Polymer-Based Biosensors, Drug Delivery and Waste Remediation Systems

by

Wei Zhang

A thesis submitted in partial fulfillment of the requirements for the degree of

Doctor of Philosophy

Department of Chemistry
University of Alberta

Abstract

Temperature responsive poly(N-isopropylacrylamide) (pNIPAm) microgels, first reported

in 1986, have attracted extensive attention due to their potential applications in many

fields, such as controlled drug delivery, chemical separation, sensors, and microreactors.

Much attention has been focused on developing biosensors because people, especially

those in resource limited areas, need inexpensive and easy-to-use technology to diagnose

quickly and accurately some common disease/health issues. Most of my work focused on

developing polymer-based sensors and polymer microgel-based drug delivery systems. In

addition to these studies, I also developed a new method to turn chewing gum waste into

materials that can be used to adsorb organic dyes, and heavy metal ions, and to reduce the

toxicity of oil sands tailings pond water. According to the focus of different chapters, I

divided my dissertation into the following three parts.

   Chapter 2 and Chapter 3 focus on the development of biosensors. In Chapter 2, I

introduce a fluorescence-based immunoassay with which I can determine the

concentration of an antigen solution containing mouse IgG by measuring the fluorescence

intensity of solution after the antigen reacts with excess antibody-modified magnetic

beads and excess FITC-modified antibody. In Chapter 3, I demonstrate the preparation of

an alkaline phosphatase-assisted pNIPAm microgel-based biosensor.

In Chapter 4, I develop near infrared-responsive etalons and utilize the etalons for

enhanced drug delivery.

In Chapter 5, I separate materials from chewing gum waste and use them to remove

organic dyes and heavy metal ions from water. These materials also can be used to reduce

the toxicity of oil sands tailing ponds water.

In Chapter 6, I draw conclusions for each chapter and give the future works of my

researches.

In addition, three appendices, A, B, and C, have been added. These contain

additional preliminary experimental results on related topics.

Preface

This thesis is the original work by Wei Zhang under the supervision of Dr. Michael J. Serpe at the University of Alberta.

Chapter 2 has been published as: Zhang, W.; Serpe, M. J., Antigen Detection Using Fluorophore-Modified Antibodies and Magnetic Microparticles, *Sensors and Actuators B: Chemical* **2017**, *238*, 441–446. I was responsible for experiment conduction, data collection, and manuscript composition. Michael J. Serpe was the supervisory author and was involved with the experimental design and manuscript composition.

Chapter 3 has been published as Zhang, W.; Wei M. L.; Carvalho, W.; Serpe, M. J., Enzyme-Assisted Polymer Film Degradation-Enabled Biomolecule Sensing with Poly (N-isopropylacrylamide)-Based Optical Devices, *Analytica Chimica Acta* **2018**, *999*, 139–143. I was responsible for experiment conduction, data collection, and manuscript composition. Menglian Wei assisted in characterization, and Wildemar Carvalho helped with useful discussions. Michael J. Serpe was the supervisory author and was involved with the experimental design and manuscript composition.

Chapter 4, Chapter 5 and Appendix materials have not been published yet. I was responsible for experiment conduction, data collection, and manuscript composition. Kevin Marakna and Huba Razzaq helped with data collecting in Chapter 4. Lei Shen

helped with the toxicity analysis in Chapter 5. Michael J. Serpe was was involved with

the experimental design.

Acknowledgements

First of all, I would like to express my deep gratitude to my supervisor, Dr. Michael J. Serpe, for giving me the opportunity to work in his lab. Dr. Serpe is one of the best supervisors I've ever met in my life. He has been a very supportive supervisor as well as a good friend. He encouraged me to attend conferences, seminars, and professional development workshops. He is like a family member, sharing with me interesting news, delicious food, etc. I am grateful that I met Dr. Serpe. With no doubt, he plays an important role in my whole life.

A big thank you to my groupmates in the Serpe lab! I spent five wonderful years with you guys! Sometimes we had disagreements, but most times we had laughter and gave each other encouragement; you were a great help in completing my PhD studies!

Next, I want to thank my committee members, Dr. Chris Le and Dr. Charles Lucy. Thank you for the precious suggestions on my research projects over the past years. In addition, I would like to extend my gratitude to Gareth from Biological Service for training me and allowing me to work in the lab. Many thanks go to Anna for helping me to edit my dissertation. You are such a kind and interesting lady!

Last but not the least, I would like to thank my family and friends for their love and support. I love you all!

Table of Contents

List of Figures

List of Schemes

List of Tables

List of Symbols and Abbreviations

G: Gibbs free energy

H: enthalpy

S: entropy

λ: wavelength maximum

m: peak order

n: dielectric index

d: spacing between the mirrors

θ: angle of incidence

A: absorbance

ε: molar extinction coefficient

b: thickness of the sample

c: concentration of the sample.

DLS: dynamic light scattering

TEM: transmission electron microscope

GPC: gel permeation chromatography

SEM: scanning electron microscope

QCM: quartz crystal microbalance

SPR: surface plasmon resonance

ELISA: enzyme-linked immunosorbent assay

LFA: lateral flow assays

LOD: limit of detection

CA19-9: carbohydrate antigen 19-9

DI: deionized

PBS: phosphate-buffered saline

pNIPAm: poly (N-isopropylacrylamide)

pAPMAH: pNIPAm-co-N-(3-Aminopropyl) methacrylamide hydrochloride

BIS: N, N- methylenebisacrylamide

AAc: acrylic acid

APS: ammonium persulfate

AP: alkaline phosphatase

CNTs: carbon nanotubes

NIR: near-infrared

LCST: lower critical solution temperature

CNTs-COOH: carboxylic acid modified carbon nanotubes

TPW: tailings ponds water

NAs: naphthenic acids

PAHs: polycyclic aromatic hydrocarbons

NPOC: non-purgeable organic carbon

TOC: total organic carbon

NDIR: non-dispersive infrared

CV: crystal violet

IgGs: Immunoglobulin Gs

FITC: fluorescein isothiocyanate

FGAM: fluorescein isothiocyanate-modified goat anti-mouse IgG

AGAR: Alexa Fluor-modified goat anti-rabbit IgG (in this thesis only, not standard)

GAM@M: goat anti-mouse IgG-modified magnetic beads

GAR@M: goat anti-rabbit IgG-modified magnetic beads

Chapter 1

Introduction to Stimuli-Responsive Hydrogels

Stimuli-responsive polymers are macromolecules that have the ability to respond chemically and/or physically to external environmental changes. [1-3] These polymers may exist as free chains,[4] polymer brushes,[5-6] and three-dimensional hydrogel networks.[7] As seen schematically in Figure 1.1a, a polymer chain can undergo a conformational change from an extended to a collapsed state in response to a certain environmental change. If the polymer chain is incorporated into a crosslinked hydrogel (Figure 1.1, b), the hydrogel network will undergo a change in response to the environmental change. The environmental change can be pH,[8] light,[9] temperature,[10] ionic strength,[11] electric field,[12] and/or mechanical pressure.[13] In many cases, the response of these polymers to environmental change are reversible and robust. This chapter discusses the general background of stimuli-responsive hydrogels with emphasis on those composed of N-isopropylacrylamide (NIPAm) monomers, which are the focus of this dissertation.

(a)   **(b)**

Figure 1.1 A stimuli-responsive polymer chain (a) and a stimuli-responsive polymer-based hydrogel (b) showing a conformational change in response to environmental change.

1.1 Introduction to Poly (N-isopropylacrylamide) Microgels

While a lot of stimuli-responsive polymers have been reported, poly

(N-isopropylacrylamide) (chemical structure shown in Figure 1.2) has received the most

attention because of its thermoresponsivity. Poly (N-isopropylacrylamide), abbreviated as

pNIPAm, was first synthesized in 1950s by polymerizing NIPAm monomers.[14]
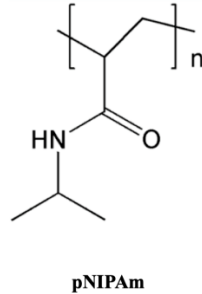
pNIPAm

Figure 1.2 Chemical structure of pNIPAm.

The thermoresponsibility of pNIPAm was discovered later by Heskins and Guillet,

who found that pNIPAm has a lower critical solution temperature (LCST) at 32 °C in

water. [15] The PNIPAm chain becomes less soluble in water at elevated temperatures; this

mainly results from dehydration of the isopropyl groups of pNIPAm. This phenomenon

also can be found in cross linked pNIPAm-based hydrogels. The Gibbs free energy

change, shown in Eq. (1.1) can be used to illustrate this phenomenon,

$$\Delta G = \Delta H - T\Delta S \qquad (1.1)$$

where ΔG is the dissolution Gibbs free energy, ΔH is the dissolution enthalpy, T is the

environmental temperature, and ΔS is the entropy change mainly due to the interaction

between water and polymer chains. A negative ΔG means that polymer dissolution is

spontaneous and that the polymer solution is homogenous in the solution, while a positive

ΔG means that polymer is insoluble in a solvent, and phase separation will occur.

For pNIPAm specifically, the interaction between water and pNIPAm plays a critical role for the phase transition. As shown in Figure 1.3, at temperatures below the LCST, pNIPAm has two different kinds of bound water: one is the bound water around the pNIPAm amide groups and the other is the water molecules with ordered structures surrounding the hydrophobic isopropyl groups and main hydrocarbon chains. As a result, negative ΔH and ΔS can be observed from the above hydration process. The enthalpy effect is dominant at low temperatures, resulting in a negative ΔG and a spontaneous polymer dissolution process. However, at elevated temperatures above the LCST, the entropy term becomes dominant, resulting in a positive ΔG and an unfavorable dissolution process and pNIPAm phase separates. Thus, the temperature-induced transition from soluble (extended coil) to collapsed (globule) state will occur. The solution transit from favorable negative ΔG to unfavorable positive ΔG.[16] At 40°C the water content of the phase separated polymer is around 52 wt%, reported by Winnik.[17]

In this chapter, I will talk about some widely studied pNIPAm-based microgels and give a few typical examples.
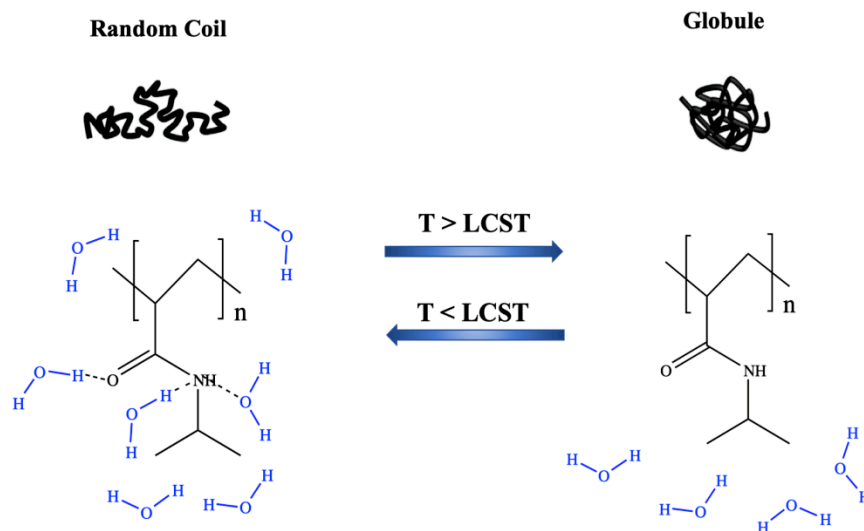
Figure 1.3 Schematic representation of pNIPAm solution's temperature-induced reversible phase transition.

1.2 Thermoresponsive pNIPAm-Based Microgels

One of the most widely studied thermoresponsive polymers is pNIPAm due to its LCST at ~32 °C in water. Thermoresponsive pNIPAm-based hydrogels were reported first by Pelton in 1978 and have been studied extensively since then. [18-20]

Figure 1.4 illustrates a typical precipitation polymerization method to synthesize hybrid microgels from NIPAm monomers and N-(3-aminopropyl)methacrylamide hydrochloride (APMAH) monomers. To synthesize this pNIPAm-co-APMAH microgel, a solution containing NIPAm, APMAH, and N,N'-methylenebisacrylamide (BIS) is purged with an inert gas, such as N_2, to remove O_2 in the solution, and allowed to heat to a temperature far above pNIPAm's LCST (~ 70 ºC) over 1 h. Then, ammonia persulfate (APS) is added to initiate polymerization. The resulting suspension is filtered to remove any large aggregates and purified with water via either centrifugation or dialysis. Note

that purification of microgels by dialysis (usually days) will take much longer time centrifugation (one day is enough).

In some cases, researchers need to decrease the size of pNIPAm-based microgels. This can be achieved by adding a surfactant, sodium dodecyl sulfate (SDS), in the solution before initiation of the polymerization. The diameter of synthesized microgels will decrease since SDS helps stabilize microgels at smaller sizes. Free-radical precipitation polymerization has been proven to be advantageous since the size distribution of microgels is narrow and the microgels' components/chemistry can be tuned easily. A key prerequisite for the success of this approach is that the monomers are dissolvable in water, while the corresponding polymers are insoluble at high temperatures.
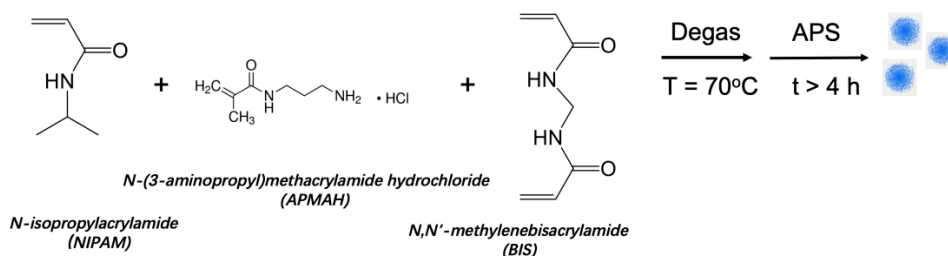
Figure 1.4 A typical precipitation polymerization method to synthesize microgels (indicated in blue) from NIPAm monomers and APMAH monomers, using BIS as the cross linker and APS as the initiator.

Richtering is among one of the pioneers who did a systematic study on the temperature responsive behavior of pNIPAm-based microgels.[21] In one example, Richtering presented a core–shell microgel consisting of pNIPAm in the shell and poly-N-isopropylmethacrylamide (PNIPMAM) in the core.[22] This microgel displayed unique properties that can be tailored easily by the synthesis and may be useful in many

different applications, such as loading of gene, protein, and drugs. The new model also can be applied with versatility to particles with core–shell.

1.3   pH-Responsive   and   Ionic   Strength-Responsive pNIPAm-Based Microgels

pH-responsive polymers usually contain poorly solvated electrolyte groups on the polymer chains, such as amino groups or carboxylic acid groups, which will accept or release protons in response to changes in the environmental pH.

An acid dissociation constant, K_a (also known as acid-ionization constant or acidity constant), is a quantitative measure of the ability of an acid to generate protons in solution. The dissociation constant usually is defined by Eq (1.2) for the reaction in equilibrium in a given solution.

$$\text{HA} \rightleftharpoons \text{A}^- + \text{H}^+ ; K_a = \frac{[\text{A}^-][\text{H}^+]}{[\text{HA}]} \tag{1.2}$$
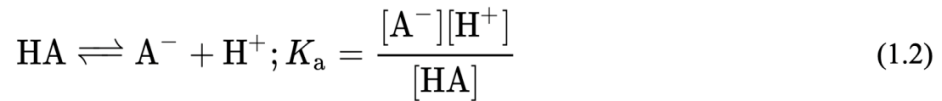
For many practical purposes, it is more convenient to discuss the logarithmic constant, pK_a, -$\log_{10} (K_a)$. The more positive the value of pK_a is, the smaller the extent of dissociation at any given pH; that is, the weaker the acid is.

As illustrated in Figure 1.5, around the pK_a of the weak electrolyte groups in the polymers, the degree of ionization of these groups changes dramatically. Acidic hydrogels become negatively charged by releasing protons at high pH and swell. In contrast, basic hydrogels prepared with basic monomers become positively charged by

accepting protons at low pH and swell. Such ionizations cause their swelling due to an increase in hydrophilicity of related groups, changes in osmolarity, and changes in ionic interactions within the gel.[23]
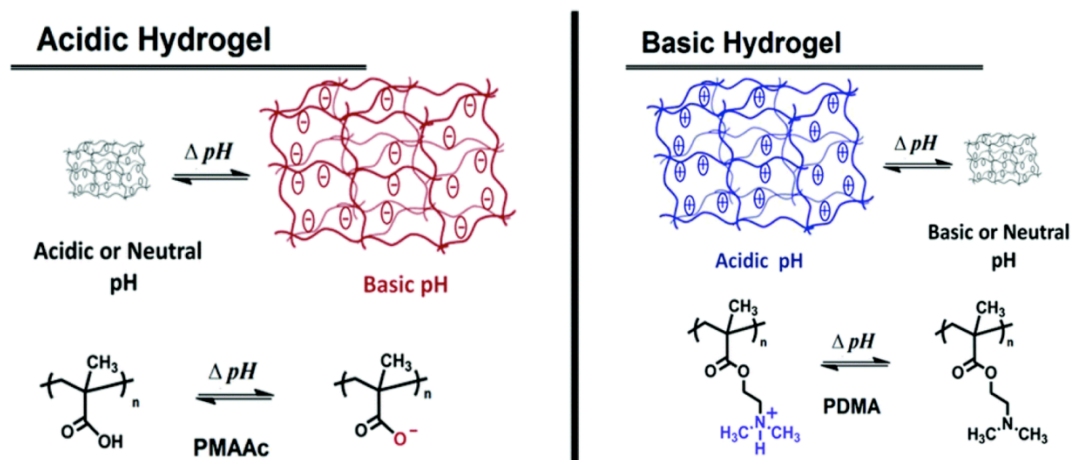
Figure 1.5 Acidic and basic hydrogels and their swelling–deswelling behaviors. PMAAc is short for Poly (methacrylic acid) and PDMA is short for poly(2,5-dimethoxyaniline). Reproduced with permission from Ref. 21. Copyright 2017, RSC.

The Serpe group carried out intense studies on pNIPAm-based microgels for controlled drug release. [24-26] They synthesized two sets of pH responsive microgels: pNIPAm-co-AAc (AAc-MG) and pNIPAm-co- 3-(acrylamido)phenylboronic acid (APBA) (APBA-MG). [26] The AAc and APBA groups are negatively charged at pH > 4.25 and 8.4, respectively, and are neutral at pHs below these respective pH values. The microgels synthesized were loaded with methylene blue (MB) by exposing them to solutions at pH 10.0, a value high enough to render both sets of microgels negatively charged, while the MB remained positively charged. This allowed the MB to be absorbed by the microgels via electrostatic interactions, as shown schematically in Figure 1.6. In a

solution with a pH above 8.4, most AAc and APBA groups are negatively charged, and positively charged MB are adsorbed via electrostatic interaction. In solutions with a pH between 4.25 and 8.4, AAc groups are negatively charged but APBA groups become neutral. In this case, the MB bound with APBA groups will release from the microgels. In solutions with a pH below 4.25, both AAc and APBA groups are neutral, and all MB will be released. As mentioned before, the chemistry of these microgels can be tuned easily. This study gives an alternative way for a complexed drug delivery system.
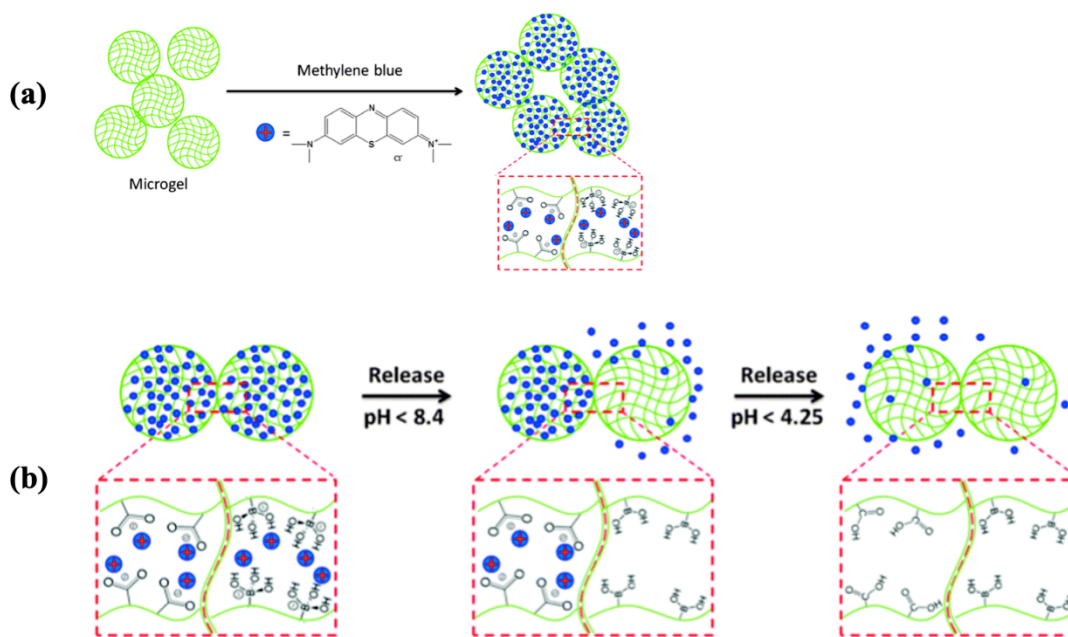
Figure 1.6 (a) Positively charged methylene blue was used as a model drug molecule that can be loaded into AAc-MG and APBA-MG at solution pH that renders them negatively charged. (b) Schematic of the pH triggered MB release from APBA-MG and AAc-MG. As each microgel is neutralized, the electrostatic interactions between the microgel and the MB are diminished, and the MB is released from the microgel. Reproduced with permission from Ref. 24. Copyright 2016, RSC.

The mechanism of pH response of pNIPAm-based microgel can be applied to others ions, such as Na^+ and K^+. Basically, ionizable groups are incorporated into the pNIPAm-based microgel either during or after the microgel synthesis process. Counterions will bind with these electrolytic groups at certain pH or ionic strength, causing the net charges of the microgel to change, and thus the volume of the microgel to change.

1.4 Bio-Responsive pNIPAm-Based Microgels

After several years' study on how these pNIPAm-based microgel responded to temperature, pH, and ions, researchers moved on to other pNIPAm-based microgels for other sensing applications. Much attention has been paid to develop pNIPAm microgel-based biosensors for various biomolecules, such as DNA, protein, saccharides, etc.

Lyon and coworkers developed a new approach to biosensing using microlenses derived from NIPAm and acrylic acid (AAc) microgels that were modified with biotin[27]. Biotin has a strong binding affinity with avidin, and the recognition event is highly specific[28-29]. They designed microlenses that would display a change in refractive index and particle diameter upon binding with avidin. This method is quite powerful and universal.

Phenylboronic acid is known for its reaction with 1,2-cisdiols such as glucose. As illustrated in Figure 1.7, PBA is in equilibrium between the charged and uncharged states in aqueous solutions, depending on the pH of the solution. Both forms of PBA can react

reversibly with glucose; this has been studied widely. However, the form of PBA in a

charged state will produce a more stable product when it reacts with glucose. Thus, when

glucose exists, the equilibrium moves to the right.
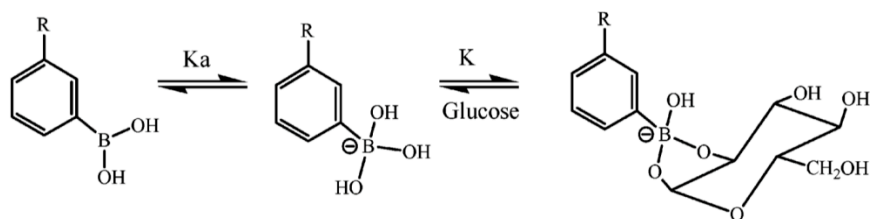
Figure 1.7 Complexation equilibrium between PBA derivative and glucose.

Zhou and coworkers prepared 3-aminophenylboronic acid (APBA) modified

pNIPAm microgels.[30] The degree of ionization of PBA on the modified microgels

increases when bound with glucose, causing the microgel to swell; thus, the detected size

of these microgels will increase. As concluded in Figure 1.8, the reaction between

glucose and PBA groups is favored at solutions with higher pH. This work inspired

research on a lot of similar glucose sensors.
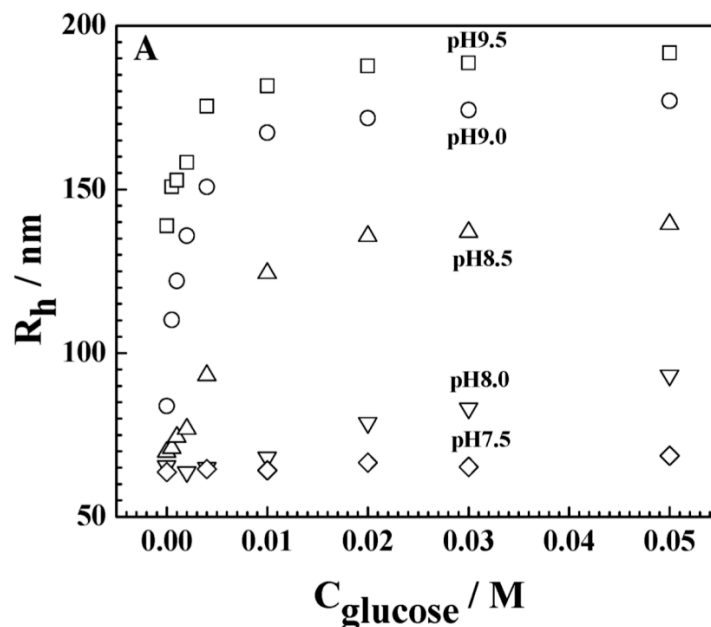
Figure 1.8 Rh values of p(NIPAM-PBA) microgels (10.0 mol % PBA) as a function of glucose concentration, measured in 0.005 M phosphate buffers of different pH values at 25 °C. Reproduced with permission from Ref. 21. Copyright 2006, American Chemical Society.

1.5 Other Stimuli-Responsive pNIPAm-Based Microgels

Attention also has been paid to other stimuli-responsive pNIPAm-based microgels, such as electricity-responsive and mechanical pressure-responsive microgels[31-34]. Electrical signals play an important role in the movement and signal recognition of living creatures. For example, Venus flytraps can trap their prey by quickly closing their lobes, which are controlled by their action potentials. Microgel-based pressure monitoring is essential in many fields, such as gas and water industries. However, research in this area is not as active as monitoring in temperature, pH, or bio-stimuli responsive microgels, but, it plays a vital role in our life

Chapter 2

Antigen Detection Using Fluorophore-modified Antibodies and Magnetic Particles

The contents of this chapter have been copied and/or adapted from the following publication: Sensors and Actuators B 238, 2017, 441–446.

2.1 Introduction

Diagnostic tools capable of detecting increasingly lower concentrations of biomarkers for disease (e.g., antigens and antibodies) have been growing in importance over the past number of decades.[35-37] This is due, in part, to the discovery of improved disease treatments, which are more efficacious when used at the early signs of disease. For example, if cancer goes untreated, it can grow, spread, and eventually lead to death[38]. Therefore, if cancer can be detected in its early stages, tumor growth can be hindered, and the risk of metastasis can be reduced dramatically. [39-41] Due to their high sensitivity and specificity, immunoassays are used frequently for quantitation of clinically relevant species like small molecules and antigenic markers.[42-44] The detection of antigens/antibodies has played a key role in early disease diagnosis and improved treatment outcomes. For example, the carbohydrate antigen 19-9 (CA19-9) is a foreign substance released by pancreatic tumor cells, and its quantitation can be used to monitor pancreatic cancer cell growth. Therefore, one could monitor CA 19-9 levels in patients to determine the efficacy of a particular treatment. [45-46] In another example, quantitation of

prostate specific antigen in bodily fluids (e.g., urine) can be used for the early detection of prostate cancer. [47] There are numerous other examples that highlight the importance of quantifying other biomarkers for disease in bodily fluids; they can lead to more effective treatment and improved quality of life. [48] Furthermore, a number of other examples exist in the literature showing sensors specific for glucose, cations, enzymes and nucleic acids. [49-52] While this is the case, there is still a need to develop novel biomolecule detection schemes that could lead to improved disease diagnostics and help improve life quality and longevity.

Antibody-based sensing schemes for the detection of specific antigens have proven to be a versatile and powerful biosensing tool. This is due to the high specificity of antibodies for the particular epitopes on corresponding antigens. So far, many techniques have been used for antigens/antibodies detection. The most common techniques used to detect them are enzyme-linked immunosorbent assay (ELISA) [53-54] and lateral flow techniques. [55-57] These techniques are well established and already are used at hospitals, clinics, and homes. While this is the case, ELISA protocols involve two separate binding steps, followed by exposure to an organic reporting group that generates a chromophore after reaction with the enzyme-tagged secondary antibody. Since there are many steps/components to this assay, and since the assay requires an enzymatic reaction, it is somewhat difficult to implement (especially in the point-of-care cases). ELISA also requires significant time to perform. Finally, the surface chemistry needs to be tuned

carefully for each analyte, which can also prohibit ELISA's utility. Compared to ELISA, lateral flow assays have many advantages, including simplicity, versatility, and low cost. However, imprecise sample volumes often are used, which reduces the assay's precision. Lateral flow assays are also difficult to implement for multianalyte sensing.[58] Other techniques have been developed to detect antigens/antibodies, e.g., surface plasmon resonance spectroscopy (SPR) [59] and microfluidic-based approaches.[60] These approaches are extremely promising, however, they often require complex sample preparation procedures, bulky and expensive equipment, and professionally trained personnel to run the tests. Therefore, new sensors capable of detecting analytes in a cost-effective manner, that are easy to use and capable of being operated in non-laboratory settings, are in demand.

Nano/microparticles have found their way into various technologies and have had a great impact on our everyday lives.[61-62] One important application of inorganic nano/microparticles is their use for disease diagnosis.[63-65] The Mirkin group was among the first to demonstrate the utility of Au nanoparticles for detecting DNA/RNA in solution.[66-68] The Van Duyne group also showed that surface bound Au nano features could be used to detect biomolecules.[69-71] Magnetic microparticles also have attracted considerable interest for biosensor applications, mainly due to their ease of separation from solutions using a simple magnet.[72-73]

In one example, the Tabrizian group showed that by using an ELISA-based approach in microfluidic devices and magnetic field induced mixing, they decreased the volume of sample needed for analysis while maintaining high sensitivity (0.1–6.7 pM).[74] While this approach is promising, it requires the use of microfluidic devices, which can be difficult to fabricate, especially if fabrication facilities are not readily available. In another example, Crowell and coworkers synthesized capture DNA aptamer-modified magnetic beads and reporter DNA aptamer-modified quantum dots. When specific bacteria exist in a sample, the capture DNA aptamer-modified magnetic beads, bacteria, and reporter DNA aptamer-modified quantum dots form a fluorescent sandwich complex, which can be collected by an external magnet and the fluorescence detected by a fluorometer.[75] While this approach is convenient, it has been designed to detect only Campylobacter. Oplatowska and coworkers demonstrated multiplex detection of plant pathogens using microsphere immunoassay technology. In their investigation, they linked an antibody specific for each plant pathogen to separate magnetic microspheres that were modified with unique fluorophores. Individual bacteria could be detected by observing the fluorescence signature of the collected microspheres.[76] Recently, our group showed that polymer-based materials combined with the use of magnetic microparticles could be used to detect biomolecules in a facile manner.[77-78] While each of these examples has its pros and cons, there is room for more technology development in this area.

In this chapter, I show that Immunoglobulin Gs (IgGs) from two different species can be detected in a single solution by utilizing fluorophore-modified antibodies and magnetic microparticles. This sensing approach showed a limit of detection of 0.65 nM, which is comparable to the current state of the art based on carbon nanotubes (LOD of 0.1–10 nM).[79-81] The approach also was capable of detecting specific IgGs and was easy to implement. While the approach has been shown to be useful for detecting two IgGs in a single solution, I envision that it can be modified easily to detect multiple analytes in a single solution, e.g., antibodies, antigens, DNA, and other small molecules of interest.

2.2 Experimental Section

2.2.1. Materials and Instruments

Mouse immunoglobulin G (IgG) (2.5 mg/mL), rabbit IgG (powder), fluorescein isothiocyanate (FITC)-modified goat anti-mouse IgG (abbreviated as FGAM, F(ab')$_2$ fragment specific to mouse IgG, emission at 520 nm, 2 mg/mL), Alexa Fluor-modified goat anti-rabbit IgG (abbreviated as AGAR, F(ab')$_2$ fragment specific to rabbit IgG, emission at 675 nm, 2 mg/mL), and phosphate-buffered saline (PBS, 1 mM KH$_2$PO$_4$, 155 mM NaCl, 3 mM Na$_2$HPO$_4$) were obtained from Thermo Fisher Scientific (Waltham, MA, USA). Mouse IgG was diluted to 1 g/ L before use. Goat anti-mouse IgG-modified magnetic beads (abbreviated as GAM@M, Fc fragment specific) and goat anti-rabbit IgG-modified magnetic beads (abbreviated as GAR@M, Fc fragment specific) were purchased from Spherotech (with an average diameter of 3.5 μm, Lake Forest, IL, USA).

The magnetic beads were washed with PBS buffer three times and later adjusted to the same concentration (0.5% w/v). As characterized by the producer, 100 μL of GAM@M was capable of binding 0.64 μg of mouse IgG in maximum and 100 μL of GAR@M is capable of binding 0.56 μg of rabbit IgG in maximum. All deionized (DI) water was filtered to have a resistivity of 18.2 M Ω cm and was obtained from a Milli-Q Plus system from Millipore (Billerica, MA). A Photon Technology International (PTI) MP1 Fluorescence System was used to measure fluorescence spectra. An ultra-high-pull Neodymium-Iron-Boron (NdFeB) magnet (5 × 5 × 1 cm) was purchased and used from McMaster-Carr Company (Elmhurst, IL). The surface magnetic strength was 1777 G. An ultraviolet lamp (Mode B100AP, BLACK-RAY CA, USA) was used to supply radiation to excite fluorescence. Photographs for each sample were obtained using a Nikon camera equipped with a 105 mm Nikon macrolens (Nikon,Ontario, Canada). The camera was placed in front of the samples.

2.2.2. Reaction Between Antigen and Antibody

The approach described here can be seen schematically in Figure 2.1. For the mouse IgG single antigen system, 150 μL of GAM@M, 450 μL of PBS buffer solution, and 1 μL (13.4 pmol) of FGAM were added in six different centrifuge tubes. Into each tube was added 0 μg (0 pmol), 0.1 μg (0.67 pmol), 0.2 μg (1.34 pmol), 0.3 μg (2.01 pmol), 0. 4 μg (2.68 pmol), and 0.5 μg (3.35 pmol) mouse IgG, respectively. The exact composition of each tube can be seen in Table 2.1. Each tube was wrapped in aluminum foil and was

shaken gently for 1 h. After 1 h, the magnetic beads were separated from the solutions by

exposing each tube to an external magnet, which pulled the magnetic particles to the

tube's inside wall, and the supernatant solution collected. The magnetic beads were

washed by adding 500 μL of PBS into the tube, mixing, magnetically separating the

particles from the solution, and collecting the supernatant solution. This process was

carried out a total of three times for each tube. Finally, all the aliquots from each

individual washing were combined, and the fluorescence intensity measured. The

excitation wavelength for FGAM was 470 nm. The emission spectra were collected from

490 nm to 650 nm, with both slit widths set at 4 nm, integration time set at 0.1 s, and the

step size was 1 nm.

Table 2.1 Reactants for mouse IgG detection by reacting with FITC-modified antibody and antibody-modified magnetic beads.

Tube No.	1	2	3	4	5	6
GAM@M	150 μL	150 μL	150 μL	150 μL	150 μL	150 μL
FGAM	1 μL	1 μL	1 μL	1 μL	1 μL	1 μL
Mouse IgG	0 μg	0.1 μg	0.2 μg	0.3 μg	0.4 μg	0.5 μg
PBS buffer solution	450 μL	450 μL	450 μL	450 μL	450 μL	450 μL

For the mouse IgG–rabbit IgG double antigen system, 150 μL of GAM@M, 150 μL

GAR@M, 300 μL PBS buffer solution, 1 μL(13.4 pmol) FGAM, and 1 μL (13.4 pmol)

AGAR were added to three different centrifuge tubes. Into each of the three tubes was

added 0.2 μg (1.34 pmol) mouse IgG and 0.6 μg (4.02 pmol) rabbit IgG, 0.4 μg (2.68 pmol) mouse IgG and 0.4 μg (2.68 pmol) rabbit IgG, and 0.6 μg (4.02 pmol) mouse IgG and 0.2 μg (1.34 pmol) rabbit IgG, respectively. The exact composition of each tube can be seen in Table 2. Note that GAM@M, GAR@M, FGAM and AGAR are in excess relative to mouse IgG and rabbit IgG. The tubes were wrapped in aluminum foil and shaken gently for 1 h. After 1 h, the magnetic beads were separated from the solutions by exposing each tube to the external magnet, which pulled the magnetic particles to the tube's inside wall, and the supernatant solution was collected. The magnetic beads were washed by adding 500 μL of PBS into the tube, mixing with pipet tips, magnetically separating the particles from the solution, and collecting the supernatant solution. This process was carried out a total of three times for each tube. Finally, all the washings from each tube were combined, and the fluorescence intensity measured. The excitation wavelength for FGAM is 470 nm and AGAM 600 nm, with both slit widths set at 4 nm. The emission spectra were collected from 490 nm to 650 nm for FGAM and 620 nm to 750 nm for AGAM, with integration time set at 0.1 s and step size of 1 nm.

Table 2.2 Reactants for mouse IgG and rabbit IgG detection by reacting mouse IgG solution and rabbit IgG solution with FITC-modified antibody and antibody-modified magnetic beads.

Tube No.	1	2	3
GAM@M	150 μL	150 μL	150 μL
GAR@M	150 μL	150 μL	150 μL
FGAM	1 μL	1 μL	1 μL
AGAR	1 μL	1 μL	1 μL
Mouse IgG	0.2 μg	0.4 μg	0.6 μg
Rabbit IgG	0.6 μg	0.4 μg	0.2 μg
PBS buffer solution	450 μL	450 μL	450 μL

2. 3 Results and Discussion

Initial experiments focused on the detection of the single analyte mouse IgG. The approach is shown schematically in Figure 2.1. As can be seen, fluorescein isothiocyanate-modified goat anti-mouse IgG (F(ab')$_2$ fragment specific) (FGAM) and goat anti-mouse IgG modified magnetic microparticles (Fc fragment specific) (GAM@M) of given (and known, as shown in Part 2.2.2) amounts were exposed to some amount of mouse IgG. For this assay to be successful, both the FGAM and GAM@M need to be added in known excesses relative to the amount of mouse IgG to be detected. Solutions were allowed to mix at room temperature for 2 h, after which the free FGAM was isolated from the rest of the components by placing the centrifuge tubes near an external

magnet, which removes any free GAM@M and GAM@M bound to mouse IgG and FGAM from solution. Then, a PBS buffer solution was added to wash the magnetic microparticles, followed by their isolation and rewashing. All the isolated/collected solutions were combined into one solution, and the fluorescence spectrum of each combined solution acquired.
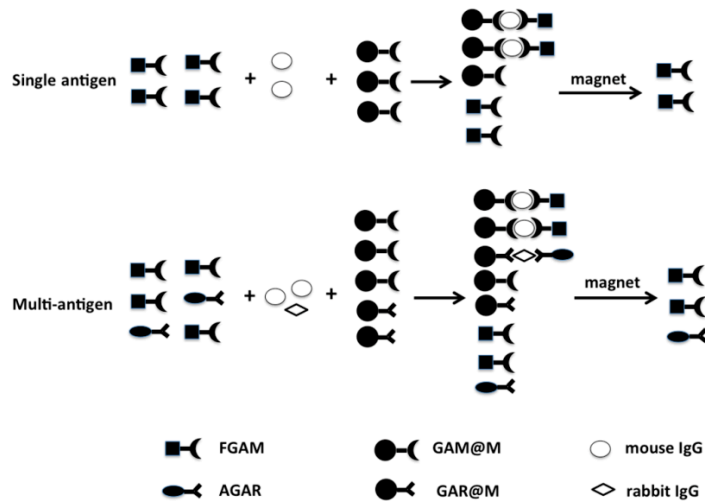
Figure 2.1 Schematic representation of the approach used to detect mouse IgG (single antigen) and mouse IgG/rabbit IgG (multi-antigen). As can be seen, in each case the amount of fluorophore-modified antibody left in solution was inversely related to the concentration of the antigens in solution.

Importantly, I showed that no fluorophore leached from the magnetic microparticles if they were left to incubate in a PBS buffer solution. Additionally, no obvious morphological change of the magnetic beads was observed after their use in the assay (see scanning electron microscope (SEM) images in Figure 2.2). The fluorescence intensity depended on the amount of FGAM left in solution, which can be related to the amount of mouse IgG in the original solution—there is an inverse relationship. Specifically, a higher concentration of mouse IgG in the initial solution yields a lower

fluorescence intensity. I note that if the fluorescence intensity from the immunoassay is not in the working range in Figure 2.2, then the amount of antibody added is likely not in excess. Therefore, specific approaches must be developed to address this problem. For example, the sample to be analyzed could be split into smaller aliquots and exposed to a range of antibody concentrations, and the fluorescence intensity from the various solutions determined. In this case, one of the solutions should have the required excess for the assay to be successful.
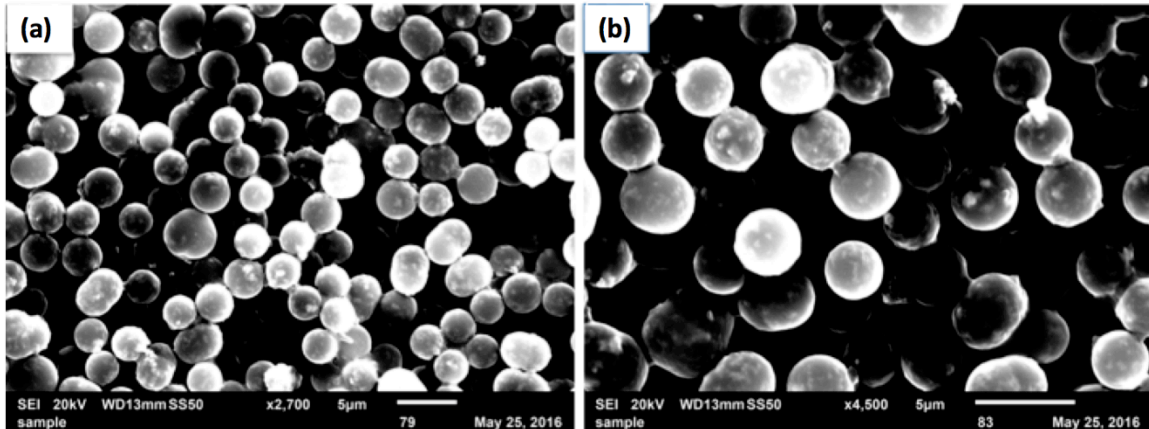
Figure 2.2 SEM images of magnetic beads before (a) and after (b) reaction. Magnetic beads for image (b) were obtained by reacting 0.5 μg (3.35 pmol) mouse IgG with 150 μL of GAM@M and 1 μL (13.4 pmol) of FGAM.

As shown in Figure 2.3a, as the amount of mouse IgG in solution increases, the fluorescence intensity of FGAM in solution decreases. This is a direct result of more FGAM being removed from solution via their bond with GAM@M, which is facilitated by the mouse IgG. As can be seen in Figure 2.3b, the fluorescence intensity of FGAM at 515 nm decreases in a linear fashion (with an R^2 of 0.991). Additionally, the error bars on

the data points obtained from multiple experiments are extremely small; therefore I conclude that the assay is highly reproducible and precise.
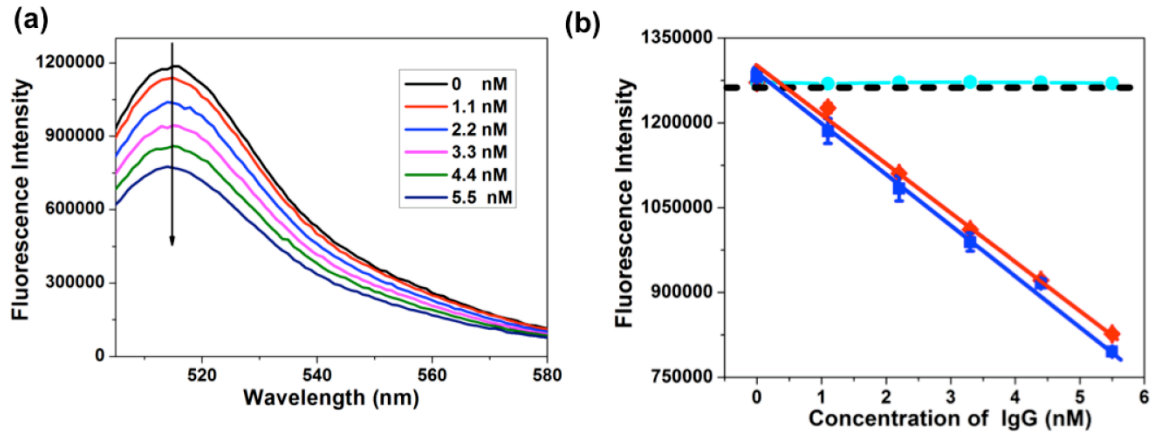
Figure 2.3 (a) Fluorescence spectra of FGAM in solution after its exposure to mouse IgG, followed by its magnetic field assisted isolation. The concentrations are indicated in the figure inset, and the arrow indicates increasing mouse IgG concentration. (b) Fluorescence intensity of FGAM (◆) for magnetic field-assisted separation and (■) for separation by filtration at the indicated mouse IgG concentrations. (●) Fluorescence intensity for the assay as a function of rabbit IgG concentration. The dashed horizontal line indicates the fluorescence intensity that corresponds to the limit of detection. Each data point is an average obtained from three individual experiments, and the error bars are the standard deviations of the measured values.

In a subsequent experiment, I showed that the magnetic microparticles could be removed from the solution using a filtration apparatus as opposed to a magnetic field. Specifically, the assay was performed using the same procedure as above, although a filter with pore size of 0.2 μm was used to remove the particles from solution as opposed to a magnet. As can be seen in Figure 2.3b, the response is inversely related to the concentration of mouse IgG in solution, with good precision. This approach also could find utility for biosensing and will allow other particles to be used, such as polystyrene

spheres and microgels. This will allow for easy multiplexing by using particles composed of different fluorophores.[82-83] Finally, approaches such as centrifugation or various separations could be used to achieve similar goals.

The selectivity of the approach also was determined by exposing FGAM and GAM@M to various amounts of rabbit IgG. Using the same approach as above for detecting mouse IgG, I isolated the remaining, unbound FGAM and measured the fluorescence intensity of the solution. As can be seen in Figure 2.3b, there is almost no response of the system to rabbit IgG, proving that the assay is specific for the IgG species.

Finally, the LOD for this assay was determined by averaging the signal obtained from the control sample (fluorescence intensity obtained from sample with no IgG added, i.e., a blank) and determining the fluorescence intensity of 3*blank. The LOD is indicated in Figure 2.3b by the dashed horizontal line and corresponds to a concentration of 0.65 nM (0.11 µg/mL), which is comparable (even better) than some other advanced technology based on carbon nanotubes (5 nM) [80] and ELISA (1.0 µg/mL) [84]. In a subsequent experiment, I showed that a similar approach could be used to quantify the amount of rabbit IgG in solution. As can be seen in Figure 2.4, a trend similar to the above experiments was observed.
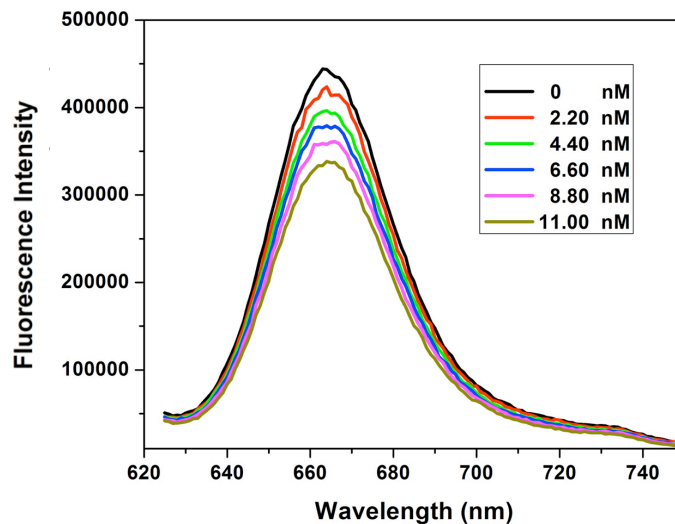
Figure 2.4 Fluorescence spectra of AGAR in solution after its exposure to rabbit IgG, followed by its magnetic field-assisted isolation. The concentrations are indicated in the figure inset, and the arrow indicates increasing rabbit IgG concentration.

For many practical applications, several antigens may coexist in one sample. The increase or decrease of the concentrations of some combination of antigens may be useful for identifying disease states more rapidly and more accurately. To determine if multiple antigens could be detected simultaneously using our assay, I quantified both mouse IgG and rabbit IgG in the same solution. As can be seen schematically in Figure 2.1 (multi-antigen), FGAM, AGAR, GAM@M, and GAR@M in known amounts were exposed to given amounts of mouse IgG and rabbit IgG. Again, for this assay to be successful, FGAM, AGAR, GAM@M, and GAR@M are added in known excess relative to the amount of mouse IgG and rabbit IgG to be detected. Solutions were allowed to mix at room temperature for 2 h, after which the free FGAM and AGAR were isolated from the rest of the components using a magnet, which can remove any free GAM@M,

GAR@M, GAM@M bound to mouse IgG and FGAM, and GAR@M bound to rabbit IgG and AGAR. After washing of the magnetic microparticles, followed by combination of the collected supernatant solutions, the fluorescence spectrum of the supernatant solution was collected. Like above, I hypothesized that the fluorescence intensity will depend on the amount of FGAM and AGAR left in solution, which can be related to the amount of mouse IgG and rabbit IgG in the original solution — again, there is an inverse relationship. Specifically, as can be seen in Figure 2.5, a higher concentration of mouse IgG and rabbit IgG in the initial solutions yielded a lower fluorescence intensity for the FGAM and AGAR. These data suggest that the approach reported here has the potential to be used to detect multiple antigens in solution.
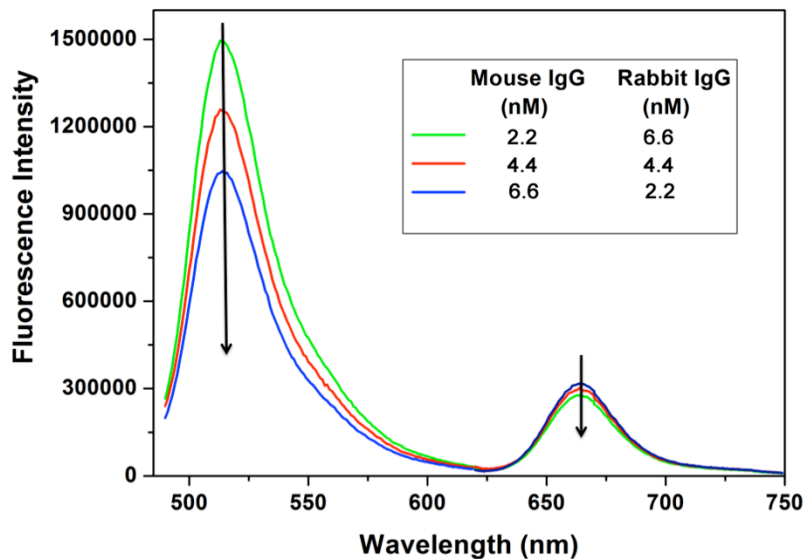
Figure 2.5 Fluorescence spectra of FGAM and AGAR in solution after their exposure to a solution of mouse and rabbit IgG, followed by their magnetic field assisted isolation. The concentrations are indicated in the figure inset, and the arrows indicate increasing mouse and rabbit IgG concentrations.

For many applications (e.g., point-of-care diagnostics) it is important to be able to quantify biomolecules without the use of specialized equipment. Therefore, it is important to show that this assay could work just by using the naked eye to determine fluorescence intensity. To prove that this is possible, I performed the mouse IgG assay, but instead of using a fluorometer to determine the fluorescence intensity of the solution, I exposed the solution to UV light (365 nm) and photographed the fluorescence. The photographs can be seen in Figure 2.6. As can be seen, the fluorescence from each solution can be seen easily, although the real figure of merit for this assay is how much of a change can be detected by the naked eye. While I did not investigate this in depth, one clearly can see the difference between the fluorescence of the individual solutions if the concentrations are different by an order of magnitude. While this may not be useful for quantifying sample concentrations, the visual detection could be useful as a "yes" or "no" assay.
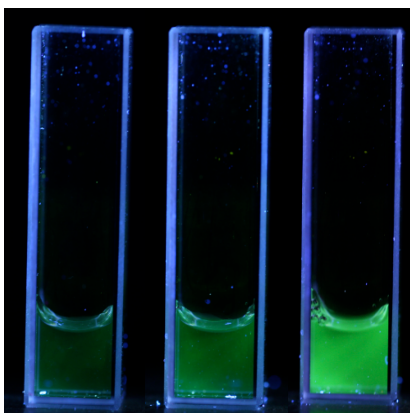
Figure 2.6 Photographs of solutions containing some amount of FGAM after exposure to various concentrations of mouse IgG. The concentrations are (left) 20 μg (13.4 pmol), (middle) 5 μg (3.35 pmol) and (right) 0.1 μg (0.67 pmol).

2.4 Conclusions

In summary, an assay that utilizes fluorophore-modified anti-bodies and antibody-modified magnetic microparticles to detect mouse and rabbit IgG was developed. I showed that the assay was able to detect the respective IgGs with good LOD and selectivity. I also demonstrated that the IgGs could be detected in a single solution simultaneously, which is important for multi-analytes sensing approaches. Finally, I showed that the assay could be performed without the use of a fluorometer by simply using the naked eye. This investigation forms the foundation for future antigen detection approaches and can find real-world applications for disease diagnosis. Though in real applications, we may need to further tune the feeding ratio of the immunoassay to allow for proper analysis.

Chapter 3

Enzyme-assisted Polymer Film Degradation-enabled Biomolecule Sensing with Poly (N-isopropylacrylamide)-Based Optical Devices

The contents of this chapter have been copied and/or adapted from the following publication: Analytica Chimica Acta 999, 2018, 139-143.

3.1 Introduction

Pathogens such as bacteria and viruses are a major class of species that can have direct negative impacts on human and animal health.[85-87] Recently, the Zika virus has emerged as a major health concern in South America and other tropical areas around the world. Oftentimes, Zika virus infection has no symptoms, which makes it very difficult to diagnose. Therefore, those infected usually are not aware that it can lead to extremely negative impacts on reproductive health.[88-89] As of 2018, there is no known cure for the Zika virus and no vaccine to prevent it. Therefore, an approach that can alert people when they are infected can help circumvent the negative impacts on those infected, especially those that are or are planning to become pregnant.

Due to the high specificity of antibodies for particular epitopes on corresponding antigens, antibody-based detection systems for specific antigens have been used as versatile and powerful tools for bioanalysis.[90-91] Thus far, many biosensors have been developed, with one of the most commonly used approaches being enzyme linked

immunosorbent assay (ELISA) that exploits antibody–antigen interactions.[62, 92] However, in many cases, ELISA requires significant time to perform; the surface chemistry needs to be tuned carefully for each specific analyte, and it requires a lab setting to achieve quantitative results. Lateral flow assays (LFA) for antibody/antigen detection also have attracted significant attention due to their ease of fabrication and the ability to use small sample volumes while maintaining high quality figures of merit (e.g., high sensitivity and low detection limits). The most common and widely used LFA is the home pregnancy test. Although LFAs are extremely useful, there are some issues with biomolecular affinities as the reaction times between the capture and analyte biomolecules are short and there is the possibility of non-specific reactivity to the LFA substrate. Much attention also has been focused on a variety of other approaches that exploit various phenomena, e.g., surface plasmon resonance (SPR),[93-95] quartz crystal microbalance (QCM),[96] and electrochemical impedance spectroscopy.[97] Even with availability of these various approaches, there is still a need for new cost-effective sensing technologies with high specificity and sensitivity, so that people, especially those in developing countries and low-income regions, will have disease diagnosis kits more readily available to them.

Recently, photonic materials/crystals have played important roles in various analytical and medical fields.[98-102] In 2010, the Serpe Group reported on a novel optical device (etalon) that can be fabricated by sandwiching a layer of poly (N-isopropylacrylamide) (pNIPAm)-based microgels between two thin, semi-transparent

metal layers (typically Au).[103] The structure of the microgel-based etalons is shown in Figure 3.1. Briefly, etalons are fabricated by painting a concentrated solution of pNIPAm-based microgels onto a gold-coated glass substrate with a pipet tip, followed by washing away the excess microgels that are not directly bound to the Au. Then, the etalon is soaked in water and rinsed further before deposition of another Au layer on top of the microgels. The etalons show visible color and exhibit unique multipeak reflectance spectra. The position of the peaks and the peak order can be predicted by Eq. (3.1)：

$$\lambda m = 2nd \cos\theta \tag{3.1}$$

where the specific wavelength maximum (λ) of a peak depends on the peak order (m), the refractive index of the dielectric (n), the spacing between the mirrors (d), and the angle of incidence (θ). As a result, the size of the microgel is one factor that can dictate the color of the devices and the position of the devices' reflectance peaks. We have used this structure for a variety of applications, primarily focused on sensing, biosensing, and drug delivery. [24, 104-107]
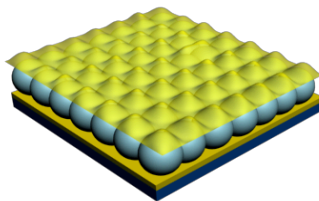
Figure 3.1 The schematic structure of a pNIPAm microgel based etalon, which consists of two 15-nm Au mirrors (yellowish layers) with 2-nm Cr adhesion layer. The mirrors sandwich a jammed layer of microgels (bluish microgel layer) built on a rigid glass substrate (dark blue bottom).

In this chapter, a new sensing motif is introduced that utilizes positively charged pNIPAm-co-N-(3-Aminopropyl) methacrylamide hydrochloride (APMAH) microgel-based etalons coated with enzyme-responsive/reactive species to detect biomolecules, specifically mouse IgG. These experiments serve as a proof of concept for sensing other antigens in real samples.

3.2 Materials and Instruments

N-isopropylacrylamide (NIPAm) was purchased from TCI (Portland, Oregon) and purified by recrystallization from hexanes (ACS reagentgrade, EMD, Gibbstown, NJ) prior to use. Carbon nanotube, N, N- methylenebisacrylamide (BIS) (99%), acrylic acid (AAc) (99%), N, N'-methylenebis(acrylamide), and ammonium persulfate (APS) (98+%) were obtained from Aldrich (St. Louis, MO) and were used as received. Phosphoric acid 2-hydroxyethyl methacrylate ester was obtained from Sigma Aldrich. Deionized (DI) water with a resistivity of 18.2 MΩ-cm was used. Fisher's finest glass coverslips were 25 × 25 mm and obtained from Fisher Scientific (Ottawa, Ontario). Cr of 99.999% purity was obtained from ESPI as flakes (Ashland, OR), while Au of 99.99% purity was obtained from MRCS Canada (Edmonton, AB). Cr/Au annealing was done in a Thermolyne muffle furnace from ThermoFisher Scientific (Ottawa, Ontario) at 250 ℃. Reflectance spectra were collected using a USB2000+ spectrophotometer, a HL-2000-FHSA tungsten light source, and a R400-7-VIS-NIR optical fiber reflectance probe, all from Ocean Optics (Dunedin, FL). The spectra were recorded using Ocean

Optics Spectra Suite Spectroscopy Software over a wavelength range of 350−1025 nm. An ellipsometer (Nano film ep4, Accurion, Germany) was used to detect the thickness of the polymer layer on top of the etalon. Transmission electron microscope (TEM) images were acquired using a JEOL, JEM 2100 (JEOL USA, Inc., MA, USA) with an accelerating voltage of 200 kV. The specimens were prepared by drying 10-μL solutions of highly diluted samples on carbon coated copper grids.

3.3 Results and Discussion

As shown in Scheme 3.1, the immunoassay is performed by adding an excess amount of alkaline phosphatase-modified goat anti-mouse IgG (AP-GAM) (F(ab')2 fragment specific to mouse IgG) to mouse IgG in solution, and allowing them to interact for 30 min. After 30 min, the AP-GAM was isolated from the unbound, excess AP-GAM via addition of goat anti-mouse IgG (Fc fragment specific)-modified magnetic microparticles (GAM@M). After application of a magnetic field, the free, unbound AP-GAM could be isolated and exposed to the etalon. The etalons used were coated with a phosphate-containing polymer that is cleaved by AP-GAM and releases phosphate. The released phosphates are then available to diffuse into the microgel layer where they neutralize the charges on the microgels; this yields a shift in the position of the peaks in the etalon's reflectance spectrum. Finally, the shift in the reflectance peak can be correlated to the initial concentration of mouse IgG. While we use a reflectance spectrometer to probe the optical properties of the devices in this investigation, we are

moving toward generating a hand-held device containing simplified optics (or even the light source/camera from a cellular phone) to probe the optical properties of the devices to make the measurements truly portable.
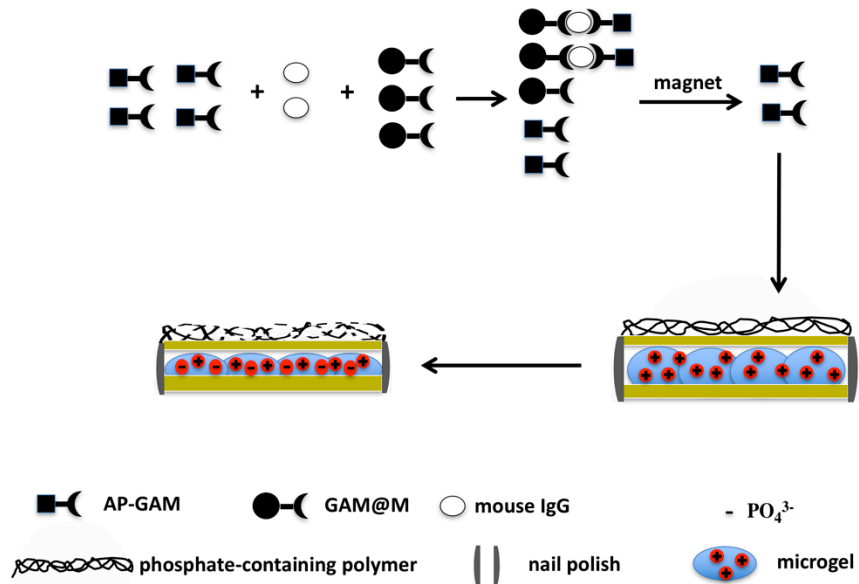
Scheme 3.1 Schematic depiction of the various steps in the immunoassay.

To accomplish this, pNIPAm-co-APMAH microgels were synthesized and used to generate etalons according to the previously published protocol [108-109]. Briefly, NIPAm and APMAH were copolymerized at 70 °C using ammonium persulfate (APS) as the initiator and N, N'-methylenebis(acrylamide) as the crosslinker. The approximate diameter of the prepared microgels was measured via dynamic light scattering (DLS) to be 1042±9 nm in water. Transmission electron microscopy (TEM) was used to characterize the microgels further, and a representative image can be seen in Figure 3.2. The size of microgels obtained from TEM decreased to about 420 nm, because of dehydration. The resulting microgels were used to fabricate etalons, as shown in the

photograph in the insert of Figure 3.2. To generate the phosphate containing polymer, phosphoric acid 2-hydroxyethyl methacrylate ester (chemical structure shown in Figure 3.3) was polymerized using APS as the initiator under a N_2 atmosphere at 60 ℃. Following the synthesis, the polymer was purified via dialysis; the concentration of the solution after dialysis was 0.01 g/mL. The molecular weight of the synthesized polymer was measured by gel permeation chromatography (GPC) to be 1.099×10^6 with a PDI 1.166. After purification, 200 mL of the polymer solution were spin-coated onto the top layer of the etalon and allowed to dry. The spin-coating process was repeated another two times to make sure that there was adequate polymer deposited on top of the Au surface. After deposition, the surface was rinsed with deionized water and soaked in PBS buffer solution. The thickness of the resultant polymer layer was measured via ellipsometry to be 156±4 nm. The XPS data, shown in Figure 3.4, is further evidence of the deposition of the polymer layer.
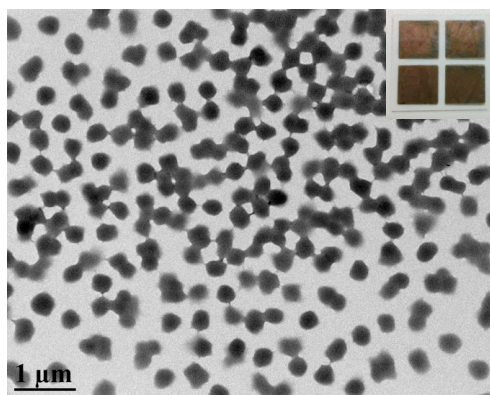
Figure 3.2 TEM image of the microgels. Insert is a photo of a representative etalon we used for performing the immunoassay.
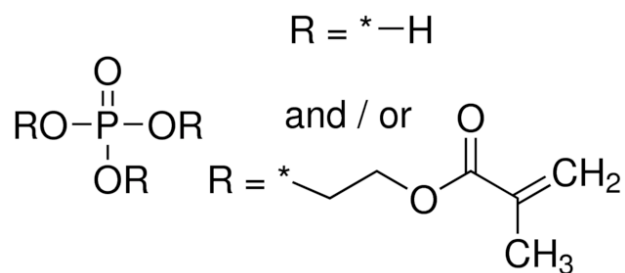
Figure 3.3 Chemical structure of phosphoric acid 2-hydroxyethyl methacrylate ester used in this submission.
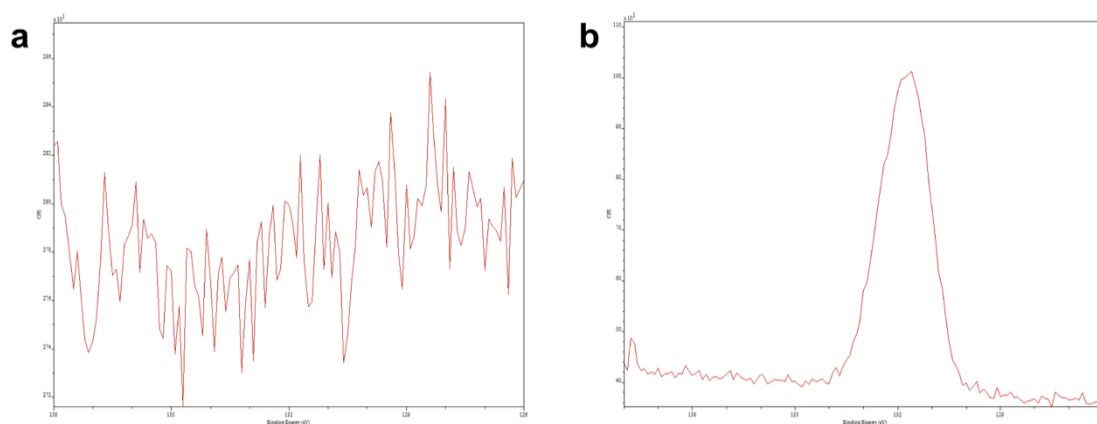
Figure 3.4 XPS spectrum for pure etalon (a) and etalon modified with poly (phosphoric acid 2-hydroxyethyl methacrylate ester) by spin-coating (b).

To perform the assay, 150 µL of GAM@M suspension, 270 µL of PBS buffer solution, and 1.7 µL (dissolved in 28 µL PBS buffer) of AP-GAM were added into six separate centrifuge tubes. Into these tubes, was added 0 µg (0 pmol), 0.1 µg (0.67 pmol), 0.2 µg (1.34 pmol), 0.3 µg (2.01 pmol), 0.4 µg (2.68 pmol), and 0.5 µg (3.35 pmol) mouse IgG, respectively. Then, each tube was wrapped in aluminum foil and gently shaken for 1 h at 37 °C. Next, the magnetic beads were separated from the solutions by exposing each tube to an external magnet, which pulled the magnetic particles to the

tube's inside wall. The supernatant solution, which contained excess AP modified GAM was collected. To ensure that all the excess AP modified GAM was collected, the magnetic beads were washed by adding 100 μL of PBS into the tube, mixing, magnetically separating the particles from the solution, and collecting the supernatant solution. This process was carried out a total of three times for each tube. Finally, all the aliquots from each individual tube were combined and used to react with the etalon. To confirm that all the magnetic beads were separated from the solution, I used DLS to measure the size of any particles in the solution. No particles with a diameter on the order of the magnetic particles used here (3.5 μm) were observed, indicating that all the magnetic particles were removed from the solution.

Next, 100 μL PBS buffer was added on top of each individual etalon (0.375 inch × 0.375 inch) to stabilize the etalon, followed by addition of 50 μL of the supernatant obtained from the reaction solutions described above. The etalon was placed on a hotplate, with the temperature set at 37 ℃. Note that while the reaction can take place at room temperature, I used 37 ℃ to mimic the conditions found in the human body. After ~5 min, a blue shift of the reflectance peak was observed that stabilized within 30 min. The reflectance spectra were collected before and after (10 min, to minimize the reaction time but still obtain an adequate sensor response) addition of the supernatant solution obtained from the reaction. Typical reflectance spectra of the etalon before and after exposure to AP-GAM solution are shown in Figure 3.5 (actual reflectance spectra for all experiments

are shown in Figure 3.6). The reflectance spectra collected at various times after exposure

to AP-GAM are shown in Figure 3.7. I observed that in the initial ~4 min, the reflectance

peaks shift slowly, stabilizing after ~10 min. For practical applications, the total peak

shift is only required to quantify the concentration of mouse IgG in solution. As can be

seen from Figure 3.8, lower initial concentrations of the mouse IgG yield high

concentrations of AP-modified GAM left in solution, which leads to larger shifts in the

peak position.
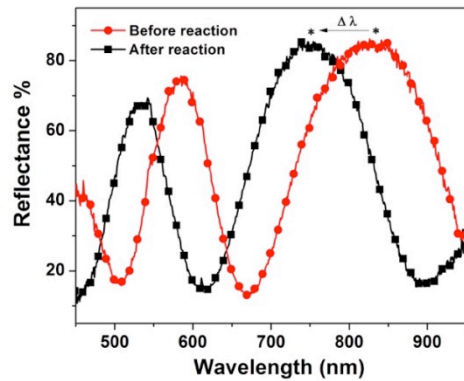
Figure 3.5 Reflectance spectra of the etalon before and after reacting with AP-GAM solution. In this case,
the AP-GAM solution was obtained after reaction with 0.1 mg mouse IgG (1.1 nM). The stars above the
respective spectra indicate the position of the reflectance peaks before and after exposure of the etalon to
excess AP-GAM.
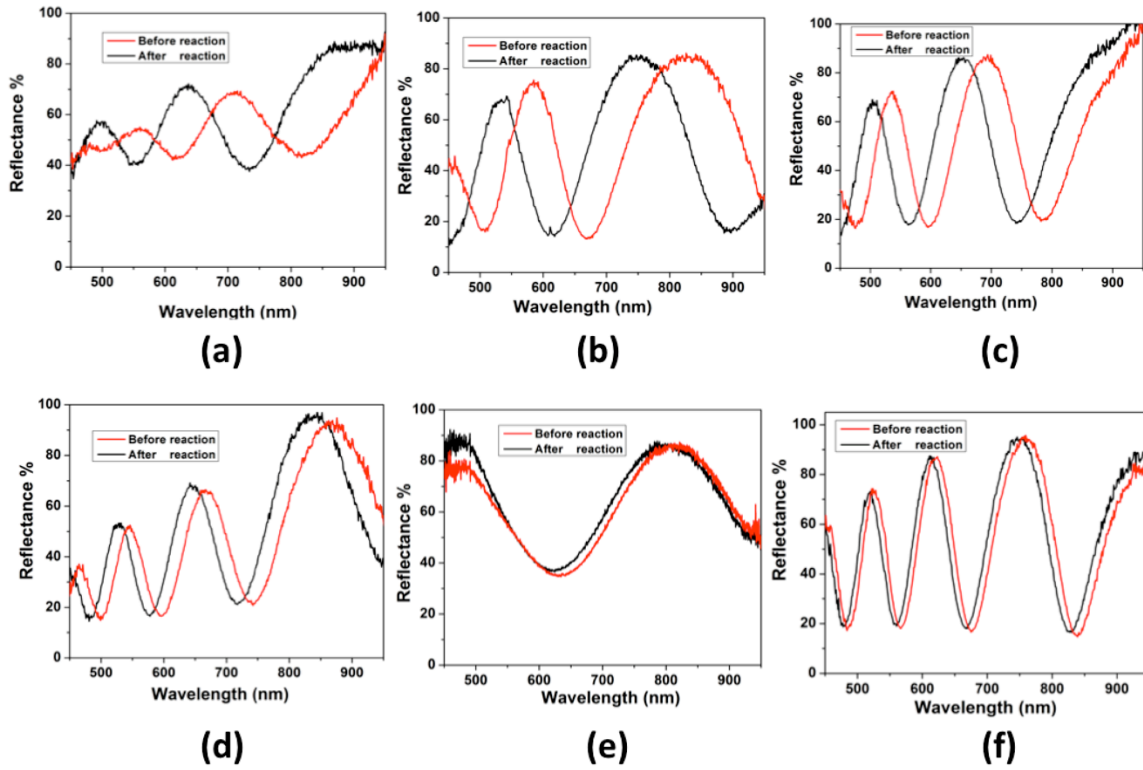
Figure 3.6 Reflectance spectra of the etalon before and after reacting with AP-goat anti-mouse IgG separated from (a) Tube No.1 (1.1 nM), (b) Tube No.2 (2.2 nM), (c) Tube No.3 (3.3 nM), (d) Tube No.4 (4.4 nM), (e) Tube No.5 (5.5 nM), and (f) Tube No.6 (6.6 nM).
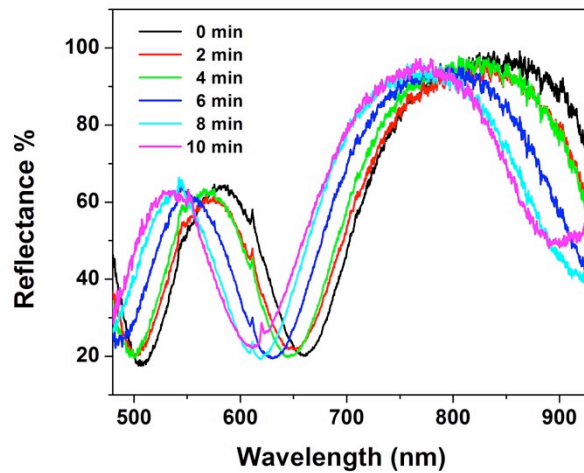
Figure 3.7 Peak shift of the etalon after reacting for different times with AP-goat anti-mouse IgG, which was separated from reacting with 0.1 μg of mouse IgG.

A proposed mechanism for the observed phenomenon is that the excess AP-GAM catalyzes the degradation of the phosphate containing polymer layer on top of the etalon, which releases negatively charged phosphate moieties. These negative phosphate moieties are capable of penetrating the etalon's microgel layer and interacting with the positively charged APMAH cations on the microgels. Before this interaction, the pNIPAm-co-APMAH microgels are positively charged, and the positive charges tend to repel one another, which causes the microgel to exist in a swollen state. The accumulation of the negative phosphate ions around/inside the microgels will neutralize the APMAH cations and cause the pNIPAm-co-APMAH microgel to deswell.

As can be seen from the reflectance spectra, a blue shift is observed, supporting the proposed mechanism. To further validate the proposed mechanism, I mixed 200 mL of the phosphate polymer solution with 20 mL PBS buffer and added 10 mL of the AP-GAM solution. As shown in Figure 3.3, the phosphate groups are part of the polymer network and are not charged fully in the polymer because the oxygen atom within the phosphate group is bound covalently to the carbon atom. After reacting with AP-GAM, the phosphate molecules with negative charges, such as monosodium phosphate and disodium phosphate, were released from the polymer network; this should result in an increase in the conductivity of the solution. After reacting for 30 min at 37 °C, I characterized the conductivity change of the solution. Before reaction the conductivity of the solution was 29.14 mS/cm (containing AP-GAM), after reaction, the conductivity

increased to 30.20 mS/cm. This is evidence supporting our hypothesized mechanism above.

The selectivity of the assay also was determined by exposing AP-GAM and GAM@M to various amounts of rabbit IgG. Using the same approach as above for detecting mouse IgG, I isolated the remaining, unbound AP-GAM and used it to react with the etalon. As can be seen in Figure 3.8, there is almost no response of the system to rabbit IgG, proving that the assay is specific for the mouse IgG. Next, I showed that mouse IgG could be quantified in the presence of rabbit IgG. As can be seen in Figure 3.8, the quantification of mouse IgG is unaffected by the presence of rabbit IgG, suggesting that this assay can be a robust method for quantifying proteins in the presence of interfering species. Finally, to determine if the buffer for AP-GAM alone affects the response of the etalon, I added 2 mL of the buffer for AP-GAM to a PBS buffer stabilized etalon; no peak shift was observed (Figure 3.9).
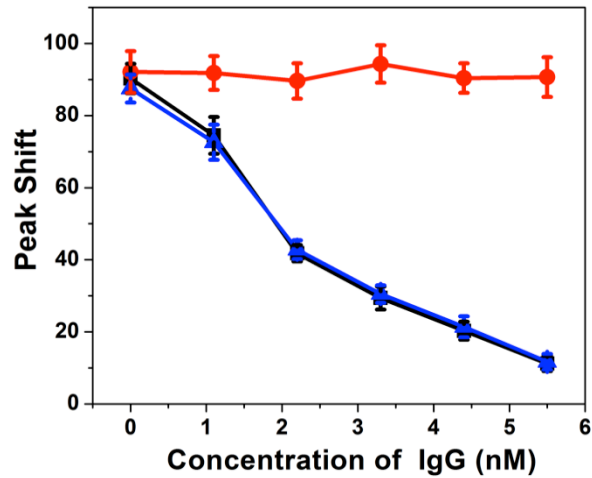
Figure 3.8 Peak shift of the reflectance spectrum from the etalon as a function of IgG concentration (■ for mouse IgG, ● for rabbit IgG, and ▲ for mouse IgG in the presence of rabbit IgG). Each data point is the average obtained from three individual experiments, and the error bars are the standard deviations of the measured values.
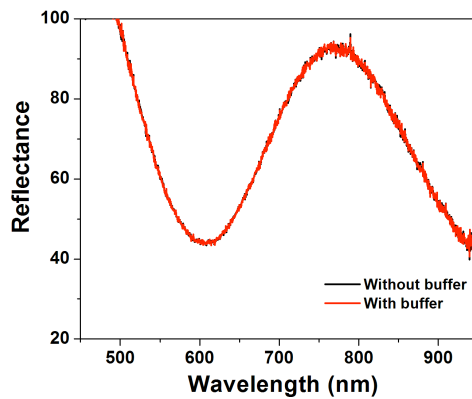
Figure 3.9 Reflectance spectra of the etalon before and after reacting with buffer in AP-goat anti-mouse IgG.

3.4 Conclusions

In summary, a novel immunoassay was developed that utilized the cleavage of a polymer coated on the surface of a responsive polymer-based etalon to result in a change in its optical properties; the change in optical properties could be related to the amount of

specific IgG in solution. It was shown that the approach is specific and can be effective in the presence of other interfering biomolecules in solution. This particular assay is simple and straightforward to carry out, and all the components are inexpensive, making this an assay that could find real world applications. While the devices here are specific to mouse IgG, the approach can be modified simply to detect other antigens and biomolecules of interest, eventually leading to the detection of whole bacteria via antibody binding to specific biomolecules on the surface of bacteria and pathogens.

Chapter 4

Near-Infrared Responsive Etalon for Enhanced Drug Delivery

4.1 Introduction

Some controlled release drugs are available on the market, but many conventional oral drugs usually do not provide rate-controlled release. In many cases, conventional drug delivery gives a sharp increase of drug concentration at potentially toxic levels in a short time, followed by a period at the therapeutic level; eventually, the drug concentration drops off to such a level that it does not function. To solve this problem, new methods of drug delivery have been developed, e.g., coating conventional drugs with rate-controlling polymer membranes[110] or integrating drugs into polymers/polymer spheres.[111] Bio-degradable/bio-friendly polymer membranes and polymer/polymer spheres play an important role in the study of controlled release drugs because they can be consumed by the body, and patients need not worry about the removal of the matrix for these drugs from their body. [112-114]

The polymer matrices used for triggered drugs release are responsive to environmental changes, such as pH and temperature, or can be disrupted by external stimuli.[115-117] When the controlled release drug systems are exposed to external stimuli, they will release the drug in a pre-dertermined way. There has been a growing interest in

light-responsive drug release systems that can be triggered by exposure to specific wavelengths of light.[118-119] It is conceivable that if the release of the encapsulated agent is triggered by light, the location of release can be determined by the applied irradiation. For example, the polymeric matrix could load anticancer drugs and release them upon light exposure. Since the light trigger could be switched between "on" and "off", it is easy to control the drug release; this is an advantage compared with other stimuli-responsive drug release systems.

Since the early nineties, there has been a tremendous amount of interest in the study of nanoscale materials because of their numerous interesting properties[120-123] that can lead to myriad applications, e.g., drug delivery, sensing, and biosensing.[124-126] A variety of nanomaterials have been developed due to the various applications envisaged for them, such as zero-dimensional nanoparticles, one-dimensional nanotubes, nanorods, nanowires and two-dimensional nanosheets.[127-129] For example, carbon nanotubes (CNTs) are capable of absorbing near-infrared radiation (NIR) and can then relax by generating localized heat.[130] NIR light is capable of penetrating into tissue and has many *in vivo* applications. This property has been studied widely and applied in the field of cancer therapy and drug delivery.[131-133]

Thermally responsive polymers, such as poly (N-isopropylacrylamide) (pNIPAm), have a wide range of applications in medicine and biotechnology.[134-135] Attributed to an alternation in the hydrogen-bonding interactions of the amide group in pNIPAm

monomer units with water, pNIPAm has a lower critical solution temperature (LCST), around 32 °C, i.e., pNIPAm becomes insoluble above this temperature and transits from an extended random coil to a collapsed globule.[14] The Serpe Group advanced a novel optical device (etalon), which can be fabricated by sandwiching a layer of pNIPAm-based microgels between two semi-transparent Au or other metal layers.[103] The structure for the etalon is shown in Figure 4.1. Briefly, etalons are made by painting a concentrated solution of pNIPAm-based microgels on a metal-coated (in our case Au-coated) glass substrate, followed by washing away the excess microgels that are not directly attached to the Au. Then, the etalon is soaked in water and further rinsed before deposition of another Au layer on top. The etalon shows visible color and has unique multipeak reflectance spectra. The position and peak order can be predicted by Eq. (1):

$$\lambda m = 2nd \cos\theta \qquad (1)$$

where the specific wavelength maximum of the peak (λ) depends on the peak order (m), refractive index of the dielectric (n), the spacing between the mirrors (d), and the angle of incidence(θ). Therefore, the size of the microgels is related closely to the wavelength shift of the reflectance peak.

Figure 4.1 The structure of a pNIPAm microgel based etalon, which consists of two 15-nm Au mirrors (a,c), with a 2-nm Cr adhesion layer. The mirrors sandwich a jammed layer of microgels (b) (dielectric) built on a rigid glass substrate (d).

Etalons have found numerous applications in our group. [49, 104, 106, 136-137] In this chapter I show that etalons can be modified with carbon nanotubes and triggered to release small molecules ("drug") by exposure to NIR light.

4. 2 Experimental Section

4.2.1 Materials

N-isopropylacrylamide (NIPAm) was purchased from TCI (Portland, Oregon) and purified by recrystallization from hexanes (ACS reagent grade, EMD, Gibbstown, NJ) prior to use. Multi-walled carbon nanotubes (with an average diameter of 9.5 nm), N, N-methylenebisacrylamide (BIS) (99%), acrylic acid (AAc) (99%), and ammonium persufate (APS) (98+%) were obtained from Aldrich (St. Louis, MO) and were used as received. Note that always wear gloves when working with carbon nanotubes. Sodium chloride was obtained from EMD (Millipore, Billerica, MA). All deionized (DI) water was filtered to have a resistivity of 18.2 M cm and was obtained from a Milli-Q Plus system from Millipore (Billerica, MA). Fisher's finest glass coverslips were 25 × 25 mm and obtained from Fisher Scientific (Ottawa, Ontario). Cr was 99.999% and obtained from ESPI as flakes (Ashland, OR), while Au was 99.99% and obtained from MRCS Canada (Edmonton, AB).

4.2.2 Instruments

Cr/Au annealing was done in a Thermolyne muffle furnace from ThermoFisher Scientific (Ottawa, Ontario). Reflectance spectra were collected using a USB2000+ spectrophotometer, a HL-2000-FHSA tungsten light source, and a R400-7-VIS-NIR optical fiber reflectance probe all from Ocean Optics (Dunedin, FL). The spectra were recorded using Ocean Optics Spectra Suite Spectroscopy Software over a wavelength range of 350−1025 nm. An IR laser (808 nm, 2W, beam divergence ＜5 mrad was used as the light source. Transition electronic microscopy (TEM) images were taken with a JEOL transmission electronic microscope (JEM 2100 USA). A scanning electron microscope (JSM-6010LA, JEOL, Peabody, MA) was used to image the microgels.

4.2.3 Synthesis of Microgels

Microgels composed of poly (N-isopropylacrylamide)-co-acrylic acid (pNIPAm-co-AAc) were synthesized via free radical precipitation polymerization, as described previously. [103] Briefly, a 3-necked round-bottom flask was fitted with a reflux condenser, nitrogen inlet, and temperature probe, and charged with a solution of NIPAm (11.9 mmol) and BIS (0.703 mmol) in 99 mL of DI water, previously filtered through a 0.2-μm filter. The solution was bubbled with N_2 gas and allowed to heat to 70 ℃ over 1 h. Then, AAc (1.43 mmol) was added to the heated reaction mixture in one aliquot and the reaction was initiated with a solution of APS (0.2 mmol) in 1 mL of DI water. The reaction was allowed to proceed at 70 °C for 4 h under a blanket of nitrogen. The resulting suspension

was allowed to cool overnight and then was filtered through a Whatman #1 paper filter to remove any large aggregates. Next, the microgel solution was distributed into centrifuge tubes and purified via centrifugation at 8300 rcf to form a pellet, followed by removal of the supernatant and resuspension with DI water; this was repeated six times. The cleaned microgels were recombined and stored in a brown glass jar. The pNIPAm microgel was synthesized in a similar procedure, without addition of AAc. The average diameter for the synthesized pNIPAm-co-AAc microgel was 752 ± 11 nm and for the pNIPAm microgel 902 ± 23 nm, determined by Dynamic Light Scattering (DLS).

4.2.4 Fabrication of Etalons

The details of the "painting" technique used to fabricate microgel-based etalons for these experiments have been reported elsewhere.[103] Briefly, 25 × 25 mm precleaned glass coverslips were immersed in piranha solution (H_2SO_4 : 30% H_2O_2 = 3:1) for 3 h, rinsed with deionized water, and dried with N_2 gas. Next, 2 nm of Cr, followed by 15 nm of Au were thermally evaporated onto them at a rate of ~0.2 and ~0.1 Å s^{-1}, respectively, using a Torr International Inc. model THEUPG thermal evaporation system (New Windsor, NY). The Cr acts as an adhesion layer to hold the Au layer on the glass. The Au coated substrates were annealed at 250 °C for 3 h in a chamber without any deoxigen treatment and then cooled to room temperature prior to use. An aliquot of about 12 mL of previously purified microgel solution was centrifuged for 30 min at 23 °C at 8500 relative centrifugal force (rcf) to pack the microgels into a pellet at the bottom of the tube. After

removal of the supernatant solution, the microgel pellet was vortexed and placed onto a hot plate at 30 °C. A previously coated Cr/Au substrate was rinsed with ethanol, dried with N_2, and then placed onto the hot plate (Corning, NY) set to 30 °C.

A 40 μL aliquot of the concentrated microgels was put onto the substrate and spread toward each edge using the side of a micropipet tip. The film was rotated 90°, and the microgel solution was spread again. The spreading and rotation continued until the microgel solution became too viscous to spread due to drying. The microgel solution was allowed to dry completely on the substrate for 2 h with the hot plate temperature set to 35 °C. After 2 h, the dry film was rinsed copiously with DI water to remove any excess microgels not bound directly to the Au. Then, the film was placed into a DI water bath and allowed to incubate overnight on a hot plate set to 30 °C. Following this step, the substrate was rinsed again with DI water to remove any remaining microgels not bound directly to the Au substrate surface. After this rinsing step, the film was dried with N_2 gas, placed into the metal evaporator, and an additional 2 nm Cr, followed by a 15-nm Au layer were deposited onto the microgel layer; the Au layer on top of the microgel is referred to as the Au overlayer.

The device was soaked in DI water overnight on a hot plate at 30 °C, rinsed with DI water, and dried with N_2. Different volumes of a suspension of carboxylic acid modified carbon nanotubes (CNTs-COOH) was drop cast onto the glass side of the etalon, allowed to dry, and subsequently rinsed with water, dried with N_2, and used for the experiments.

It is believed that the interaction between the hydroxyl group on the glass slide and the carboxylic acid group in the carbon nanotubes helps the deposition of carbon nanotubes onto the glass slide.

4.2.5 NIR Sensing

The CNTs were dispersed in pure ethanol at a concentration of 1 mg/mL. The suspension was found to be stable for at least 15 days, i.e., no obvious precipitation was detected at the bottom. To modify the etalon with CNTs, 500 μL (0.5 g) and a 1-mL (1 g) CNTs suspension were drop cast onto the other side of the etalon that had been pretreated with pNIPAm-co-AAc microgel, and the etalon was allowed to dry at ambient temperature. Following rinsing with DI water, I could see that no CNTs had leaked from the etalon. The etalon was placed in a plastic Petri dish, and 1 mL of deionized water was added onto the top of the etalon to saturate the microgel and stabilize the etalon. The IR source was placed 1 cm behind the Petri dish, and the optical probe was placed at the corner of the etalon and used to detect the reflectance of the etalon (shown in Figure 4.2).
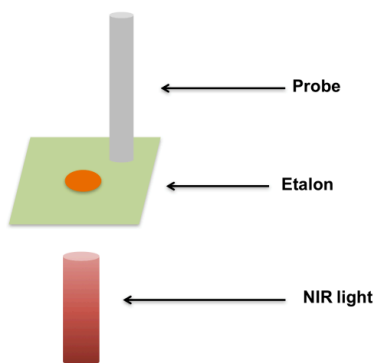
Figure 4.2 Schematic diagram of the setup for NIR-response of a CNTs-COOH modified etalon.

4.2.6 Drug Delivery

As shown in Scheme 1, a layer of 2 nm of Cr and 15 nm of Au were deposited onto piranha solution treated glass. Then, a monolayer of pNIPAm-co-AAc microgel was coated onto the surface of the Au (see details in 4.2.4). After deposition of the pNIPAm-co-AAc microgel, the slide was immersed in a 1-mg/mL crystal violet solution for 12 h. Next, the slide was rinsed with DI water to remove the unbound crystal violet, followed by deposition of a layer of Cr (2 nm) and another layer of Au (50 nm). The sides of the slide were sealed with nail polish to prevent the release of crystal violet from the sides, therefore, all crystal violet molecules will be released from small pores on the top Au layer. The sealed slide was placed in a plastic petri dish, immersed in 20 mL DI water, and put on top of the NIR source. A circulating pump system and UV-vis spectrometry were used to collect and detect the absorbance of the solution.
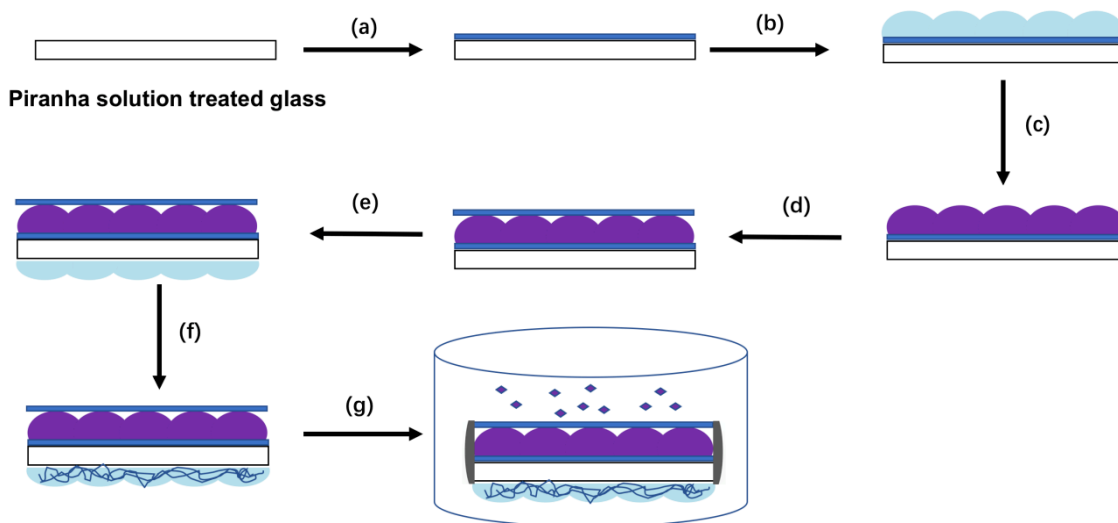
Scheme 4.1 Schematic flow chart of how the etalon was made for drug release: (a) deposition of bottom Cr/Au; (b) coated with pNIPAm-co-AAc microgel; (c) loaded with crystal violet in DI water; (d) deposition of the top Cr/Au layer; (e) coated with pNIPAm-co-AAc microgel on the back side of the glass slide; (f) deposition of CNT-COOH; (g) drug release when exposed to NIR light.

4. 3 Results and Discussion

4.3.1 Synthesis and Characterization

The TEM images and DLS data indicate that the synthesized pNIPAm-co-AAc and pNIPAm microgels are uniform in size and shape. Poly (N-isopropylacrylamide)-co-acrylic acid can assemble well on the piranha solution treated glass slides (Figure 4.3(a)). Inserted at the right corner on Figure 4.3(a) is a picture of the glass slide deposited with pNIPAm-co-AAc. Figure 4.3(b) shows the TEM image of the poly (N-isopropylacrylamide) microgel. A typical fiber-like structure of the CNT-COOH can be seen in the TEM images on Figure 4.3(c). The CNT-COOH sticks with pNIPAm-co-AAc microgel on the glass slide. To mimic the interaction between

CNT-COOH and the pNIPAm-co-AAc microgel, I modified the copper grid with a pNIPAm-co-AAc microgel (the same way I did for making etalons, discussed in 4.2.4) and then drop cast 10 µL of a CNTs-COOH suspension on top of it. After it dried at ambient temperature, I rinsed the copper grid with deionized water and found that the CNT-COOH did not leach from the copper grid by the naked eye. From the TEM image (Figure 4.3(d)), we can see clearly that the CNT-COOH binds with pNIPAm-co-AAc microgel. Inserted on the top right corner of Figure 4.3(d) is a photo of a glass slide modified with microgel and later carbon nanotubes.
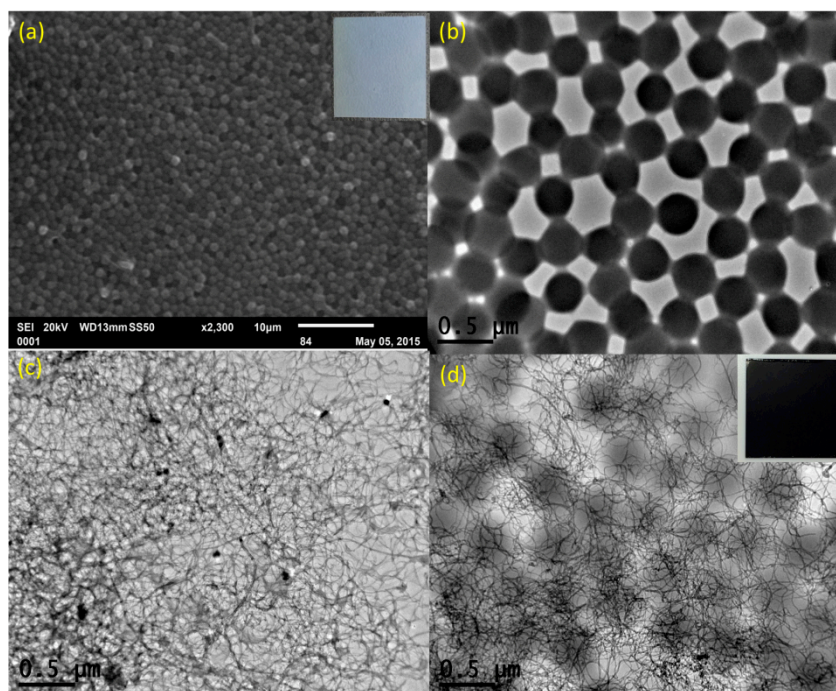
Figure 4.3 (a) SEM image of the glass slide deposited with pNIPAm-co-AAc microgel; (b) TEM images of the pNIPAm-co-AAc microgel; (c) TEM images of the carbon nanotubes and (d) pNIPAm-co-AAc microgel after being soaked in carbon nanotube solution.

4.3.2 NIR Response

It is well known that carbon nanotubes generate heat when exposed to NIR. When modified with carbon nanotubes, the etalons show obvious IR response by changing their color, therefore, an optical probe was used to track the color change of etalons. Figure 4.4 shows the reflectance spectra obtained for etalons deposited with 0.5 mg carbon nanotubes (0.5 mL *1mg/mL). As the radiation time increases, the reflectance peak shows a blue shift. This phenomenon became more obvious when the etalon was modified with 1 mg carbon nanotubes (1 mL * 1mg/mL), i.e., in a given radiation time, the peak shift is larger for the etalon modified with 1 mg carbon nanotubes than with 0.5 mg carbon nanotubes. As a control, the etalon without any modification shows a very slight change in response to IR. It is reasonable that 1 mg carbon nanotubes on the etalon generates more heat than 0.5 mg carbon nanotubes, which causes the localized microgel to collapse to a larger extent. Thus, a larger peak shift is observed. Figure 4.5 indicates the peak shift for different kinds of etalons. As a control experiment, I investigated how the IR radiation affects etalons without modification with CNTs. Figure 4.6 clearly shows that, compared with etalons modified with CNTs, no obvious peak shift from the etalon with no CNTs is observed.
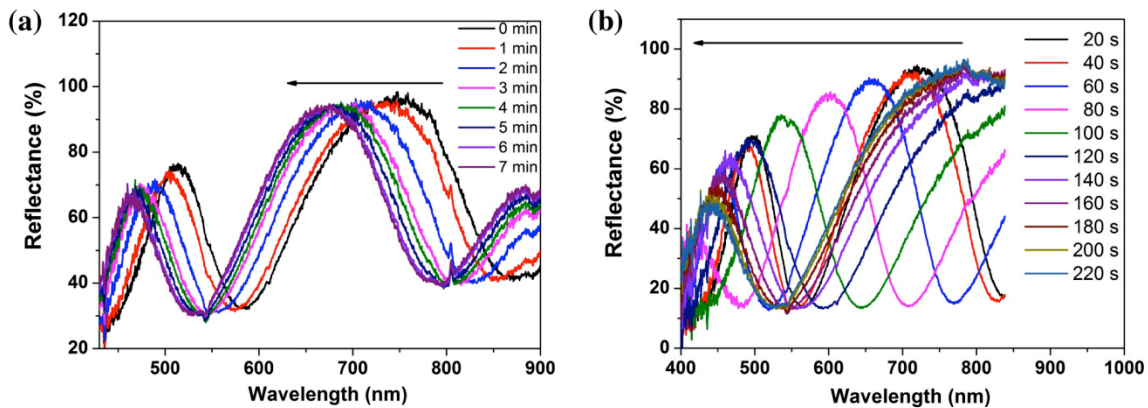
Figure 4.4 Reflectance spectra for an etalon modified with a different mass of carbon nanotubes (a, 0.5 mg; b, 1 mg) when exposed to NIR for different times.
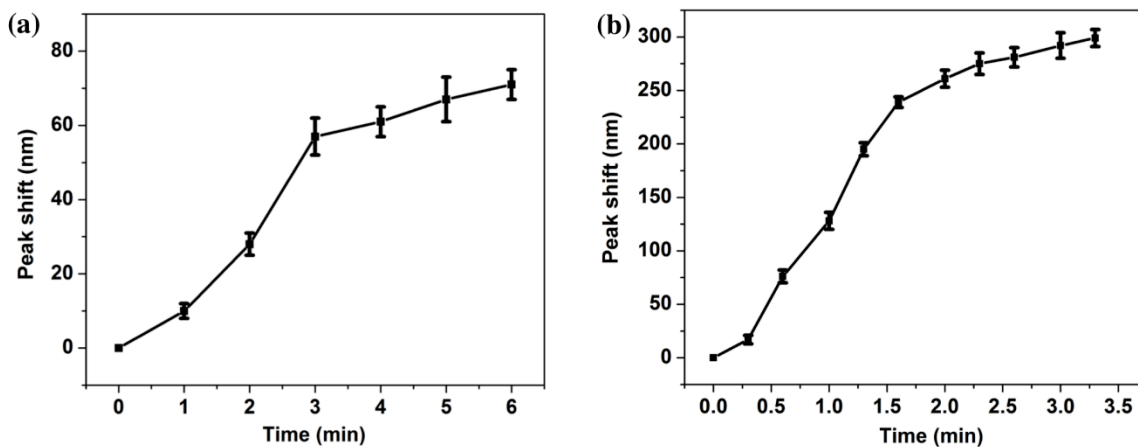
Figure 4.5 Maximum peak shift of reflectance for an etalon modified with a different mass of carbon nanotubes (a, 0.5 mg; b, 1 mg) when exposed to NIR for different times.
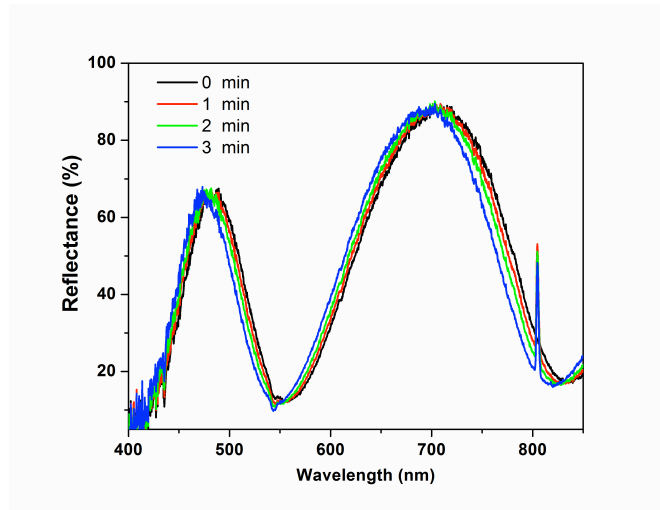
Figure 4.6 Reflectance spectra for an etalon without modification with carbon nanotubes with NIR on for different times.

As shown in Figure 4.7, the etalon itself responds significantly to temperature. When the temperature increases, the pNIPAm-based microgel shrinks in DI water. According to Eq. (1), when d decreases, λ will decrease, thus a blue-shift of the spectrum is observed. This explains why the CNT-modified etalon responds to NIR. The CNTs generate localized heat when exposed to NIR, and the heat will cause shrinking of localized microgels, resulting in a the peak shift in the spectrum. The more CNTs exposed to NIR, the more localized is the heat generated, and the bigger is the peak shift observed.
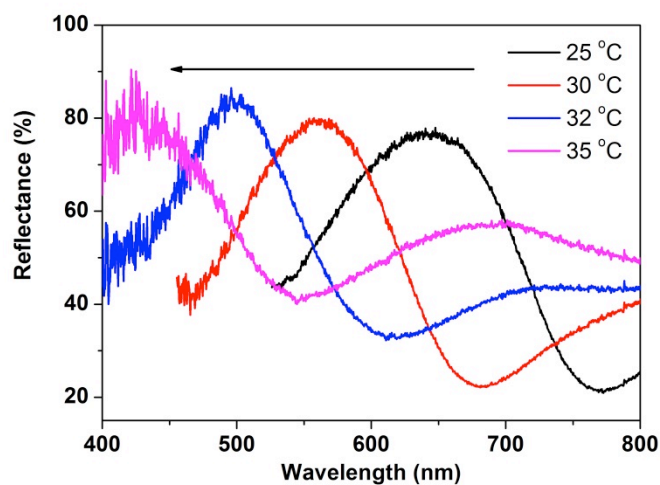
Figure 4.7 Reflectance spectra for an etalon modified with 0.5 mg of carbon nanotubes when exposed to different temperatures when placed in a chamber.

The thermal-responsive property of the etalon is due to the pNIPAm microgel sandwiched between metal layers. This can be confirmed by the UV-vis absorbance spectra of a pNIPAm microgel suspension. It is well-known that pNIPAm has a lower critical solution temperature (LCST) of around 32 °C, i.e., the pNIPAm chain disperses well in water below LCST and changes conformation above LCST. As can be seen from Figure 4.8, the pNIPAm microgel swells in the suspension and lowers the transmittance of the solution. This further confirms why the etalon responded to NIR, while the solution put on top of the etalon did not change temperature significantly.
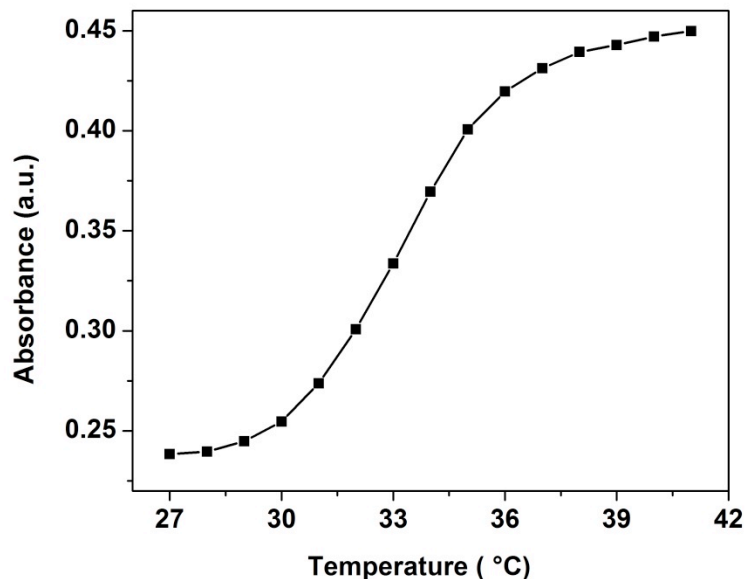
Figure 4.8 Absorbance of a pNIPAm microgel suspension in water at various temperatures at 520 nm.

4.3.3 Drug Delivery

In many cases, we want to manipulate the drug delivery rate so that patients get proper doses. For example, when a patient needs a higher dose, it would be so convenient if the patient can just easily do it with no professional training required.

The NIR response of the CNTs-modified etalon can be applied to enhanced drug delivery. We used crystal violet as a model drug and loaded it into a pNIPAm-co-AAc microgel deposited on the bottom of an Au layer.[25] By increasing the amount of CNT deposited onto the etalon, an enhanced drug delivery is observed (Figure 4.9). This is attributed to the localized heat generated by the CNTs when exposed to NIR. The top Au layer in the etalon is porous. When heat is generated, crystal violet is released easier from the microgel and finally easier from the etalon. The more CNTs exposed to NIR, the

59

more heat is generated, thus the faster is crystal violet released from the etalon. The tunability of the releasing rate of drugs makes the device promising in real applications.
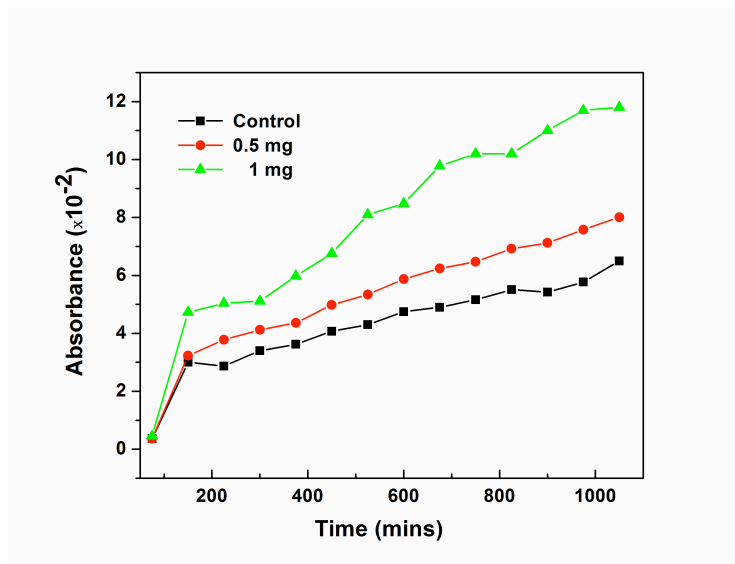
Figure 4.9 Crystal violet release profile for etalons modified with different masses of carbon nanotubes. Absorbance of the solution was collected by tracking at 590 nm wavelength with NIR on for different times.

4.4 Conclusions

In summary, a polymer-based NIR sensing etalon was fabricated. The etalon shows fast response toward NIR by changing its color, which was characterized by an optical probe. The etalon can be developed further for drug delivery. Introducing carbon nanotubes onto the etalon obviously can enhance the drug release from the etalon. The platform we developed can be applied for NIR enhanced drug delivery systems.

Chapter 5

Using Waste Chewing Gum to Treat Wastewater

5.1 Introduction

Industrial waste water has attracted much attention from both industry and academia, because of the potential harm waste water has on the environment and human health.[138-140] Most common contaminants in industrial waste water are organic dyes and heavy metal ions. In Alberta, Canada particularly, there is a lot of oil sands tailings water; this is a huge environmental problem.[141]

Organic dyes are used widely in various fields, such as textile, paper, rubber, leather, and pharmaceutical industries. Their discharge into water could cause severe environmental pollution because most of the used dyes are toxic, and some are considered carcinogenic for animals.[142-145]

Heavy metals, like Pb, Fe, Cu, and Cr, are mainly generated from mining and industrial waste, vehicle emissions, lead acid batteries, fertilizers, paints, treated woods, and aging water supply infrastructure. Heavy metals have high solubility in aquatic environments and hence can be absorbed by living organisms. Exposure to heavy metals can produce serious health issues like reduced development and growth, nervous system damage, organ damage, and cancer; in extreme cases, it may even lead to death.[146-148]

The oil sands in Alberta, Canada is one of the largest oil deposits in the world. With the ongoing expansion of the Canadian oil sands industry, there is an ever growing need for a sustainable supply of fresh water for mining operations.[141] The volume of water stored in impounded tailings currently exceeds 700 million m^3, which eventually will have to be disposed of. Tailings ponds water is composed of a mixture of salts, suspended solids, and other dissolvable chemical compounds, such as acids, benzene, hydrocarbons and residual bitumen. Dissolved solids are dominated by sodium bicarbonate (~500 to 700 mg/L), sodium chloride (~75 to 550mg/L), and sodium sulphate (~200 to 300mg/L). Organic compounds detected in tailings ponds water (TPW) include bitumen, naphthenic acids (NAs), asphaltenes, benzene, creosols, phenols, phthalates, polycyclic aromatic hydrocarbons (PAHs), and toluene. [149] Naphthenic acid is the primary source of toxicity in TPW, with lower molecular weight NAs being the primary contributors to mixture toxicity.[150]

The treatment of these industrial effluents is a top issue in environmental science and technology.[151] Recently, numerous approaches have been studied to increase the efficiency and reduce the cost of organic dye and heavy metal removal from wastewater and oil sands TPW treatment. Common organic dyes treatment methods include organic dyes adsorption,[152] electrochemical,[153] photocatalysis,[154] and fungal degradation.[155] Common heavy metal ion treatment methods include chemical precipitation [156], ion exchange,[157] adsorption,[158] membrane filtration,[159] flotation coagulation, and

flocculation.[160] Water treatment technologies are evolving rapidly to meet the needs of the oil industry, but the viability of these technologies is unclear. While it is true that dewatering technologies have proven successful, the reclamation of these large tailings ponds may depend on the detoxification of water in lakes and wetland, yet the viability of these processes is uncertain.[161] Also, most of these techniques involve expensive or bulky instruments, and some of them consume high energy like electricity. It would be highly desirable to find new techniques to treat industrial waste water in an easier, more versatile, and cost effective way.

It is estimated that the total cost of cleaning chewing gum streets is estimated at £10 million (17.2 Canadian dollars) in London alone. Even when disposed of in bins, chewing gum ends up in landfill where it never biodegrades. A piece of chewing gum may not seem like a great deal of trash, but if one considers that around the world people chew 100,000 tons of gum every year, it starts to add up[162]. It would be a great idea if we could make use of this waste gum; it would help reduce the release of gum to the environment and generate a huge economic effect in this field.

In this chapter, I use waste chewing gum to adsorb organic dyes and heavy metal ions and to decrease the toxicity of oil sands TPW with waste gum treatment. I believe this work will shine light on how to make full use of the waste chewing gum to solve environmental issues in the future.

5.2 Experimental Section

5.2.1 Materials and Instruments

Excel Peppermint chewing gum (gum 1), Trident Peppermint chewing gum (gum 2), and Dubble Bubble Crybaby Sour Gumballs (gum3) were bought from the market. Rhodamine B, methylene blue, crystal violet, activated charcoal powder, flash silica, and sand were purchased from Sigma Aldrich (Oakville, Ontario) and used without further purification. Filters with a pore size of 0.2 μm were purchased from Fisher Scientific. Salts used for preparing different metal ions are $FeCl_3$ (Sigma Aldrich, Germany), $CuSO_4 \cdot 5H_2O$ (Sigma Aldrich, Japan), $AgNO_3$ (Sigma Aldrich, Ontario), $Hg(NO_3)_2 \cdot H_2O$ (J.I. Baker Chemical Co. Phillipsburg, N.J.), $Cd(NO_3)_2$ (Anachemia Canada Inc., Montreal), $Pb(NO_3)_2$ (Anachemia Canada Inc., Montreal), and $Zn(NO_3)_2$ (Anachemia Canada Inc., Montreal). Hydrogen chloride and sodium hydroxide were obtained from Fisher Scientific (Ottawa, Ontario), 95% ethanol, and 99.9% Toluene was purchased from Sigma-Aldrich (St. Louis, Missouri) and was used as received. Deionized water (DI) water was filtered to have a resistivity of 18.2 MΩ-cm by a Milli-Q Plus system (Millipore Co.).

A Shimadzu TOC-V CHS/CSN Model Total Organic Carbon Analyzer was used to determine non-purgeable organic carbon (NPOC). NPOC Total organic carbon (TOC) was measured as NPOC in water. NPOC was measured by acidifying an aliquot of water sample and then sparking the sample to remove any purgeable organic and inorganic

carbon. Then, the sample was injected onto a strip of platinum catalyst within a combustion chamber at 720 ^{o}C. Due to the redox reaction, CO_2 evolved and was detected by non-dispersive infrared (NDIR) detector for carbon.

An Agilent 8453 UV−vis spectrophotometer was used to collect absorbance spectra for dyes. Perkin Elmer ICP-OES was used to evaluate heavy metals in the water. A 25-mm Syringe Filter w/ 0.2 μm Nylon Membrane made by VWR International in USA was used.

5.2.2 Separate Polymers from Chewing Gum

All chewing gum was chewed for more than 30 min as received from stores. The gum was washed with toluene, ethanol, and water, and this was carried out another three times to remove any soluble matters. The solid product was separated from the gum/solvent mixture by centrifugation. After being washed, the solid products were dried in a vacuum overnight.

5.2.3 Chewing Gum Used for Organic Dye Removal

5.2.3.1 Gum for Crystal Violet Removal at Different pH Solutions

Solutions with pH 3, pH 7 and pH 11 were prepared by adjusting the distilled water with either 1 M HCl or 1 M NaOH solutions. Solid gum (0, 60, 120, 180, 240, and 300 mg) was dispersed in individual 10-mL centrifuge tubes containing an 8-mL solution of different pHs. Then, 100 μL of 4 g/L crystal violet solution was added to the gum

dispersion prepared above. After being shaken for 20 min, the solid gum powder was separated by centrifugation, and the absorbance of the supernatant was detected.

5.2.3.2 Maximum Adsorption of Different Dyes by 100 mg of Gum

(a) Crystal violet: 100 mg of solid gum powder was dispersed in 5 mL distilled water in a 10-mL centrifuge tube. Then, 15 µL of 4 g/L crystal violet solution was added to the gum dispersion prepared above. After being shaken for 20 min, the solid gum was separated by centrifugation, and the absorbance of the supernatant was measured.

(b) Rhodamine B: 100 mg of solid gum powder was dispersed in 5 mL distilled water in a 10-mL centrifuge tube. Then, 1 mL of 100 mg/L rhodamine B solution was added to the gum dispersion prepared above. After being shaken for 20 min, the solid gum was separated by centrifugation, and the absorbance of the supernatant was measured.

(c) Methylene blue: 100 mg of solid gum was dispersed in 5 mL distilled water in a 10-mL centrifuge tube. Then, 2 mL of 20 mg/L methylene blue solution was added to the gum dispersion prepared above. After being shaken for 20 min, the solid gum powder was separated by centrifugation, and the absorbance of the supernatant was measured.

5.2.3.3 Regeneration of Chewing Gum

Gum loaded with dyes was immersed in 3 mL of ethanol (95%) and was shaken for 10 min. Then, the solid gum was then separated by centrifugation. These two steps were carried out another two times.

5.2.3.4 Calculation of the Concentrations of Dye Solution

The concentrations of the samples were calculated using the Beer-Lambert law ($A = \varepsilon b c$), where A is the absorbance, ε is the molar extinction coefficient, b is the thickness of the sample in cm, and c is the concentration of the sample. For a specific dye solution, A is proportional to c in a certain range. By comparing the absorbance of an unknown sample with that of a sample of known concentration, we can obtain the concentration of the unknown sample.

5.2.4 Chewing Gum used for Heavy Metal Ion Removal

A solution of each heavy metal solution with a concentration of 50 ppm was prepared. A 10-ml sample of the solution was taken in a 15-mL centrifuge tube, and 0.1 g of gum powder was put in the tube and shaken for 1 h. After 1 h, the supernatant was decanted to a separate test tube after centrifuging and was analyzed by ICP-OES for the heavy metal presence. The concentration was obtained by making a standard calibration curve with heavy metal ions of different concentrations.

5.2.5 Chewing Gum Used for Oil Sand TPW Treatment

5.2.5.1 Column Filtration of TPW

For this study, four column preparations were evaluated, as shown schematically in Figure 5.1. Table 5.1 lists the composition of the columns used to filter TPW; 100 mL of TPW was filtered through each of these columns.
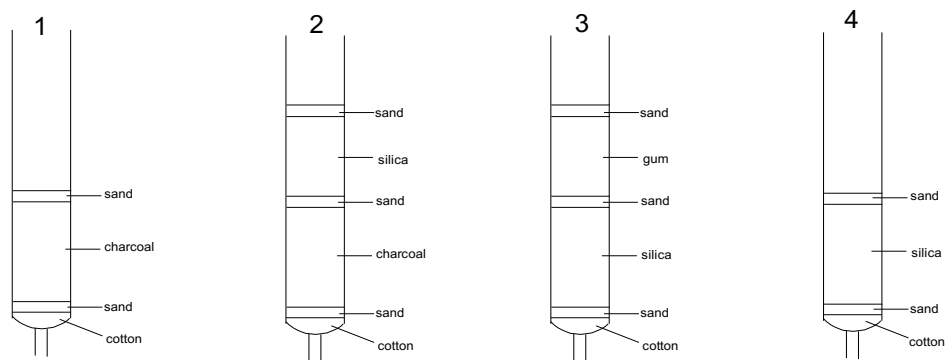
Figure 5.1 Composition of the columns used to filter TPW.

Table 5.1 Composition of the columns used to filter TPW; 100 mL of TPW was filtered through each of these columns and separated into two 50-mL samples. The first 50-mL sample was not used as it was contaminated by DI water that was used to pack the columns.

Column 1	Column 2	Column 3	Column 4
Charcoal 5.14g ±0.01g	Charcoal 3.00g ±0.01g	Silica 3.01g ±0.01g	Silica 7.47g ±0.01g
	Silica 3.01g ±0.01g	Gum 1.51g ±0.01g	

5.2.5.2 Toxicity Test

In vitro photothermal cytotoxicity of TPW and filtered TPW was measured by performing TPW assays on HeLa cells.[132] The cells were added into a 96-well cell culture plate at 5×10^4 per well. After that, TPW was added to each well, and the plates were incubated for 4 h at 30 $^{\circ}$C under 5% CO_2. After the 4 h incubation period, 10% sodium dodecyl sulfate was added (50 mL per well), and the assay plate was allowed to stand at room temperature for 12 h. The optical density (OD_{570}) value (Abs) of each well, with background subtraction at 690 nm, was measured by means of a Tecan Infinite M200 monochromator-based multifunction microplate reader. The toxicity of TPW was calculated based on the inhibition of cell growth with the following Eq 5.1:

$$\text{Cell viability} = (\text{mean OD}_{570} \text{ from sample/mean OD}_{570} \text{ from control}) * 100\% \qquad (5.1)$$

5.3 Results and Discussions

5.3.1 Chewing Gum used for Organic Dye Removal

Initially, I used crystal violet (CV) as a model dye; CV has a typical absorbance at 590 nm. As expected, when more gum is added into a certain amount of CV solution, more CV is removed from the solution, thus a lower absorbance is detected. Figure 5.2 shows the absorbance of the CV solution after reacting with different amounts of gum powder at pH 3 (solution diluted 10-fold for UV-Vis detection, same for pH 7 and pH 11). Similar results are found for pH 7 solutions (Figure 5.3). Note that CV is not stable at high pH solutions, but we can detect the decrease in absorbance by increasing the amount of gum (Figure 5.4). This indicates that the gum can be used to remove dyes in solutions with different pH values.
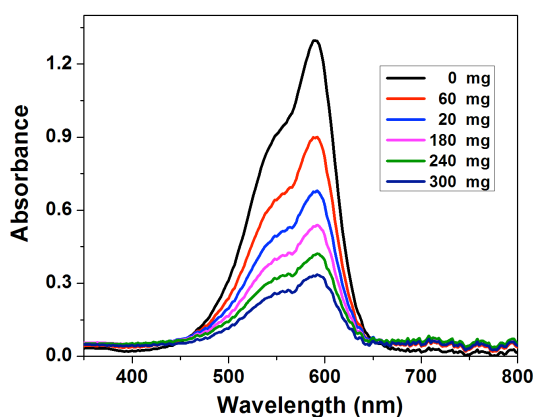
Figure 5.2. UV-vis spectra of crystal violet solution (pH 3) after reacting with different amounts of gum.
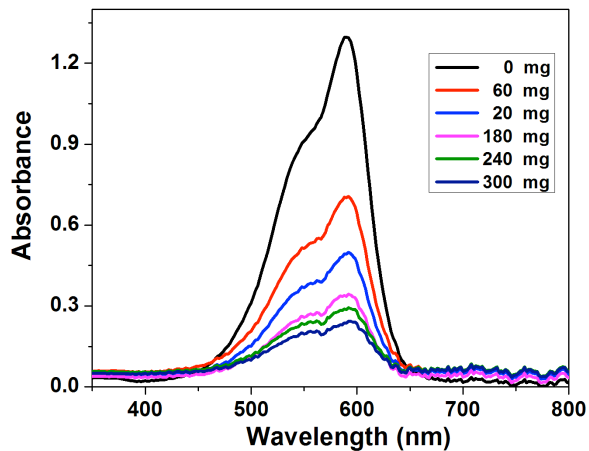
Figure 5.3 UV-vis spectra of crystal violet solution (pH 7) after reacting with different amounts of gum.
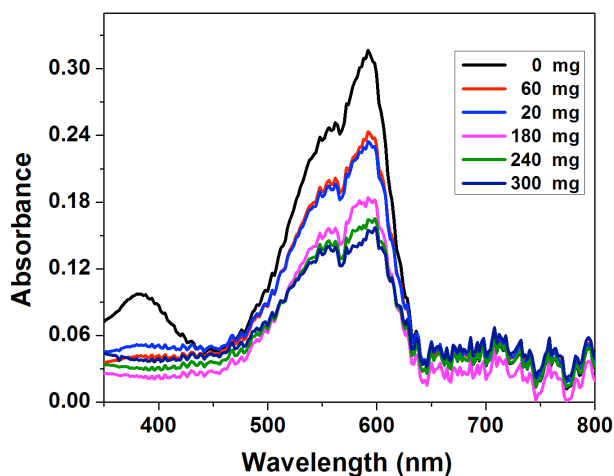
Figure 5.4 UV-vis spectra of crystal violet solution (pH 11) after reacting with different amounts of gum.

The adsorption rate of dyes by adsorbent play an important role in real applications. Faster adsorption allows for shorter reaction time and thus lowers energy consumption, such as electricity and water. I reacted the gum with CV for 2, 4, 6, 8, and 10 min. As can be seen in Figure 5.5, the absorbance stays almost constant after 2 min, showing that the

dye removal is really fast. This is of great importance when we use gum to remove organic dyes in practical application.
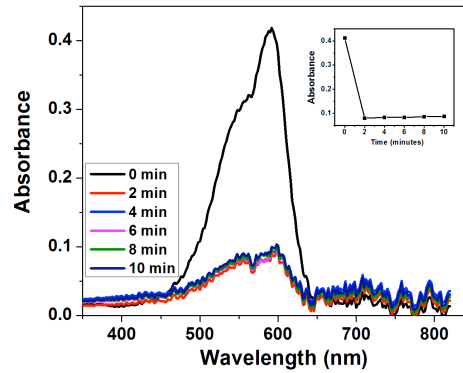
Figure 5.5 UV-vis spectra of crystal violet solutions after reacting with gum for a different time (inserted is the absorbance at 590 nm with a different reaction time).

Then, I modified a filter with a pore size of 0.2 μm by injecting a gum suspension into the filter so that gum powder was stuck in the filter, and I injected CV solutions through the modified filter. Interestingly, compared with the unmodified filters, the filtrate from the modified filter is colorless (Figure 5.6). This is because the gum can adsorb the dye really quickly and completely. Undoubtedly, this gave us an inspiration for the design of novel dye removal devices.
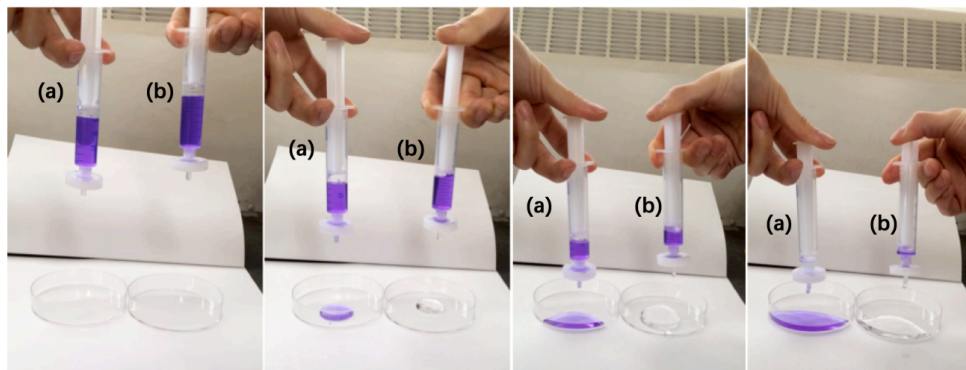
Figure 5.6 Unmodified (a) and modified (b) filters used for CV solution removal from the beginning to the end of the separation.

It is desirable that the gum can be reused so that I can decrease the cost for dye removal further. As shown in Figure 5.7, the pure gum suspension is white. After CV was added and allowed to react for a while, the solid gum was loaded with dye from the solution. The dye adsorbed was washed away from the gum with ethanol several times, and after washing, the gum precipitate became white again. No obvious absorbance at 590 nm was found from the UV-Vis spectrum for the supernatant, showing that there was a complete separation of dyes from gum. The regenerated gum can be used for dye removal in aqueous solution; details are shown later in this chapter.
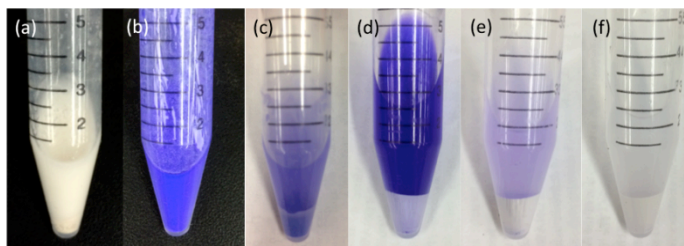
Figure 5.7 Photos of (a) gum powder suspension, (b) gum reacted with CV, (c) after precipitation of (b), (d) precipitate from (c) washed with ethanol, (e) precipitate from (d) further washed with ethanol, (f) precipitate from (e) further washed with ethanol.

Given that the gum works well for CV removal, I tried two other dyes, rhodamine B and methylene blue which both are commonly used in the lab research . I used 100 mg gum of three different brands to treat crystal violet, rhodamine B, and methylene blue solutions. All these gums can be used to adsorb the dyes, but the adsorbing capability differs between gums for various dyes. As can be seen from Table 5.2, Gum 3 works best for methylene blue, probably because of the strong interaction between methylene and

gum 3. This hypothesis is confirmed by the FT-IR peak at around 2520 cm^{-1} in FT-IR

spectra (Figure 5.8), which is attributed to C≡C or C≡N stretching. This bond is capable

of reacting with highly conjugated methylene blue backbone by π-π stacking. Overall,

these gum can be used to remove various dyes in aqueous solutions.

Table 5.2 Maximum mass of various dyes adsorbed by 100 mg of gums of different brands.

	Gum 1 (µg)	Gum 2 (µg)	Gum 3 (µg)
Crystal violet	50.85 ± 2.23	52.61 ± 2.56	56.33 ± 3.10
Rhodamine B	58.72 ± 1.71	22.25 ± 1.68	40.17 ± 1.94
Methylene blue	9.090 ± 0.47	17.45 ± 1.01	450.1 ± 12.97
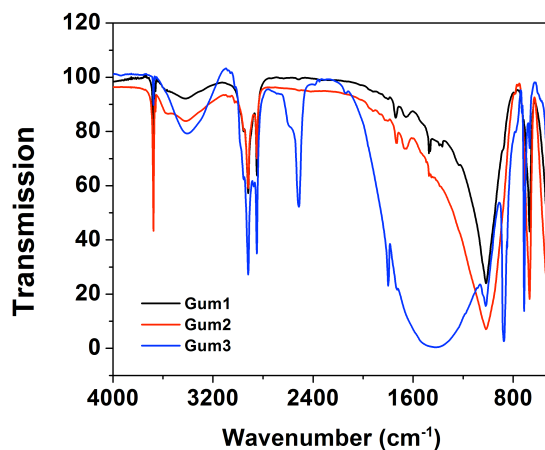
Figure 5.8 FT-IR spectra for gums of three different brands.

Finally, I performed the reusability of Gum 1 for dye removal. The removal

efficiency was defined by taking the amount of the dye absorbed to that of the dye added

at the beginning. As can be seen in Figure 5.9, after being used for four times, there is no

significant decrease in removal efficiency of the gum toward crystal violet and rhodamine B. A decrease of removal efficiency for methylene blue is found, probably because the methylene blue molecule binds with the gum more tightly. The gum loaded with methylene blue cannot be fully regenerated even in saturated salt sodium chloride solution, ruling out the possibility that methylene blue is adsorbed onto gum by electrostatic interaction. Being reusable is economically beneficial in considering using gum to remove dyes in practical applications.
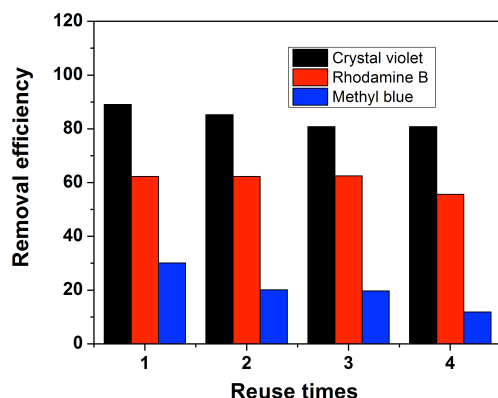
Figure 5.9 Dye removal efficiency with gum after being used multiple times.

5.3.2 Chewing Gum Used for Heavy Metal Ion Removal

As a proof of concept, I studied if gum (gum 1) powder could be used to remove heavy metal ions. There is usually more than one single heavy metal ion in wastewater, so various kinds of heavy metal ions were selected to react with gum powder. All the concentrations of heavy metal ion solutions used were 50 ppm. The concentrations of resulting solutions were different after reacting with the same amount of gum powder (Figure 5.10). This is because the capability of the gum powder binding with various ions

differs. As can be seen from Figure 5.10, the binding of a certain amount of gum powder

was a maximum with Pb^{2+}, followed by Fe^{3+}, Cu^{2+}, Zn^{2+}, Hg^{2+}, Ag^+, and Cd^{2+}.
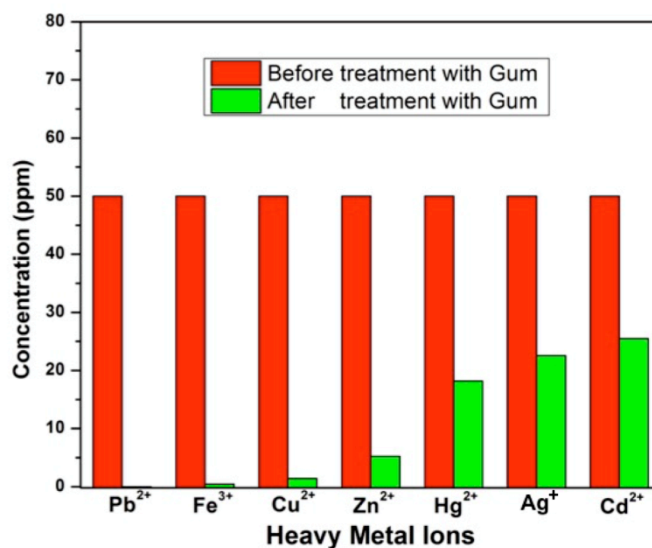
Figure 5.10 Concentrations of heavy metals in water before and after treatment with gum powder.

I was interested in finding out more about the interaction between metal ions and

gum powder. Taking Pb^{2+} and Fe^{3+} as examples, I studied how the feeding ratio affects

the binding event. Samples of 10, 20, 30, 40, 50, and 100 mg of gum powder were

reacted individually with 10 mL of $Pb(NO_3)_2$ and $Fe(NO_3)_3$ solutions (50 ppm). The

results in Figure 5.11 and Figure 5.12 show that 20 mg of gum powder is enough to

capture Pb^{2+} in the solution, while 10 mg of gum powder is enough to remove almost all

the Fe^{3+} in the solution.
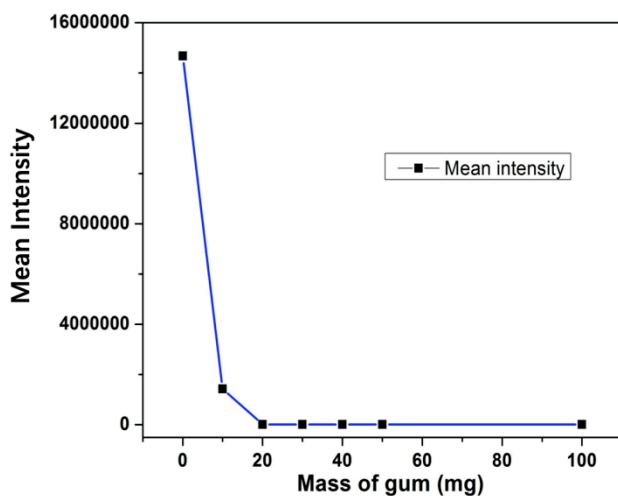
Figure 5.11 Graph of intensity of Pb^{2+} with increasing amount of gum when the solution was analyzed by ICP-OES after treatment with gum.
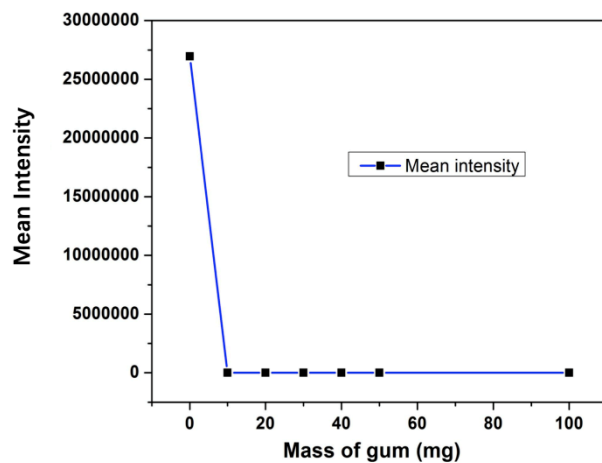
Figure 5.12 Graph of intensity of Fe^{3+} with increasing amount of gum when the solution was analyzed by ICP-OES after treatment with gum.

Then, I prepared a solution containing an unknown concentration of $Pb(NO_3)_2$, $Fe(NO_3)_3$, $CuSO_4 \cdot 5H_2O$, and $Hg(NO_3)_2 \cdot H_2O$ in order to mimic an industrial wastewater scenario. The solution was analyzed before and after treatment with 10 mg of gum powder to get the net intensity of each particular ion. We can see from Figure 5.13 that

the intensity of the metal ions decreases to different degrees. Note that the exact net

intensities do not make too much sense here; I just wanted to confirm that gum powder

works even in the existence of various ions.
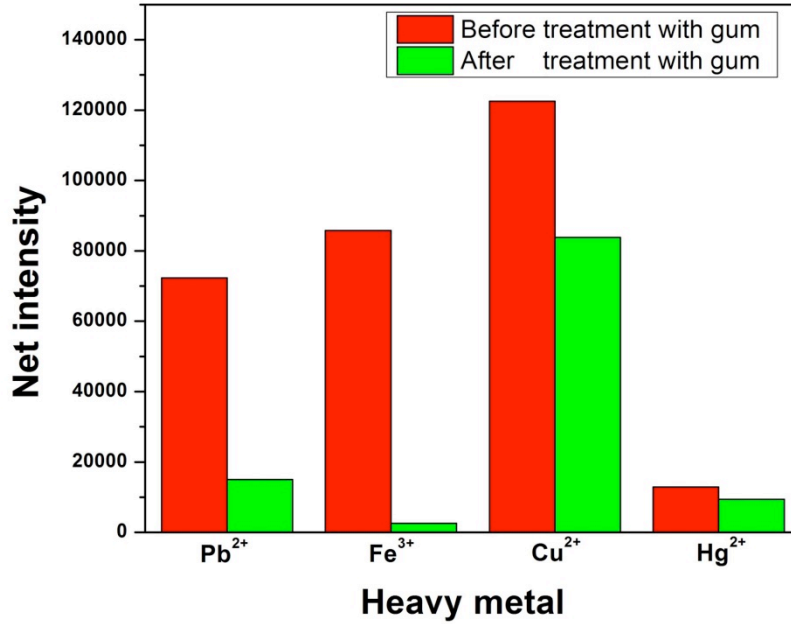
Figure 5.13 Graph of net intensity of heavy metals given by ICP-OES analysis before and after treatment.

Similar to what I did in 5.3.1, I modified a filter with gum powder. When I passed

the $FeCl_3$ solution through the modified filter, the solution became colorless, while the

commercially available filter could not block anything, as tested by naked eye (Figure

5.14).
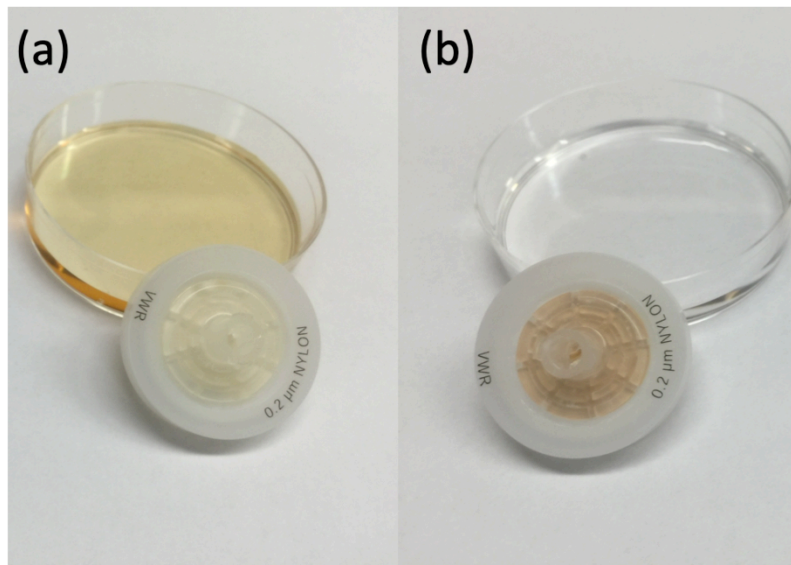
Figure 5.14 (a) shows the result when 1000 ppm of Fe^{3+} is passed through the unmodified filter and (b) shows the result when the filter is modified with gum.

5.3.3 Chewing Gum Used for Oil Sand TPW Treatment

Note that always wear gloves when working with oil sand TPW. Oil sand TPW was supplied from a local oil company. Column treatment of TPW was an attempt to reduce toxicity with waste chewing gum. Charcoal was chosen to compare chewing gum effectiveness against the gold standard of filtration. All columns were prepared with a 24-mL syringe and a 1-cm layer of cotton. For the charcoal column, a layer of dry sand was added on top of the cotton, followed by 5.1 g of charcoal suspended in DI water, which was allowed to compact for 4 h before a layer of dry sand was added on top. While the column was still wet, TPW was added drop by drop, and the resulting solution was collected over six days as the charcoal allowed very slow filtration. From Figure 5.15 we can see that charcoal filtered TPW results to a very transparent filtrate, signifying that

most organic molecules have been adsorbed onto the surface of the activated charcoal; this is due to the porous nature of activated charcoal, which allows binding of toxins to exposed sites by π-π interaction on the charcoal. We compared this filtrate with the TPW from Figure 5.15, which is cloudy and yellowish in color, signifying that most dissolved chemicals and solids have not been removed.
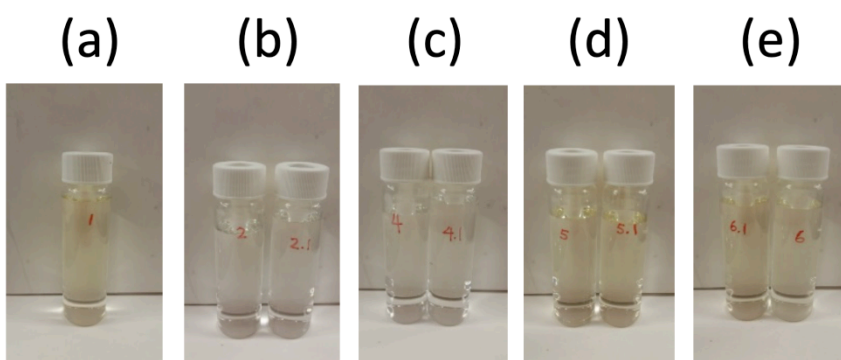
Figure 5.15 Photo of sample (a): TPW, sample (b): TPW filtered by charcoal, sample (c): TPW filtered by charcoal + silica, sample (d): TPW filtered by silica+ gum, sample (e): TPW filtered by silica.

Charcoal and silica columns were prepared similarly with a layer of sand, followed by 3 g of suspended charcoal, sand, 3 g of flash silica suspended in DI water, and another layer of sand. TPW was added drop by drop into this column, and the resulting filtrate was as clear as the filtrate from the charcoal column. This is due mainly to the adsorptive properties of charcoal, which are very effective at removing organic molecules.

The column containing silica and gum was prepared with a layer of sand, 3 g of suspended silica in DI water, sand, 1.5 g of gum, and finally another layer of sand. The gum was kept above the silica because silica is able to keep the gum from infiltrating into the sand/cotton layer and escaping the column. Also, only 1.5 g of gum was used because

it is very impermeable, and more than 2 g of gum makes the column impermeable to water. TPW was added drop by drop, and a filtrate that is slightly darker than TPW filtered by charcoal was obtained. A column containing 1.5 g of gum and 3 g of charcoal was made, however, it was impermeable to TPW.

The column that contains only silica filtered the fastest. Silica is very permeable compared to charcoal and gum, and from the filtrate in Figure 5.15 we can see that it has a very similar dark brown color to the filtrate obtained from silica and gum. However, from Table 5.3 the cell viability for this solution is only 43.8%, which means it removed less toxicity than gum and charcoal.

An in vitro photothermal cytotoxicity test was performed for each column filtration with five replicates for each of them, and the average value of all treatment groups was taken. Cell viability was calculated against the control group and showed that TPW had the lowest cell viability, as expected, with a cell viability of 22%. TPW that was filtered by charcoal had a 54% cell viability. TPW that was filtered by the column with charcoal and silica showed a cell viability of 54%, which is the same as TPW filtered by charcoal. This result is expected because activated charcoal is the single most effective agent for removing organic acids, and organic acids are the primary reasons for TPW toxicity.

Table 5.3 In vitro photothermal cytotoxicity test results for HeLa Cells and cell viability

	Oil Sand	Charcoal	Charcoal and Silica	Silica and Gum	Silica	Control
1	0.118	0.261	0.256	0.313	0.182	0.454
2	0.111	0.279	0.255	0.288	0.226	0.491
3	0.063	0.278	0.270	0.318	0.212	0.456
4	0.061	0.215	0.247	0.346	0.219	0.491
5	0.166	0.241	0.246	0.376	0.200	0.475
average	0.104	0.255	0.255	0.328	0.208	0.473
standard deviation	0.044	0.027	0.009	0.033	0.017	0.018
Cell viability %	22	54	54	69	44	100

The result for TPW filtered by silica confirms that silica is a less effective agent compared to charcoal, with a cell viability of only 44% even though a higher mass of silica was used compared to charcoal.

TPW that was filtered by the column containing silica and gum had the highest cell viability of 69%. This supports the fact that gum can be used as an effective agent for reducing TPW toxicity, given that it is more effective at reducing the toxicity of TPW than even activated carbon.

Non-purgeable organic carbon (NPOC) data was taken to confirm if the gum adsorbed or reacted with TPW (Table 5.4). TPW had 67.4 mg/ L of NPOC, which was expected as TPW contains a high amount of organic carbons. The charcoal column had NPOC of 3.7 mg/ L, and the charcoal with silica column had 1.77 mg/L, which was expected given the adsorption properties of activated charcoal. Contrary to expectation,

NPOC data for the silica and gum column showed a higher NPOC count of 71.2 mg/L compared to pure TPW. This means that gum has reacted most likely with the naphthenic acid in TPW, given the reduction in toxicity previously measured. More research is needed to understand what gum are left after washing, what is being reacted in our samples, and what is being produced.

Table 5.4 NPOC results of TPW and filtrates.

Lab ID	Sample ID	NPOC (mg/L)	%RSD
1	TPW	67.4	1.28
2	Charcoal Filtrate	3.7	9.36
4	Charcoal + Silica	1.77	9.64
5	Silica + Gum	71.2	1.09
6	Silica	68.9	1.13

5.4 Conclusions

I successfully removed the dissolved materials from waste chewing gum and used the remaining gum to remove dyes and heavy metal ions from water. The gum also can be used to reduce the toxicity of oil sands TPW. The gum powder adsorbs many kinds of dyes and can be reused several times. This finding plays a role in solving environmental wastewater issues. On the one hand, I make use of the waste gum, reducing the gum pollution; on the other hand, I help solve environmental water pollution. Overall, this study opens the door for further investigation of new resources that can be used to solve environmental water

contamination. Though it worked as a proof of concept, we may encounter many problems in real application, such as the recovery of gum waste and how to improve the removal efficiency.

Chapter 6

Conclusions and Future Outlook

6.1 Conclusions and Future Outlooks of Biosensors

Two sets of biosensors are developed. In Chapter 2, a biosensor was developed by utilizing fluorophore-modified anti-bodies and antibody-modified magnetic microparticles to detect mouse and rabbit IgG. The assay was able to detect the respective IgGs with good LOD and selectivity. The IgGs could be detected in a single solution simultaneously, which is important for multi-analytes sensing approaches. The assay could be performed without the use of a fluorometer by simply using the naked eye.

In Chapter 3, another biosensor was developed by utilizing the cleavage of a polymer coated on the surface of a responsive polymer-based etalon to result in a change in its optical properties. It was shown that the approach is specific to mouse IgG and can be effective in the presence of other interfering biomolecules in solution. This particular assay is simple and straightforward to carry out, and all the components are inexpensive, making this an assay that could find real world applications.

For the future outlook of this part, we would like to apply our sensors for real sample analysis, which is really important in disease diagnosis. For a certain disease diagnosis, one can either detect the concentration of an antigen causing the disease or the concentration of the corresponding antibody. We can try detecting both the antigen and

the antibody concentrations with our sensors and see what progress will we obtain and what potential problems we may encounter.

6.2 Conclusions and Future Outlooks of NIR Enhanced Drug Delivery

In Chapter 4, we developed a NIR responsive etalons by incorporating carbon nanotubes onto the etalons. The etalon shows fast response toward NIR by changing its color, which was characterized by an optical probe. This phenomenon then was utilized for enhanced drug delivery. Introducing carbon nanotubes onto the etalon obviously can enhance the drug release from the etalon. The platform we developed can be applied for NIR enhanced drug delivery systems.

For the future outlook of this part, we would apply this finding to animals such as rabbits and mouse. The preliminary idea is that we put the etalon loaded with drugs in animals that have a certain kind of disease. Then we shine NIR on these animals for various time and observe the health conditions over time.

6.3 Conclusions and Future Outlooks of Chewing Gum Waste for Water Treatment

In Chapter 5, chewing gum waste could be processed to remove dyes and heavy metal ions from water. The gum also can be used to reduce the toxicity of oil sands TPW. The gum powder adsorbs many kinds of organic dyes and can be reused several times.

For the future outlook of this part, more attention will be focused on analyzing the composition of the chewing gum waste after treatment with water, ethanol, and toluene respectively. And how are these dyes and heavy metal ions are adsorbed onto the gum, as well as the mechanism how gum powder decreased the toxicity of oil sands tailing ponds water.

6.4 Conclusions and Future Work of Chewing Gum Waste for Controlled Release Fertilizer

In Appendix A, we separated materials from chewing gum waste and then used them to make controlled released fertilizer. The release rate can be controlled by change the size of the fertilizer and the chemistry (addition of some chemicals) of the fertilizer. This will lead to future innovations, which will decrease our ecological footprint while solving some of the problems faced today.

For the future outlook of this part, we will design an experiment to use the controlled released fertilizers we synthesized for canola plants and compare the difference form traditional fertilizer.

6.5 Conclusions and Future Work of High Frequency Magnetism Respnsive Etalons

In Appendix B, we obtained preliminary results from high frequency magnetic field response etalons. So far we have confirmed that we are able to use iron (0) to replace

gold to fabricate etalons in order to enhance the high frequency-magnetic field response. This property could be used in enhanced drug delivery.

For the future outlook of this part, we will study how the thickness of iron layer will affect the high frequency magnetic field response and drug release. Increasing the thickness of iron will probably give us better high frequency magnetic field response but will hinder the release of drugs. We may need to find a balance between both cases.

6.6   Conclusions and Future Work of E.coli Detection Project

In Appendix C, we developed an E.coli sensor. DNA aptamer which is specific to Ecoli was reacted with urease and used to react with E.coli solution; the excess DNA-urease will be left in the solution, which can degrade urea into ammonia that will interact with the microgels in the etalon, causing the size change of these microgels. The size change of the microgels can be tracked and recorded with an optical probe by collecting the reflectance spectrum. As the concentration of E.coli changes, the total reflectance peak shift changes accordingly. This might be deployed as a cheap and hand held E.coli sensor.

For the future outlook of this part, we need to study the specificity of this sensor. And we will see what problems we may encounter when we analyze real water sample or drinks.

Bibliography

1. Stuart, M. A. C.; Huck, W. T.; Genzer, J.; Müller, M.; Ober, C.; Stamm, M.; Sukhorukov, G. B.; Szleifer, I.; Tsukruk, V. V.; Urban, M., Emerging applications of stimuli-responsive polymer materials. *Nature Materials* **2010,** *9* (2), 101.

2. Ahn, S.-k.; Kasi, R. M.; Kim, S.-C.; Sharma, N.; Zhou, Y., Stimuli-responsive polymer gels. *Soft Matter* **2008,** *4* (6), 1151-1157.

3. Li, M.-H.; Keller, P., Stimuli-responsive polymer vesicles. *Soft Matter* **2009,** *5* (5), 927-937.

4. Ma, X.; Tian, H., Stimuli-responsive supramolecular polymers in aqueous solution. *Accounts of Chemical Research* **2014,** *47* (7), 1971-1981.

5. Lee, H.-i.; Pietrasik, J.; Sheiko, S. S.; Matyjaszewski, K., Stimuli-responsive molecular brushes. *Progress in Polymer Science* **2010,** *35* (1-2), 24-44.

6. Chen, T.; Ferris, R.; Zhang, J.; Ducker, R.; Zauscher, S., Stimulus-responsive polymer brushes on surfaces: Transduction mechanisms and applications. *Progress in Polymer Science* **2010,** *35* (1-2), 94-112.

7. Yan, X.; Wang, F.; Zheng, B.; Huang, F., Stimuli-responsive supramolecular polymeric materials. *Chemical Society Reviews* **2012,** *41* (18), 6042-6065.

8. Lynn, D. M.; Amiji, M. M.; Langer, R., pH-responsive polymer microspheres: Rapid release of encapsulated material within the range of intracellular pH. *Angewandte Chemie* **2001,** *113* (9), 1757-1760.

9. Nicoletta, F. P.; Cupelli, D.; Formoso, P.; De Filpo, G.; Colella, V.; Gugliuzza, A., Light responsive polymer membranes: A review. *Membranes* **2012,** *2* (1), 134-197.

10. Laloyaux, X.; Fautré, E.; Blin, T.; Purohit, V.; Leprince, J.; Jouenne, T.; Jonas, A. M.; Glinel, K., Temperature-responsive polymer brushes switching from bactericidal to cell-repellent. *Advanced Materials* **2010,** *22* (44), 5024-5028.

11. Zhao, B.; Moore, J. S., Fast pH-and ionic strength-responsive hydrogels in microchannels. *Langmuir* **2001,** *17* (16), 4758-4763.

12. Ge, J.; Neofytou, E.; Cahill III, T. J.; Beygui, R. E.; Zare, R. N., Drug release from electric-field-responsive nanoparticles. *ACS Nano* **2011,** *6* (1), 227-233.

13. Katsuno, C.; Konda, A.; Urayama, K.; Takigawa, T.; Kidowaki, M.; Ito, K., Pressure-Responsive Polymer Membranes of Slide-Ring Gels with Movable Cross-Links. *Advanced Materials* **2013,** *25* (33), 4636-4640.

14. Schild, H. G., Poly (N-isopropylacrylamide): experiment, theory and application. *Progress in Polymer Science* **1992,** *17* (2), 163-249.

15. Heskins, M.; Guillet, J. E., Solution properties of poly (N-isopropylacrylamide). *Journal of Macromolecular Science—Chemistry* **1968,** *2* (8), 1441-1455.

16. Pelton, R., Poly (N-isopropylacrylamide)(PNIPAM) is never hydrophobic. *Journal of Colloid and Interface Science* **2010,** *348* (2), 673-674.

17. Kujawa, P.; Aseyev, V.; Tenhu, H.; Winnik, F. M., Temperature-sensitive properties of poly (N-isopropylacrylamide) mesoglobules formed in dilute aqueous solutions heated above their demixing point. *Macromolecules* **2006,** *39* (22), 7686-7693.

18. Hoare, T.; Pelton, R., Charge-switching, amphoteric glucose-responsive microgels with physiological swelling activity. *Biomacromolecules* **2008,** *9* (2), 733-740.

19. Xu, Y.; Pharand, L.; Wen, Q.; Gonzaga, F.; Li, Y.; Ali, M. M.; Filipe, C. D.; Pelton, R., Controlling biotinylation of microgels and modeling streptavidin uptake. *Colloid and Polymer Science* **2011,** *289* (5-6), 659-666.

20. Hoare, T.; Pelton, R., Engineering glucose swelling responses in poly (N-isopropylacrylamide)-based microgels. *Macromolecules* **2007,** *40* (3), 670-678.

21. Senff, H.; Richtering, W., Temperature sensitive microgel suspensions: Colloidal phase behavior and rheology of soft spheres. *The Journal of Chemical Physics* **1999,** *111* (4), 1705-1711.

22. Berndt, I.; Pedersen, J. S.; Richtering, W., Temperature-Sensitive Core–Shell Microgel Particles with Dense Shell. *Angewandte Chemie* **2006,** *118* (11), 1769-1773.

23. Kocak, G.; Tuncer, C.; Bütün, V., pH-Responsive polymers. *Polymer Chemistry* **2017,** *8* (1), 144-176.

24. Gao, Y.; Ahiabu, A.; Serpe, M. J., Controlled drug release from the aggregation–disaggregation behavior of pH-responsive microgels. *ACS Applied Materials & Interfaces* **2014,** *6* (16), 13749-13756.

25. Gao, Y.; Zago, G. P.; Jia, Z.; Serpe, M. J., Controlled and triggered small molecule release from a confined polymer film. *ACS Applied Materials & Interfaces* **2013,** *5* (19), 9803-9808.

26. Gao, Y.; Wong, K. Y.; Ahiabu, A.; Serpe, M. J., Sequential and controlled release of small molecules from poly (N-isopropylacrylamide) microgel-based reservoir devices. *Journal of Materials Chemistry B* **2016,** *4* (30), 5144-5150.

27. Kim, J.; Nayak, S.; Lyon, L. A., Bioresponsive hydrogel microlenses. *Journal of the American Chemical Society* **2005,** *127* (26), 9588-9592.

28. Guesdon, J.-L.; Ternynck, T.; Avrameas, S., The use of avidin-biotin interaction in immunoenzymatic techniques. *Journal of Histochemistry & Cytochemistry* **1979,** *27* (8), 1131-1139.

29. Weber, P. C.; Ohlendorf, D.; Wendoloski, J.; Salemme, F., Structural origins of high-affinity biotin binding to streptavidin. *Science* **1989,** *243* (4887), 85-88.

30. Zhang, Y.; Guan, Y.; Zhou, S., Synthesis and volume phase transitions of glucose-sensitive microgels. *Biomacromolecules* **2006,** *7* (11), 3196-3201.

31. Rivero, R. E.; Molina, M. A.; Rivarola, C. R.; Barbero, C. A., Pressure and microwave sensors/actuators based on smart hydrogel/conductive polymer nanocomposite. *Sensors and Actuators B: Chemical* **2014,** *190*, 270-278.

32. Haq, M. A.; Su, Y.; Wang, D., Mechanical properties of PNIPAM based hydrogels: A review. *Materials Science and Engineering: C* **2017,** *70*, 842-855.

33. Nöjd, S.; Mohanty, P. S.; Bagheri, P.; Yethiraj, A.; Schurtenberger, P., Electric field driven self-assembly of ionic microgels. *Soft Matter* **2013,** *9* (38), 9199-9207.

34. Zhou, J.; Wei, J.; Ngai, T.; Wang, L.; Zhu, D.; Shen, J., Correlation between dielectric/electric properties and cross-linking/charge density distributions of thermally sensitive spherical PNIPAM microgels. *Macromolecules* **2012,** *45* (15), 6158-6167.

35. Stern, E.; Vacic, A.; Rajan, N. K.; Criscione, J. M.; Park, J.; Ilic, B. R.; Mooney, D. J.; Reed, M. A.; Fahmy, T. M., Label-free biomarker detection from whole blood. *Nature Nanotechnology* **2010,** *5* (2), 138.

36. Arasaradnam, R.; Covington, J.; Harmston, C.; Nwokolo, C., Next generation diagnostic modalities in gastroenterology–gas phase volatile compound biomarker detection. *Alimentary Pharmacology & Therapeutics* **2014,** *39* (8), 780-789.

37. Mohammed, M.-I.; Desmulliez, M. P., Lab-on-a-chip based immunosensor principles and technologies for the detection of cardiac biomarkers: a review. *Lab on a Chip* **2011,** *11* (4), 569-595.

38. Etzioni, R.; Urban, N.; Ramsey, S.; McIntosh, M.; Schwartz, S.; Reid, B.; Radich, J.; Anderson, G.; Hartwell, L., Early detection: The case for early detection. *Nature Reviews Cancer* **2003,** *3* (4), 243.

39. Uludag, Y.; Tothill, I. E., Cancer biomarker detection in serum samples using surface plasmon resonance and quartz crystal microbalance sensors with nanoparticle signal amplification. *Analytical Chemistry* **2012,** *84* (14), 5898-5904.

40. Wulfkuhle, J. D.; Liotta, L. A.; Petricoin, E. F., Early detection: proteomic applications for the early detection of cancer. *Nature reviews cancer* **2003,** *3* (4), 267.

41. Smith, R. A.; Cokkinides, V.; von Eschenbach, A. C.; Levin, B.; Cohen, C.; Runowicz, C. D.; Sener, S.; Saslow, D.; Eyre, H. J., American Cancer Society guidelines for the early detection of cancer. *CA: a Cancer Journal for Clinicians* **2002,** *52* (1), 8-22.

42. Yalow, R. S.; Berson, S. A., Immunoassay of endogenous plasma insulin in man. *The Journal of Clinical Investigation* **1960,** *39* (7), 1157-1175.

43. Arenkov, P.; Kukhtin, A.; Gemmell, A.; Voloshchuk, S.; Chupeeva, V.; Mirzabekov, A., Protein microchips: use for immunoassay and enzymatic reactions. *Analytical Biochemistry* **2000,** *278* (2), 123-131.

44. Porstmann, T.; Kiessig, S., Enzyme immunoassay techniques an overview. *Journal of Immunological Methods* **1992,** *150* (1-2), 5-21.

45. Ni, X.; Bai, X.; Mao, Y.; Shao, Y.; Wu, J.; Shan, Y.; Wang, C.; Wang, J.; Tian, Y.; Liu, Q., The clinical value of serum CEA, CA19-9, and CA242 in the diagnosis and

prognosis of pancreatic cancer. *European Journal of Surgical Oncology (EJSO)* **2005,** *31* (2), 164-169.

46. Goonetilleke, K.; Siriwardena, A., Systematic review of carbohydrate antigen (CA 19-9) as a biochemical marker in the diagnosis of pancreatic cancer. *European Journal of Surgical Oncology (EJSO)* **2007,** *33* (3), 266-270.

47. Schröder, F. H.; van der CRUIJSEN-KOETER, I.; de KONING, H. J.; Vis, A. N.; Hoedemaeker, R. F.; Kranse, R., Prostate cancer detection at low prostate specific antigen. *The Journal of Urology* **2000,** *163* (3), 806-812.

48. Jain, R. K.; Duda, D. G.; Willett, C. G.; Sahani, D. V.; Zhu, A. X.; Loeffler, J. S.; Batchelor, T. T.; Sorensen, A. G., Biomarkers of response and resistance to antiangiogenic therapy. *Nature reviews Clinical Oncology* **2009,** *6* (6), 327.

49. Islam, M. R.; Gao, Y.; Li, X.; Serpe, M. J., Responsive polymers for biosensing and protein delivery. *Journal of Materials Chemistry B* **2014,** *2* (17), 2444-2451.

50. Islam, M.; Ahiabu, A.; Li, X.; Serpe, M., Poly (N-isopropylacrylamide) microgel-based optical devices for sensing and biosensing. *Sensors* **2014,** *14* (5), 8984-8995.

51. Zhu, Y.; Fang, Q., Analytical detection techniques for droplet microfluidics—A review. *Analytica Chimica Acta* **2013,** *787*, 24-35.

52. Craw, P.; Balachandran, W., Isothermal nucleic acid amplification technologies for point-of-care diagnostics: a critical review. *Lab on a Chip* **2012,** *12* (14), 2469-2486.

53. MacBeath, G., Protein microarrays and proteomics. *Nature Genetics* **2002,** *32* (4s), 526.

54. Voller, A.; Bartlett, A.; Bidwell, D., Enzyme immunoassays with special reference to ELISA techniques. *Journal of Clinical Pathology* **1978,** *31* (6), 507-520.

55. Fan, Z.; Chen, J.; Zou, J.; Bullen, D.; Liu, C.; Delcomyn, F., Design and fabrication of artificial lateral line flow sensors. *Journal of Micromechanics and Microengineering* **2002,** *12* (5), 655.

56. Delmulle, B. S.; De Saeger, S. M.; Sibanda, L.; Barna-Vetro, I.; Van Peteghem, C. H., Development of an immunoassay-based lateral flow dipstick for the rapid detection of

aflatoxin B1 in pig feed. *Journal of Agricultural and Food Chemistry* **2005,** *53* (9), 3364-3368.

57. Zhang, G.; Wang, X.; Yang, J.; Yang, Y.; Xing, G.; Li, Q.; Zhao, D.; Chai, S.; Guo, J., Development of an immunochromatographic lateral flow test strip for detection of β-adrenergic agonist Clenbuterol residues. *Journal of Immunological Methods* **2006,** *312* (1-2), 27-33.

58. Posthuma-Trumpie, G. A.; Korf, J.; van Amerongen, A., Lateral flow (immuno) assay: its strengths, weaknesses, opportunities and threats. A literature survey. *Analytical and Bioanalytical Chemistry* **2009,** *393* (2), 569-582.

59. Singh, S.; Gupta, A. K.; Gupta, S.; Gupta, S.; Kumar, A., Surface Plasmon Resonance (SPR) and cyclic voltammetry based immunosensor for determination of teliosporic antigen and diagnosis of Karnal Bunt of wheat using anti-teliosporic antibody. *Sensors and Actuators B: Chemical* **2014,** *191*, 866-873.

60. Sackmann, E. K.; Fulton, A. L.; Beebe, D. J., The present and future role of microfluidics in biomedical research. *Nature* **2014,** *507* (7491), 181.

61. Upadhyayula, V. K., Functionalized gold nanoparticle supported sensory mechanisms applied in detection of chemical and biological threat agents: a review. *Analytica Chimica Acta* **2012,** *715*, 1-18.

62. Liu, B.-H.; Tsao, Z.-J.; Wang, J.-J.; Yu, F.-Y., Development of a monoclonal antibody against ochratoxin A and its application in enzyme-linked immunosorbent assay and gold nanoparticle immunochromatographic strip. *Analytical Chemistry* **2008,** *80* (18), 7029-7035.

63. Nam, J.-M.; Thaxton, C. S.; Mirkin, C. A., Nanoparticle-based bio-bar codes for the ultrasensitive detection of proteins. *Science* **2003,** *301* (5641), 1884-1886.

64. Alivisatos, P., The use of nanocrystals in biological detection. *Nature Biotechnology* **2004,** *22* (1), 47.

65. Salata, O. V., Applications of nanoparticles in biology and medicine. *Journal of Nanobiotechnology* **2004,** *2* (1), 3.

66. Cao, Y. C.; Jin, R.; Mirkin, C. A., Nanoparticles with Raman spectroscopic fingerprints for DNA and RNA detection. *Science* **2002,** *297* (5586), 1536-1540.

67. Taton, T. A.; Mirkin, C. A.; Letsinger, R. L., Scanometric DNA array detection with nanoparticle probes. *Science* **2000,** *289* (5485), 1757-1760.

68. Park, S.-J.; Taton, T. A.; Mirkin, C. A., Array-based electrical detection of DNA with nanoparticle probes. *Science* **2002,** *295* (5559), 1503-1506.

69. Haes, A. J.; Van Duyne, R. P., A nanoscale optical biosensor: sensitivity and selectivity of an approach based on the localized surface plasmon resonance spectroscopy of triangular silver nanoparticles. *Journal of the American Chemical Society* **2002,** *124* (35), 10596-10604.

70. Haes, A. J.; Hall, W. P.; Chang, L.; Klein, W. L.; Van Duyne, R. P., A localized surface plasmon resonance biosensor: First steps toward an assay for Alzheimer's disease. *Nano Letters* **2004,** *4* (6), 1029-1034.

71. Haes, A. J.; Chang, L.; Klein, W. L.; Van Duyne, R. P., Detection of a biomarker for Alzheimer's disease from synthetic and clinical samples using a nanoscale optical biosensor. *Journal of the American Chemical Society* **2005,** *127* (7), 2264-2271.

72. Zhu, H.-Y.; Fu, Y.-Q.; Jiang, R.; Yao, J.; Xiao, L.; Zeng, G.-M., Novel magnetic chitosan/poly (vinyl alcohol) hydrogel beads: preparation, characterization and application for adsorption of dye from aqueous solution. *Bioresource Technology* **2012,** *105*, 24-30.

73. Zhang, Y.; Liu, R.; Hu, Y.; Li, G., Microwave heating in preparation of magnetic molecularly imprinted polymer beads for trace triazines analysis in complicated samples. *Analytical Chemistry* **2009,** *81* (3), 967-976.

74. Herrmann, M.; Veres, T.; Tabrizian, M., Enzymatically-generated fluorescent detection in micro-channels with internal magnetic mixing for the development of parallel microfluidic ELISA. *Lab on a Chip* **2006,** *6* (4), 555-560.

75. Bruno, J. G.; Phillips, T.; Carrillo, M. P.; Crowell, R., Plastic-adherent DNA aptamer-magnetic bead and quantum dot sandwich assay for Campylobacter detection. *Journal of Fluorescence* **2009,** *19* (3), 427.

76. Charlermroj, R.; Himananto, O.; Seepiban, C.; Kumpoosiri, M.; Warin, N.; Oplatowska, M.; Gajanandana, O.; Grant, I. R.; Karoonuthaisiri, N.; Elliott, C. T.,

Multiplex detection of plant pathogens using a microsphere immunoassay technology. *PLoS One* **2013,** *8* (4), e62344.

77. Islam, M. R.; Serpe, M. J., Label-free detection of low protein concentration in solution using a novel colorimetric assay. *Biosensors and Bioelectronics* **2013,** *49*, 133-138.

78. Islam, M. R.; Serpe, M. J., Polyelectrolyte mediated intra and intermolecular crosslinking in microgel-based etalons for sensing protein concentration in solution. *Chemical Communications* **2013,** *49* (26), 2646-2648.

79. Chen, R. J.; Bangsaruntip, S.; Drouvalakis, K. A.; Kam, N. W. S.; Shim, M.; Li, Y.; Kim, W.; Utz, P. J.; Dai, H., Noncovalent functionalization of carbon nanotubes for highly specific electronic biosensors. *Proceedings of the National Academy of Sciences* **2003,** *100* (9), 4984-4989.

80. Abe, M.; Murata, K.; Kojima, A.; Ifuku, Y.; Shimizu, M.; Ataka, T.; Matsumoto, K., Quantitative detection of protein using a top-gate carbon nanotube field effect transistor. *The Journal of Physical Chemistry C* **2007,** *111* (24), 8667-8670.

81. Wohlstadter, J. N.; Wilbur, J. L.; Sigal, G. B.; Biebuyck, H. A.; Billadeau, M. A.; Dong, L.; Fischer, A. B.; Gudibande, S. R.; Jameison, S. H.; Kenten, J. H., Carbon nanotube-based biosensor. *Advanced Materials* **2003,** *15* (14), 1184-1187.

82. Su, S.; Ali, M. M.; Filipe, C. D.; Li, Y.; Pelton, R., Microgel-based inks for paper-supported biosensing applications. *Biomacromolecules* **2008,** *9* (3), 935-941.

83. Shmanai, V. V.; Nikolayeva, T. A.; Vinokurova, L. G.; Litoshka, A. A., Oriented antibody immobilization to polystyrene macrocarriers for immunoassay modified with hydrazide derivatives of poly (meth) acrylic acid. *BMC biotechnology* **2001,** *1* (1), 4.

84. Hurley, I. P.; Coleman, R. C.; Ireland, H. E.; Williams, J. H., Measurement of bovine IgG by indirect competitive ELISA as a means of detecting milk adulteration. *Journal of dairy science* **2004,** *87* (3), 543-549.

85. Walsh, T. R.; Weeks, J.; Livermore, D. M.; Toleman, M. A., Dissemination of NDM-1 positive bacteria in the New Delhi environment and its implications for human health: an environmental point prevalence study. *The Lancet Infectious Diseases* **2011,** *11* (5), 355-362.

86. Lundberg, J. O.; Weitzberg, E.; Cole, J. A.; Benjamin, N., Nitrate, bacteria and human health. *Nature Reviews Microbiology* **2004,** *2* (7), 593.

87. Peiris, J. M.; De Jong, M. D.; Guan, Y., Avian influenza virus (H5N1): a threat to human health. *Clinical Microbiology Reviews* **2007,** *20* (2), 243-267.

88. Duffy, M. R.; Chen, T.-H.; Hancock, W. T.; Powers, A. M.; Kool, J. L.; Lanciotti, R. S.; Pretrick, M.; Marfel, M.; Holzbauer, S.; Dubray, C., Zika virus outbreak on Yap Island, federated states of Micronesia. *New England Journal of Medicine* **2009,** *360* (24), 2536-2543.

89. Brasil, P.; Pereira Jr, J. P.; Moreira, M. E.; Ribeiro Nogueira, R. M.; Damasceno, L.; Wakimoto, M.; Rabello, R. S.; Valderramos, S. G.; Halai, U.-A.; Salles, T. S., Zika virus infection in pregnant women in Rio de Janeiro. *New England Journal of Medicine* **2016,** *375* (24), 2321-2334.

90. Holford, T. R.; Davis, F.; Higson, S. P., Recent trends in antibody based sensors. *Biosensors and Bioelectronics* **2012,** *34* (1), 12-24.

91. Lanciotti, R. S.; Kosoy, O. L.; Laven, J. J.; Velez, J. O.; Lambert, A. J.; Johnson, A. J.; Stanfield, S. M.; Duffy, M. R., Genetic and serologic properties of Zika virus associated with an epidemic, Yap State, Micronesia, 2007. *Emerging Infectious Diseases* **2008,** *14* (8), 1232.

92. Lee, P.; Plavina, T.; Castro, A.; Berman, M.; Jaiswal, D.; Rivas, S.; Schlain, B.; Subramanyam, M., A second-generation ELISA (STRATIFY JCV™ DxSelect™) for detection of JC virus antibodies in human serum and plasma to support progressive multifocal leukoencephalopathy risk stratification. *Journal of Clinical Virology* **2013,** *57* (2), 141-146.

93. Tran, D. T.; Knez, K.; Janssen, K. P.; Pollet, J.; Spasic, D.; Lammertyn, J., Selection of aptamers against Ara h 1 protein for FO-SPR biosensing of peanut allergens in food matrices. *Biosensors and Bioelectronics* **2013,** *43*, 245-251.

94. Breault-Turcot, J.; Chaurand, P.; Masson, J.-F., Unravelling nonspecific adsorption of complex protein mixture on surfaces with SPR and MS. *Analytical Chemistry* **2014,** *86* (19), 9612-9619.

95. de Juan-Franco, E.; Caruz, A.; Pedrajas, J.; Lechuga, L. M., Site-directed antibody immobilization using a protein A–gold binding domain fusion protein for enhanced SPR immunosensing. *Analyst* **2013,** *138* (7), 2023-2031.

96. Cooper, M. A.; Singleton, V. T., A survey of the 2001 to 2005 quartz crystal microbalance biosensor literature: applications of acoustic physics to the analysis of biomolecular interactions. *Journal of Molecular Recognition: An Interdisciplinary Journal* **2007,** *20* (3), 154-184.

97. Lisdat, F.; Schäfer, D., The use of electrochemical impedance spectroscopy for biosensing. *Analytical and Bioanalytical Chemistry* **2008,** *391* (5), 1555.

98. Satapathy, S. S.; Bhol, P.; Chakkarambath, A.; Mohanta, J.; Samantaray, K.; Bhat, S. K.; Panda, S. K.; Mohanty, P. S.; Si, S., Thermo-responsive PNIPAM-metal hybrids: an efficient nanocatalyst for the reduction of 4-nitrophenol. *Applied Surface Science* **2017,** *420*, 753-763.

99. Zhang, W.; Jiang, P.; Chen, J.; Zhu, C.; Mao, Z.; Gao, C., Application of melatonin-loaded poly (N-isopropylacrylamide) hydrogel particles to reduce the toxicity of airborne pollutes to RAW264. 7 cells. *Journal of Colloid and Interface Science* **2017,** *490*, 181-189.

100. Elashnikov, R.; Mares, D.; Podzimek, T.; Švorčík, V.; Lyutakov, O., Sandwiched gold/PNIPAm/gold microstructures for smart plasmonics application: towards the high detection limit and Raman quantitative measurements. *Analyst* **2017,** *142* (16), 2974-2981.

101. Wang, T.; Yu, Y.; Chen, D.; Wang, S.; Zhang, X.; Li, Y.; Zhang, J.; Fu, Y., Naked eye plasmonic indicator with multi-responsive polymer brush as signal transducer and amplifier. *Nanoscale* **2017,** *9* (5), 1925-1933.

102. Wang, Z.; Zhang, J.; Wang, Z.; Shen, H.; Xie, J.; Li, Y.; Lin, L.; Yang, B., Biochemical-to-optical signal transduction by pH sensitive organic–inorganic hybrid Bragg stacks with a full color display. *Journal of Materials Chemistry C* **2013,** *1* (5), 977-983.

103.   Sorrell, C. D.; Serpe, M. J., Reflection order selectivity of color-tunable poly (N-isopropylacrylamide) microgel based etalons. *Advanced Materials* **2011,** *23* (35), 4088-4092.

104.   Islam, M. R.; Lu, Z.; Li, X.; Sarker, A. K.; Hu, L.; Choi, P.; Li, X.; Hakobyan, N.; Serpe, M. J., Responsive polymers for analytical applications: A review. *Analytica Chimica Acta* **2013,** *789*, 17-32.

105.   Gao, Y.; Li, X.; Serpe, M. J., Stimuli-responsive microgel-based etalons for optical sensing. *RSC Advances* **2015,** *5* (55), 44074-44087.

106.   Islam, M. R.; Gao, Y.; Li, X.; Zhang, Q. M.; Wei, M.; Serpe, M. J., Stimuli-responsive polymeric materials for human health applications. *Chinese Science Bulletin* **2014,** *59* (32), 4237-4255.

107.   Zhang, W.; Guo, S.; Carvalho, W. S. P.; Jiang, Y.; Serpe, M. J., Portable point-of-care diagnostic devices. *Analytical Methods* **2016,** *8* (44), 7847-7867.

108.   Islam, M. R.; Serpe, M. J., A novel label-free colorimetric assay for DNA concentration in solution. *Analytica Chimica Acta* **2014,** *843*, 83-88.

109.   Islam, M. R.; Serpe, M. J., Polymer-based devices for the label-free detection of DNA in solution: low DNA concentrations yield large signals. *Analytical and Bioanalytical Chemistry* **2014,** *406* (19), 4777-4783.

110.   Folkman, J.; Long, D. M., The use of silicone rubber as a carrier for prolonged drug therapy. *Journal of Surgical Research* **1964,** *4* (3), 139-142.

111.   Desai, S. J.; Simonelli, A.; Higuchi, W., Investigation of factors influencing release of solid drug dispersed in inert matrices. *Journal of Pharmaceutical Sciences* **1965,** *54* (10), 1459-1464.

112.   Jalil, R.; Nixon, J., Biodegradable poly (lactic acid) and poly (lactide-co-glycolide) microcapsules: problems associated with preparative techniques and release properties. *Journal of Microencapsulation* **1990,** *7* (3), 297-325.

113.   Kamaly, N.; Yameen, B.; Wu, J.; Farokhzad, O. C., Degradable controlled-release polymers and polymeric nanoparticles: mechanisms of controlling drug release. *Chemical Reviews* **2016,** *116* (4), 2602-2663.

114.   Weiser, J. R.; Saltzman, W. M., Controlled release for local delivery of drugs: barriers and models. *Journal of Controlled Release* **2014,** *190*, 664-673.

115.   Gupta, P.; Vermani, K.; Garg, S., Hydrogels: from controlled release to pH-responsive drug delivery. *Drug Discovery Today* **2002,** *7* (10), 569-579.

116.   Kim, M. R.; Park, T. G., Temperature-responsive and degradable hyaluronic acid/Pluronic composite hydrogels for controlled release of human growth hormone. *Journal of Controlled Release* **2002,** *80* (1), 69-77.

117.   Tokarev, I.; Minko, S., Stimuli-Responsive Porous Hydrogels at Interfaces for Molecular Filtration, Separation, Controlled Release, and Gating in Capsules and Membranes. *Advanced Materials* **2010,** *22* (31), 3446-3462.

118.   Yavuz, M. S.; Cheng, Y.; Chen, J.; Cobley, C. M.; Zhang, Q.; Rycenga, M.; Xie, J.; Kim, C.; Song, K. H.; Schwartz, A. G., Gold nanocages covered by smart polymers for controlled release with near-infrared light. *Nature Materials* **2009,** *8* (12), 935-939.

119.   Choi, S. K.; Thomas, T.; Li, M.-H.; Kotlyar, A.; Desai, A.; Baker Jr, J. R., Light-controlled release of caged doxorubicin from folate receptor-targeting PAMAM dendrimer nanoconjugate. *Chemical Communications* **2010,** *46* (15), 2632-2634.

120.   De Heer, W. A.; Chatelain, A.; Ugarte, D., A carbon nanotube field-emission electron source. *Science* **1995,** *270* (5239), 1179-1181.

121.   Fan, S.; Chapline, M. G.; Franklin, N. R.; Tombler, T. W.; Cassell, A. M.; Dai, H., Self-oriented regular arrays of carbon nanotubes and their field emission properties. *Science* **1999,** *283* (5401), 512-514.

122.   Stankovich, S.; Dikin, D. A.; Dommett, G. H.; Kohlhaas, K. M.; Zimney, E. J.; Stach, E. A.; Piner, R. D.; Nguyen, S. T.; Ruoff, R. S., Graphene-based composite materials. *Nature* **2006,** *442* (7100), 282-286.

123.   Hummers Jr, W. S.; Offeman, R. E., Preparation of graphitic oxide. *Journal of the American Chemical Society* **1958,** *80* (6), 1339-1339.

124.   Ipe, B. I.; Mahima, S.; Thomas, K. G., Light-induced modulation of self-assembly on spiropyran-capped gold nanoparticles: a potential system for the controlled release of amino acid derivatives. *Journal of the American Chemical Society* **2003,** *125* (24), 7174-7175.

125.   Lal, S.; Link, S.; Halas, N. J., Nano-optics from sensing to waveguiding. *Nature Photonics* **2007,** *1* (11), 641-648.

126.   Portney, N. G.; Ozkan, M., Nano-oncology: drug delivery, imaging, and sensing. *Analytical and Bioanalytical Chemistry* **2006,** *384* (3), 620-630.

127.   Daniel, M.-C.; Astruc, D., Gold nanoparticles: assembly, supramolecular chemistry, quantum-size-related properties, and applications toward biology, catalysis, and nanotechnology. *Chemical Reviews* **2004,** *104* (1), 293-346.

128.   Smalley, R. E.; Dresselhaus, M. S.; Dresselhaus, G.; Avouris, P., *Carbon nanotubes: synthesis, structure, properties, and applications*. Springer Science & Business Media: 2003; Vol. 80.

129.   Wang, Q.; O'Hare, D., Recent advances in the synthesis and application of layered double hydroxide (LDH) nanosheets. *Chemical Reviews* **2012,** *112* (7), 4124-4155.

130.   Kavan, L.; Rapta, P.; Dunsch, L.; Bronikowski, M. J.; Willis, P.; Smalley, R. E., Electrochemical tuning of electronic structure of single-walled carbon nanotubes: in-situ Raman and Vis-NIR study. *The Journal of Physical Chemistry B* **2001,** *105* (44), 10764-10771.

131.   Kam, N. W. S.; O'Connell, M.; Wisdom, J. A.; Dai, H., Carbon nanotubes as multifunctional biological transporters and near-infrared agents for selective cancer cell destruction. *Proceedings of the National Academy of Sciences of the United States of America* **2005,** *102* (33), 11600-11605.

132.   Markovic, Z. M.; Harhaji-Trajkovic, L. M.; Todorovic-Markovic, B. M.; Kepić, D. P.; Arsikin, K. M.; Jovanović, S. P.; Pantovic, A. C.; Dramićanin, M. D.; Trajkovic, V. S., In vitro comparison of the photothermal anticancer activity of graphene nanoparticles and carbon nanotubes. *Biomaterials* **2011,** *32* (4), 1121-1129.

133.   Klingeler, R.; Hampel, S.; Büchner, B., Carbon nanotube based biomedical agents for heating, temperature sensing and drug delivery. *International Journal of Hyperthermia* **2008,** *24* (6), 496-505.

134.   Hoffman, A. S., Applications of thermally reversible polymers and hydrogels in therapeutics and diagnostics. *Journal of Controlled Release* **1987,** *6* (1), 297-305.

135.   Schmaljohann, D., Thermo-and pH-responsive polymers in drug delivery. *Advanced Drug Delivery Reviews* **2006,** *58* (15), 1655-1670.

136.   Hu, L.; Serpe, M. J., The influence of deposition solution ph and ionic strength on the quality of poly (N-isopropylacrylamide) microgel-based thin films and etalons. *ACS Applied Materials & Interfaces* **2013,** *5* (22), 11977-11983.

137.   Zhang, Q. M.; Guo, S.; Duan, J.; Serpe, M. J., Ordered Responsive Materials for Sensing Applications. In *Photonic Materials for Sensing, Biosensing and Display Devices*, Springer: 2016; pp 1-31.

138.   Hung, Y.-T.; Wang, L. K.; Lo, H. H.; Yapijakis, C., *Hazardous industrial waste treatment*. CRC Press: 2006.

139.   Samanlioglu, F., A multi-objective mathematical model for the industrial hazardous waste location-routing problem. *European Journal of Operational Research* **2013,** *226* (2), 332-340.

140.   Gupta, V. K.; Jain, R.; Varshney, S., Electrochemical removal of the hazardous dye Reactofix Red 3 BFN from industrial effluents. *Journal of Colloid and Interface Science* **2007,** *312* (2), 292-296.

141.   Swart, N. C.; Weaver, A. J., The Alberta oil sands and climate. *Nature Climate Change* **2012,** *2* (3), 134.

142.   O'Neill, C.; Hawkes, F. R.; Hawkes, D. L.; Lourenco, N. D.; Pinheiro, H. M.; Delee, W., Colour in textile effluents–sources, measurement, discharge consents and simulation: a review. *J. Chem. Technol. Biotechnol.* **1999,** *74* (11), 1009-1018.

143.   Kuo, W., Decolorizing dye wastewater with Fenton's reagent. *Water Research* **1992,** *26* (7), 881-886.

144.   Miller, J. A.; Miller, E. C., The carcinogenic aminoazo dyes. *Advanced Cancer Research* **1953,** *1*, 339-396.

145.   Brown, M. A.; De Vito, S. C., Predicting azo dye toxicity. *Critical reviews in Environmental Science and Technology* **1993,** *23* (3), 249-324.

146.   Rehwoldt, R.; Lasko, L.; Shaw, C.; Wirhowski, E., The acute toxicity of some heavy metal ions toward benthic organisms. *Bulletin of Environmental Contamination and Toxicology* **1973,** *10* (5), 291-294.

147.   Ryan, J. A.; Hightower, L. E., Evaluation of heavy-metal ion toxicity in fish cells using a combined stress protein and cytotoxicity assay. *Environmental Toxicology and Chemistry* **1994,** *13* (8), 1231-1240.

148.   Duruibe, J. O.; Ogwuegbu, M.; Egwurugwu, J., Heavy metal pollution and human biotoxic effects. *International Journal of Physical Sciences* **2007,** *2* (5), 112-118.

149.   Allen, E. W., Process water treatment in Canada's oil sands industry: I. Target pollutants and treatment objectives. *Journal of Environmental Engineering and Science* **2008,** *7* (2), 123-138.

150.   West, C. E.; Scarlett, A. G.; Pureveen, J.; Tegelaar, E. W.; Rowland, S. J., Abundant naphthenic acids in oil sands process-affected water: studies by synthesis, derivatisation and two-dimensional gas chromatography/high-resolution mass spectrometry. *Rapid Communications in Mass Spectrometry* **2013,** *27* (2), 357-365.

151.   Mondal, S., Methods of dye removal from dye house effluent-an overview. *Environmental Engineering Science* **2008,** *25* (3), 383-396.

152.   He, Y.-C.; Yang, J.; Kan, W.-Q.; Zhang, H.-M.; Liu, Y.-Y.; Ma, J.-F., A new microporous anionic metal–organic framework as a platform for highly selective adsorption and separation of organic dyes. *Journal of Materials Chemistry A* **2015,** *3* (4), 1675-1681.

153.   Brillas, E.; Martínez-Huitle, C. A., Decontamination of wastewaters containing synthetic organic dyes by electrochemical methods. An updated review. *Applied Catalysis B: Environmental* **2015,** *166*, 603-643.

154.   Kaviyarasu, K.; Kotsedi, L.; Simo, A.; Fuku, X.; Mola, G. T.; Kennedy, J.; Maaza, M., Photocatalytic activity of ZrO2 doped lead dioxide nanocomposites: Investigation of structural and optical microscopy of RhB organic dye. *Applied Surface Science* **2017,** *421*, 234-239.

155.   Sen, S. K.; Raut, S.; Bandyopadhyay, P.; Raut, S., Fungal decolouration and degradation of azo dyes: a review. *Fungal Biology Reviews* **2016,** *30* (3), 112-133.

156.   Gunatilake, S., Methods of removing heavy metals from industrial wastewater. *Methods* **2015,** *1* (1).

157.	Ahmed, M. J. K.; Ahmaruzzaman, M., A review on potential usage of industrial waste materials for binding heavy metal ions from aqueous solutions. *Journal of Water Process Engineering* **2016,** *10*, 39-47.

158.	Abbas, A.; Al-Amer, A. M.; Laoui, T.; Al-Marri, M. J.; Nasser, M. S.; Khraisheh, M.; Atieh, M. A., Heavy metal removal from aqueous solution by advanced carbon nanotubes: critical review of adsorption applications. *Separation and Purification Technology* **2016,** *157*, 141-161.

159.	Zeng, G.; He, Y.; Zhan, Y.; Zhang, L.; Pan, Y.; Zhang, C.; Yu, Z., Novel polyvinylidene fluoride nanofiltration membrane blended with functionalized halloysite nanotubes for dye and heavy metal ions removal. *Journal of Hazardous Materials* **2016,** *317*, 60-72.

160.	Al-Zoubi, H.; Ibrahim, K. A.; Abu-Sbeih, K. A., Removal of heavy metals from wastewater by economical polymeric collectors using dissolved air flotation process. *Journal of Water Process Engineering* **2015,** *8*, 19-27.

161.	Mahdavi, H.; Prasad, V.; Liu, Y.; Ulrich, A. C., In situ biodegradation of naphthenic acids in oil sands tailings pond water using indigenous algae–bacteria consortium. *Bioresource Technology* **2015,** *187*, 97-105.

162.	Deshpande, A.; Jadad, A. R., The impact of polyol-containing chewing gums on dental caries: a systematic review of original randomized controlled trials and observational studies. *The Journal of the American Dental Association* **2008,** *139* (12), 1602-1614.

163.	Zhong, W.; Gu, T.; Wang, W.; Zhang, B.; Lin, X.; Huang, Q.; Shen, W., The effects of mineral fertilizer and organic manure on soil microbial community and diversity. *Plant and Soil* **2010,** *326* (1-2), 511-522.

164.	Delgado, C. L., Rising consumption of meat and milk in developing countries has created a new food revolution. *The Journal of Nutrition* **2003,** *133* (11), 3907S-3910S.

165.	Jarosiewicz, A.; Tomaszewska, M., Controlled-release NPK fertilizer encapsulated by polymeric membranes. *Journal of Agricultural and Food Chemistry* **2003,** *51* (2), 413-417.

166.   Azeem, B.; KuShaari, K.; Man, Z. B.; Basit, A.; Thanh, T. H., Review on materials & methods to produce controlled release coated urea fertilizer. *Journal of Controlled Release* **2014,** *181*, 11-21.

167.   Han, X.; Chen, S.; Hu, X., Controlled-release fertilizer encapsulated by starch/polyvinyl alcohol coating. *Desalination* **2009,** *240* (1-3), 21-26.

168.   Tomaszewska, M.; Jarosiewicz, A.; Karakulski, K., Physical and chemical characteristics of polymer coatings in CRF formulation. *Desalination* **2002,** *146* (1-3), 319-323.

169.   Hanafi, M.; Eltaib, S.; Ahmad, M.; Syed Omar, S., Evaluation of controlled-release compound fertilizers in soil. *Communications in Soil Science and Plant Analysis* **2002,** *33* (7-8), 1139-1156.

170.   Gan, L. H.; Ravi, P.; Mao, B. W.; Tam, K. C., Controlled/living polymerization of 2-(diethylamino) ethyl methacrylate and its block copolymer with tert-butyl methacrylate by atom transfer radical polymerization. *Journal of Polymer Science Part A: Polymer Chemistry* **2003,** *41* (17), 2688-2695.

Appendix A: Turning Chewing Gum Waste into a Structure for Controlled Release of Fertilizers

A.1 Introduction

As the world's population continues to grow, there will be a greater demand for agricultural products to provide nutrition to the masses. Fertilizers dramatically improve crop yields and have played an important role in providing food for nations. Mineral fertilizers are responsible for supporting half of the world's current food production.[163] Reliance on fertilizers will intensify as land available for agriculture decreases and as developing nations shift to demanding more meat in their diets.[164] Not only will it be important to continue to use fertilizers in agriculture production, it will also be important to make sure that we use them more efficiently. This places special emphasis on developing methods that allow crops to increase their absorption of these nutrients to maximize the increase in yield per unit of fertilizer applied. This is a major reason why continuous research has been put into developing methods to control the release rate of fertilizer as this will increase application efficiency.[165-167]

With increasing environmental concerns in regard to how human activity is affecting the Earth's ecosystems, there has been increased pressure on the agricultural industry to make sure that the chemicals and fertilizers used to increase production yields have a minimal effect on the surrounding environment. A common problem faced by this

industry is fertilizer leaching that occurs when heavy rain dissolves the fertilizer that is spread over the field, washing it in the streams and rivers.[166] This is unfavorable for both the environment and farmers, i.e., it causes an imbalance of nutrients available in rivers and streams, which affects biodiversity there,[167] and it causes farmers to engage in the costly procedure of reapplying fertilizer in order to get the desired production yield. One method that has been utilized to deal with this problem has been to coat granular fertilizers with hydrophobic polymer coatings in order to control the release rates of these fertilizers, alleviating some of the negative effects of fertilization.[168]

Hydrophobic polymer coatings work by limiting the contact of water to the hydrophilic fertilizers inside the coating.[165] Without the coating, the water would dissolve the fertilizers very quickly, and the fertilizer would be washed away in any runoff that occurs in a heavy rainfall. The hydrophobic polymers do not dissolve in water; however, they are slightly permeable, allowing water to seep slowly through the coating coming in contact with the fertilizer. Then, the fertilizer is able to be dissolved and flows out of the coating in a controlled manner. The rate of release can be manipulated by changing, for example, the coating permeability and/or thickness.[169] Ideally, it is best to have a steady release throughout the entire growing season of the crop.

One of the major components of chewing gum is hydrophobic polymers. Every year 100,000 tons of chewing gum are consumed worldwide and end up as litter or make their way into landfills; this is not an efficient use of this material.[9] In this investigation, we

wanted to determine if consumed and recovered gum could be processed and used to embed fertilizers and, therefore, control the rate of release.

The method used should be inexpensive and environmentally friendly, while producing a good polymer that adequately embeds the fertilizer, allowing it to control the rate of release. The process also needs to be scaled up easily to enable large scale production. It will be important to look at what effect the polymer has on the soil after the fertilizer is released and whether it is able to biodegrade in the soil. These factors will be the key in determining whether the results of the experiment could be applied to industry. So far, our experiments have shown that this concept is feasible, and that it could be used as an alternative to traditional polymers for controlling the release of fertilizers to the environment. In addition, we are able to tune the release rate of fertilizers in a certain environment by mixing them with some additive polymer.

A.2 Experimental Section

A.2.1 Materials and Instruments

99.9% Toluene was purchased from Sigma-Aldrich (St. Louis, Missouri) and was used as received. 99.9% Dimethyl sulphoxide and granular 99.0% potassium phosphate and potassium chloride (fertilizer) were purchased from Caledon Chemicals (Georgetown, Ontario). 99.9% Dimethylformamide and 100% tetrachloroethylene used in the experiments were purchased from Fisher Scientific (Ottawa, Ontario). 99.8%

Chloroform-d and 98% 1-bromohexene also were obtained from Sigma-Aldrich (St. Louis, Missouri). Two brands of chewing gum of two brands were purchased from a local store and used in this research: Excel Peppermint chewing gum (Brand 1) and Trident Peppermint chewing gum (Brand 2).

Fourier transform infrared spectroscopy (FT-IR) was conducted on a Nicolet ContinuμM microscope (Waltham, MA). Thermogravimetric analysis (TGA) was performed on a Perkin Elmer Thermogravimetric Analyzer (Waltham, MA). Both Vortex and sonication baths were purchased from Fisher Scientific (Ottawa, Ontario), and a Dynac centrifuge from BD (Mississauga, Ontario). National Appliance CO. (Portland, Oregon) vacuum chamber equipment was used throughout the experiment. A Thermo Scientific Orion Star A212 conductivity meter was used. Corning CentriStar 15 mL and 50 mL centrifuge tubes, obtained from Corning incorporated (Corning, NY), and Fisher's finest glass coverslips 25 × 25 mm, obtained from Fisher Scientific (Ottawa Ontario), were used throughout the experiment.

A.2.2 Separation of Gum Powder

For our experiments, the different brands of chewing gum that were used to prepare polymer solutions will be referred to as Brand 1 and Brand 2. First, we determined which organic solvents were the most effective for dispersing the gum. It was found that 1-bromohexane, tetrachloroethylene, chloroform-d, dimethyl sulfoxide, dimethylformamide, and toluene all worked to disperse the gum in organic solvent, with

toluene being able to disperse the gum the quickest with the least amount of solvent. The rate of dispersion was increased by sonication.

Once the gum was dispersed, the hydrophobic polymers could be isolated by centrifugation in a Dynac centrifuge at 6000 rpm; this forced them to the bottom of the centrifuge tube, which was isolated from the supernatant solution. The isolated gum was washed with ethanol, followed by centrifugation, and then washing/centrifuging three times with deionized (DI) water. Then, the organic polymers were freeze-dried overnight in a vacuum oven in order to remove any remaining water. A picture of the isolated polymer is shown in Figure A.1.
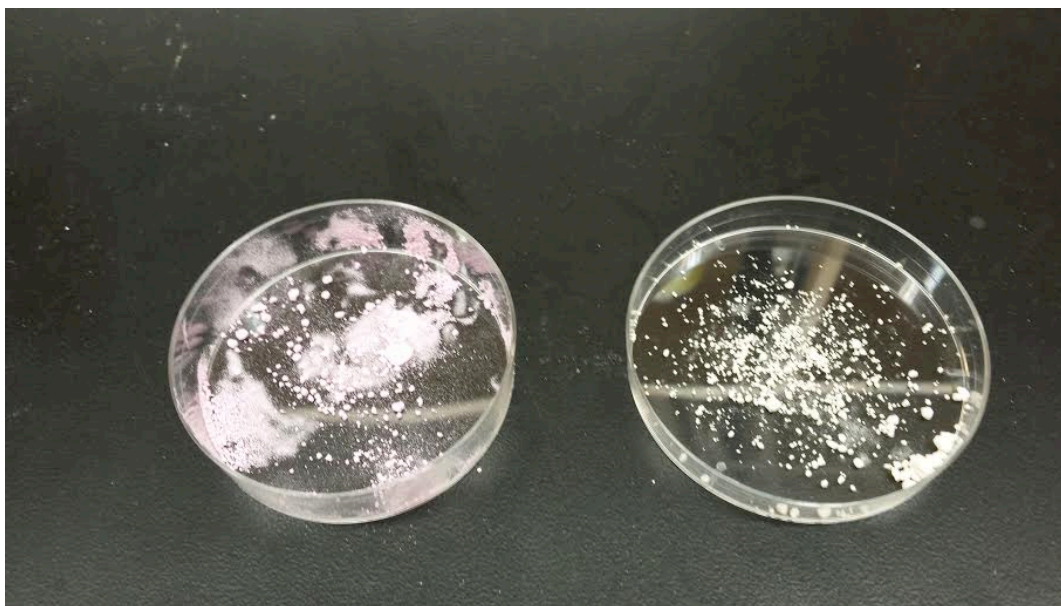
Figure A.1 On the left is the isolated organic polymer from Brand 1 after being freeze-dried. On the right is the organic polymer and potassium phosphate mixture after being freeze-dried.

A.2.3 Mechanical Mixing of the Fertilizer and Gum

Mechanical mixing of the fertilizer and gum also was determined to be an effective method of developing a structure that can control the release rate of fertilizer into the environment. In this process, chewing gum waste was washed in ethanol and water and mixed with potassium phosphate that had been ground into a powder. Next, the chewing gum waste was stretched and folded repeatedly until a uniform blend of fertilizer and gum waste mixture was formed. After the blend was formed, the rate of release was able to be tracked by placing the structure in water and measuring the change in conductivity of the water as the potassium and phosphate ions were released from the chewing gum waste.

A.2.4 Conductivity Test of Controlled Release of Prepared Fertilizer

In the first release experiment that was conducted, three different samples were made containing different ratios of potassium phosphate to chewing gum waste. The first sample contained 0.2041 g of chewing gum waste and no potassium phosphate. The second sample was 20.07% potassium phosphate to gum sample by weight, weighing a total of 0.2286 g. The final sample in this experiment was 32.75% potassium phosphate to gum sample by weight, weighing a total of 0.2922 g. Each of these samples was broken up into four equal sized pieces that were rolled into spheres and placed in vials with 10.0 mL of DI water. The conductivity was recorded over time to track the release rate of the fertilizer into the water.

Once it was determined that chewing gum waste could be used to control the release rate of the fertilizer in the environment, the next challenge was to figure out how that release rate could be manipulated. By increasing the surface area to volume ratio of the sample, the rate of release also was increased. In this experiment, we prepared samples that were 39.58% potassium phosphate to gum sample by weight, weighing a total of 0.3454 g per sample. The first sample was broken up into 10 equal pieces and rolled into spheres, the second was broken into four pieces and rolled into spheres, and the third was just one big sphere. As in the previous experiment, the samples were placed in vials with 10 mL of DI water, and the conductivity was measured over time.

Finally, to confirm that the gum waste would release the fertilizer slowly in soil as well as water, we performed a similar experiment in soil. To do this, a Buchner funnel with a piece of filter paper was placed inside a 400 mL glass beaker. About 10 g of soil that had been washed previously with DI water until its ionic content in soil was negligible was placed in the funnel. Sample 1 contained only soil in the funnel, Sample 2 contained soil along with 0.7530 g of potassium phosphate embedded in 1.1092 g of chewing gum waste that were broken into 20 equal spheres, and Sample 3 contained just soil and 0.7317 g potassium phosphate. Next, 50 mL of DI water was passed through the soil, collected in the beaker, and the conductivity of the water tested. In order to determine the release rate of the fertilizer in soil, this water was tested and then passed through the soil every 24 h until the release of potassium phosphate was complete.

A.2.5 Addition of CO_2-Responsive Synthetic Polymer

We also tested whether the controlled released fertilizer can be functionalized so that that can be used in soil of a specific pH, such as an acidic environment where there are acidic rains. We mixed a CO_2-responsive crosslinked poly (N,N-dimethylaminoethylmethacrylate) (PDMAEMA) with the gum, which increased the releasing rate of fertilizers. This crossed linked polymer was synthesized by adding BIS as the cross linker, according to a published method. [170]

A.3 Results and Discussion

To determine whether potassium phosphate (fertilizer) was coated by the organic polymers found in the gum, we looked at how the properties of the gum changed after processing. Thermogravimetric analysis (TGA) was used to evaluate the physical properties of the gum, i.e., at what temperature the gum decomposes and eventually vaporizes, as shown in Figure A.2 under a nitrogen atmosphere. This works by determining masses at different temperatures and comparing them to the initial masses at the initial temperature. The organic polymers in our control sample of Brand 1 show a mass decrease at ~ 400 °C and then another major mass decrease at ~ 650 °C as the polymers decompose, reducing the weight of the sample. When compared to the sample of potassium phosphate coated by the polymers dispersed in DMSO from Brand 1, we see that the sample decomposes at the same temperatures, however, the percent weight decrease is less because the potassium phosphate found in the sample is not decomposing.

We can determine that the fertilizer is coated by the gum, otherwise it would have been

removed when we washed the sample with DI water during processing.
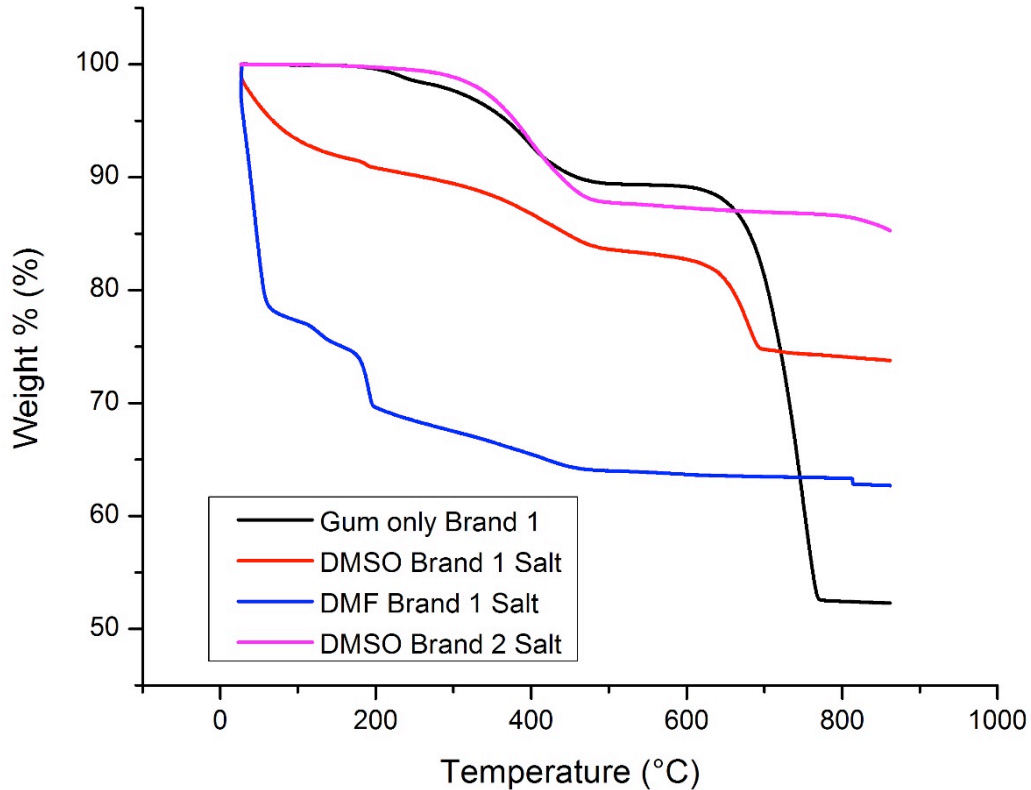
Figure A.2 Thermogravimetric analysis (TGA) comparing the % weight as a function of temperature in a sample containing only organic polymers found in gum to mixtures of polymers and potassium phosphate, confirming that fertilizer is found in the polymer coating. Analysis was performed on a platinum pan in a nitrogen atmosphere with a scan rate of 10 ^{0}C /min.

Brand 2 also experiences a mass decrease at ~ 400 °C just as Brand 1, however, not

with the same decrease at ~ 650 °C. We believe that this is due to the differences in the

polymer blend of the two brands of gum, which exhibit different physical properties and,

therefore, have different decomposition temperatures. However, both brands were able to

embed the potassium phosphate successfully as Brand 2 only decreased to about 85% of

the original weight. This indicates that the potassium phosphate was embedded in the gum; however, we are unable to conclude that the gum encapsulated a potassium phosphate core, which was the goal initially desired for the experiment.

To understand further how the organic polymer affects the fertilizer, we conducted FTIR for Brand 1 dispersed in DMSO. As can be seen in Figure A.4, once the fertilizer is mixed with the polymer, it takes on similar absorbance characteristics as the sample of organic polymer. This is to be expected from the IR spectrum of the organic polymer coated on the outside of the potassium phosphate. In the FTIR data in Figure A.3, we see that the sample containing both the polymer and potassium phosphate has a strong absorption between 1000 and 1200 cm^{-1} due to the P–O bonds present in the structure. There also is a peak around 1675 cm^{-1}, which is believed to be absorption of the P=O. However, the FTIR results confirm that we are able to make a mixture containing both the organic polymer and the potassium phosphate.
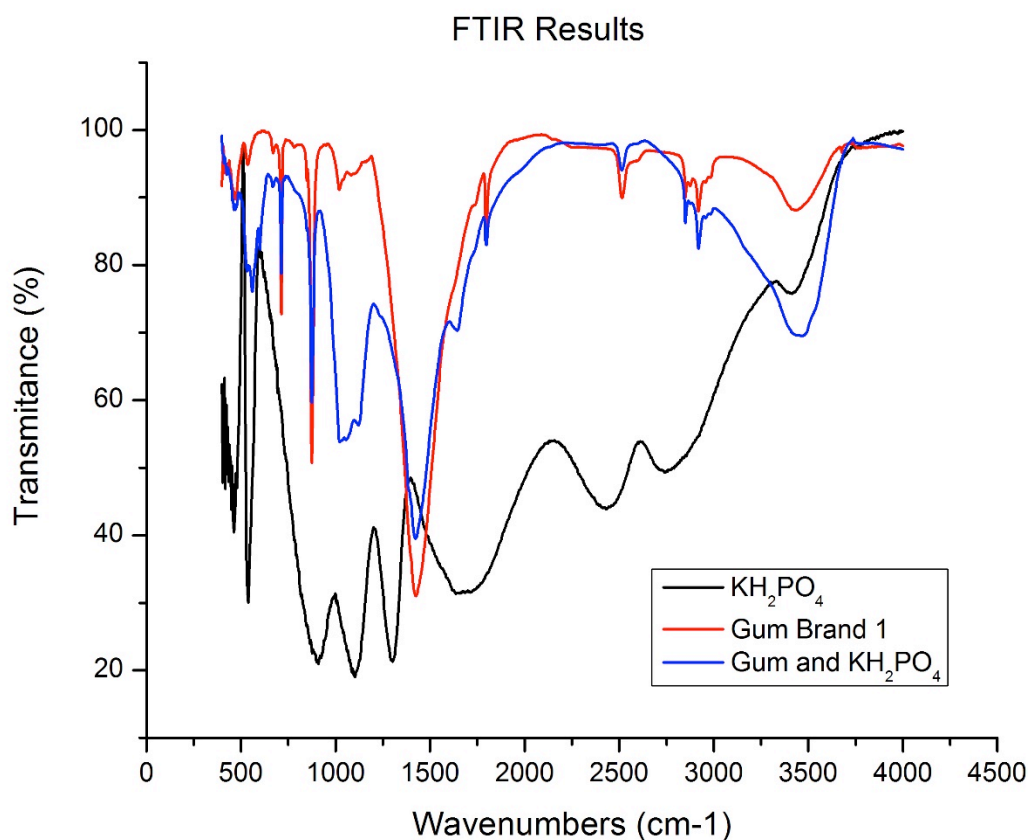
Figure A.3 Fourier transform infrared (FTIR) of potassium phosphate, organic polymer synthesized from gum, and potassium phosphate coated by gum.

As we were unable to conclude definitively that the polymer derived from the chewing gum waste completely surrounded a potassium phosphate core, we decided that it was better to embed the fertilizer mechanically throughout the gum waste. By preforming this procedure, we were able to reduce the need for organic solvents that are harmful to the environment as well as the time needed to prepare the potassium phosphate and the gum sample.

When we placed the sample in water, we found that it was successful in decreasing the release rate of the potassium phosphate into the environment, as show in Figure A.4,

taking just over 1500 min to see a complete release. As the weight percentage of salt in the controlled release fertilizer increases, the total salt released in the solution increases, thus the conductivity of the solution increases.
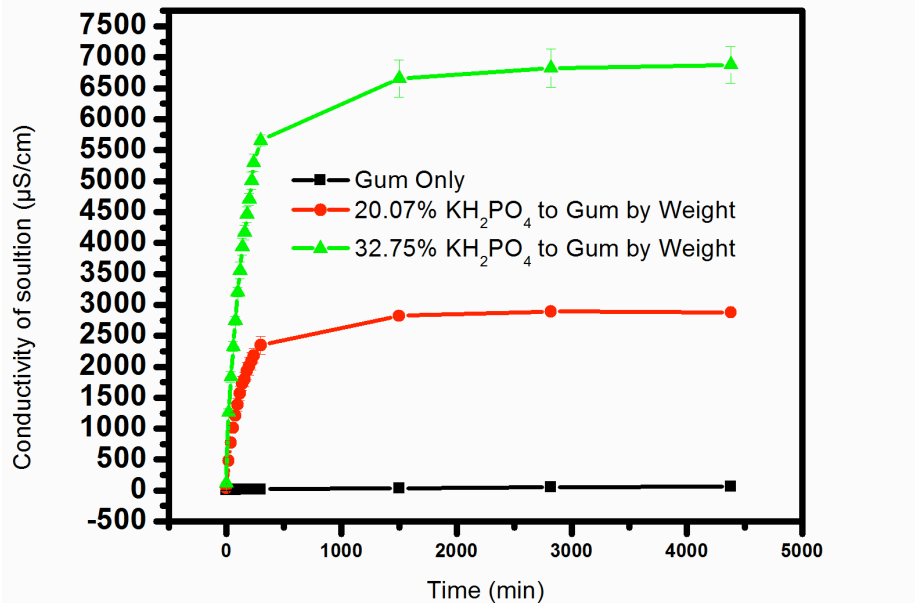
Figure A.4 The change in conductivity of 10 mL of DI water as potassium phosphate is released from chewing gum waste over time. The green line represents a 32.75% potassium phosphate to gum ratio sample, the red line a 20.07% potassium phosphate to gum ratio sample, the black line a sample containing only gum.

An important characteristic of controlled release fertilizers is being able to manipulate the release rate of the fertilizer. One method of manipulating the release rate is to change the size (surface area to volume ratios) of the fertilizer. By changing these ratios, we control how much water is able to penetrate the semipermeable compound as well as the distance that it must travel to reach the center of the compound. When the surface area to volume ratio was increased, so was the rate of release, as shown in Figure A.5. This is one method that can be used to control the rate of release.
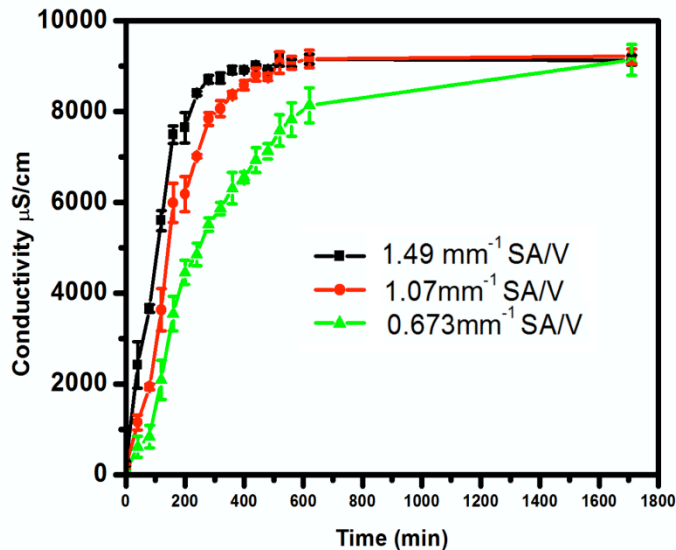
Figure A.5 Change in conductivity in 10 mL of DI water as potassium phosphate is released from chewing gum wastes with varying surface area to volume ratios.

Just as the gum based polymer structure can control the release of potassium phosphate in water, it also can control effectively the release rate in the soil where moisture is present. The release was slower, as expected, compared to the release rate when the structure is placed in water. It took just over 100 h for the complete release of fertilizer from the polymer structure into the environment with a surface area to volume ratio of 0.95, as shown in Figure A.6. From these data we can infer that the polymer derived from the chewing gum waste could be used as an effective material for controlled release of fertilizer.
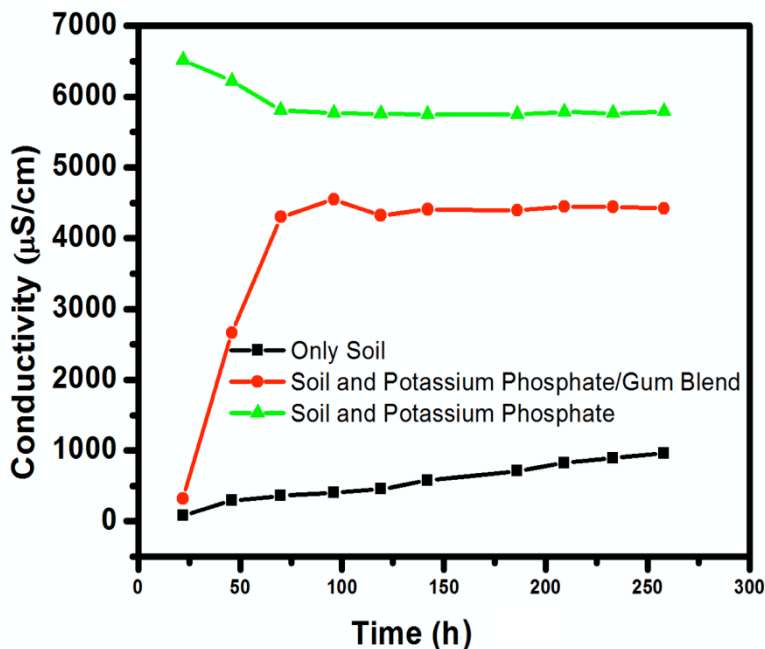
Figure A.6 Release of potassium phosphate in 10 g of soil that was saturated with 50 mL of water. The black line represents only soil, the red line potassium phosphate embedded in chewing gum waste, and the green line granular potassium phosphate.

We made another batch of controlled release fertilizer by mechanically mixing Brand 1 chewing gum waste with KCl (Gum/S) in a method mentioned before and cut it into small balls of very similar sizes. Then half of the gum loaded with KCl was mixed with crosslinked PDMAEMA. We used a pipet tip to bubble air into the solution, as shown in Figure A.7. As a control, we prepared the same gum with polymer (Gum/P), with double the amount of polymer (Gum/DP), and into several smaller sizes labeled "s".

Figure A.7 Air bubbled into the solution with a pipet tip.

From the conductivity data (Figure A.8), we found that the conductivity of the pure gum and gum mixed with polymer does not change much. If we look at the conductivity 1 h after we mixed the salt in the gum, the conductivity increases as the salt is released into water. The conductivity further increases when the gum is mixed with CO_2–responsive PDMAEMA. We can tune the feeding ratio of salt in the gum. In this case, we doubled the amount of salt, so we see a higher conductivity of the solution. When we make the fertilizers into smaller sizes, the releasing rate increases; this would be applied to change the release rate of controlled release fertilizer. Finally, we doubled the amount of salt polymer mixed in the gum and found we were able to increase the

release of salt further. This indicates that addition of crosslinked PDMAEMA can tune the chemistry of slow release fertilizer; this is promising in different environment.
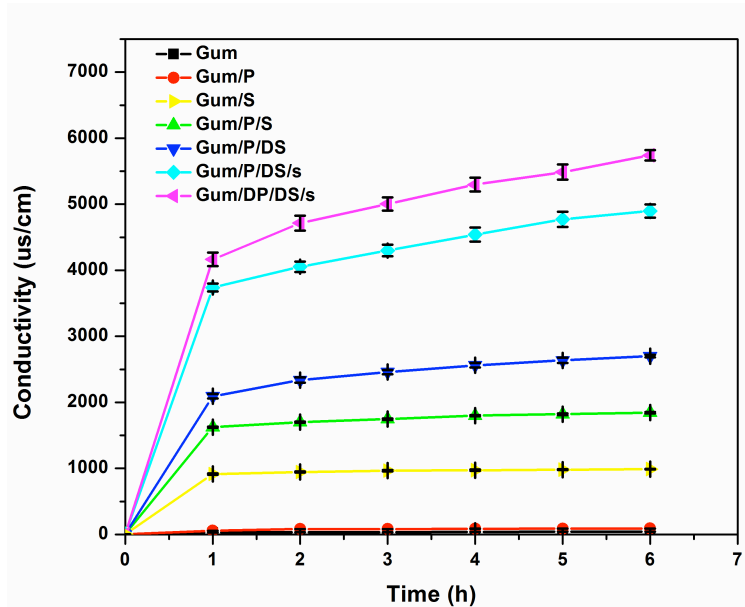
Figure A.8 Conductivity of the solution with different kinds of gum when bubbled with air for different times.

A.4 Conclusions

Overall, there is a great opportunity to be able to use chewing gum waste as a source in which hydrophobic organic polymers can be synthesized. They have been shown to be able to embed hydrophilic fertilizers effectively, allowing them to fill a market niche in the agriculture industry as society becomes more aware of human impact on the environment. A lot of work still needs to be done before it can be scaled up for industrial production; however, there is a foundation on which we can build upon. Not only can this foundation and model be applied to control the release of fertilizers, but our understanding of the properties of the organic polymers also can be applied to other

industries, particularly in the pharmaceutical industry and in the production of construction materials.[17] This will lead to future innovations, which will decrease our ecological footprint while solving some of the problems faced today. We will investigate into the recycle of the gum waste after use in the future.

Appendix B: Preliminary Results of High Frequency Magnetic Field Responsive Etalon and its Application in Drug Delivery

B.1 Experimental Section

B.1.1 Materials

N-isopropylacrylamide (NIPAm) was purchased from TCI (Portland,Oregon) and purified by recrystallization from hexanes (ACS reagentgrade, EMD, Gibbstown, NJ) prior to use. N, N- methylenebisacrylamide (BIS) (99%), acrylic acid (AAc) (99%), and ammonium persufate (APS) (98+%) were obtained from Aldrich (St. Louis, MO) and used as received. Sodium chloride was obtained from EMD (Millipore, Billerica, MA). Deionized (DI) water with a resistivity of 18.2 $M\Omega \cdot cm$ was used. Cr was 99.999% and obtained from ESPI as flakes (Ashland, OR), while Au was 99.99% and obtained from MRCS Canada (Edmonton, AB). Fisher's finest glass coverslips were 25 × 25 mm and obtained from Fisher Scientific (Ottawa, Ontario).

B.1.2 Instruments

Cr/Au annealing was done in a Thermolyne muffle furnace from ThermoFisher Scientific (Ottawa, Ontario). A JUV electron beam evaporator was used to deposit iron. Reflectance spectra were collected using a USB2000+ spectrophotometer, a HL-2000-FHSA tungsten light source, and a R400-7-VIS-NIR optical fiber reflectance probe, all from Ocean Optics (Dunedin, FL).

The spectra were recorded using Ocean Optics Spectra Suite Spectroscopy Software over a wavelength range of 350−1025 nm.

B.1.3 Synthesis of Microgels

Microgels composed of poly (N-isopropylacrylamide)-co-acrylic acid (pNIPAm-co-AAc) were synthesized via free radical precipitation polymerization, as described previously. Briefly, a 3-necked round-bottom flask was fitted with a reflux condenser, nitrogen inlet, and temperature probe, and charged with a solution of NIPAm (11.9 mmol) and BIS (0.703 mmol) in 99 mL of DI water that was filtered previously through a 0.2 μm filter. The solution was bubbled with N_2 gas and allowed to heat to 70 °C for 1 h. AAc (1.43 mmol) was added to the heated reaction mixture in one aliquot. The reaction was initiated with a solution of APS (0.2 mmol) in 1 mL of DI water and allowed to proceed at 70 °C for 4 h under a blanket of nitrogen. The resulting suspension was allowed to cool

overnight and filtered through a Whatman #1 paper filter to remove any large aggregates. Then, the microgel solution was distributed into centrifuge tubes and purified via centrifugation at 8300 rcf to form a pellet, followed by removal of the supernatant and resuspension with DI water, 6 ×. The cleaned microgels were recombined and stored in a brown glass jar. Poly (N-isopropylacrylamide) microgel was synthesized in a similar procedure, without addition of AAc.

B.1.4 Fabrication of Etalon

The details of the "painting" technique used to fabricate microgel-based etalons for these experiments have been reported elsewhere. Briefly, 25 × 25 mm precleaned glass coverslips were rinsed with DI water and ethanol and dried with N_2 gas. Then, 2 nm of Cr, followed by 15 nm of Au, were evaporated thermally onto them at a rate of ~0.2 and ~0.1 Å s^{-1}, respectively, using a Torr International Inc. model THEUPG thermal evaporation system (New Windsor, NY). The Cr acts as an adhesion layer to hold the Au layer on the glass. The Au coated substrates were annealed at 250 °C for 3 h and then cooled to room temperature prior to use.

An aliquot of about 12 mL of previously purified microgel solution was centrifuged for 30 min at 23 °C at 8500 relative centrifugal force (rcf) to pack the microgels into a pellet at the bottom of the tube. After removal of the supernatant solution, the microgel pellet was vortexed and placed onto a hot plate at 30 °C. A previously coated Cr/Au

substrate was rinsed with ethanol, dried with N_2, and then placed onto the hot plate (Corning, NY) set to 30 °C. A 40 μL aliquot of the concentrated microgels was put onto the substrate and then spread toward each edge using the side of a micropipet tip. The film was rotated 90°, and the microgel solution was spread again. The spreading and rotation continued until the microgel solution became too viscous to spread due to drying. The microgel solution was allowed to dry completely on the substrate for 2 h with the hot plate temperature set to 35 °C. After 2 h, the dry film was rinsed copiously with DI water to remove any excess microgels not bound directly to the Au. The film was then placed into a DI water bath and allowed to incubate overnight on a hot plate set to 30 °C. Following this step, the substrate was rinsed again with DI water to remove any microgels not bound directly to the Au substrate surface. Following this rinsing step, the film was dried with N_2 gas, placed into the metal evaporator, and an additional 2 nm Cr, followed by an Au layer of 15 nm, was deposited onto the microgel layer. The Au layer on top of the microgels is referred to as the Au overlayer. Following Au overlayer deposition, the device was soaked in DI water overnight on a hot plate at 30 °C, rinsed with DI water, dried with N_2, and subsequently used for experiments.

Etalons composed of iron are prepared in a similar way. In total, we prepared four kinds of etalons: iron as bottom layer/iron as top layer, iron as bottom layer/gold as top layer, gold as bottom layer/iron as top layer, and gold as bottom layer/gold as top layer.

B.1.5 Loading of Crystal Violet into Etalons

The loading of crystal violet into etalons was carried out by the same method that was used in Chapter 3.

B.1.6 High Frequency Magnetic Field Sensing

A home-built high frequency generator was built by assembling the power supply, cooling system, and copper coil, as shown in Figure A.1. A piece of tape was inserted into the copper coil so that it can hold a small container like the glassware on top of it. For the sensing experiment, an etalon was placed into the glass vial which was filled with 1 mL DI water, making sure the surface of the etalon was fully immersed in water. An optical probe was placed on top of the etalon, and cooling water was run before turning on the power. The reflectance spectra were collected at different time periods.
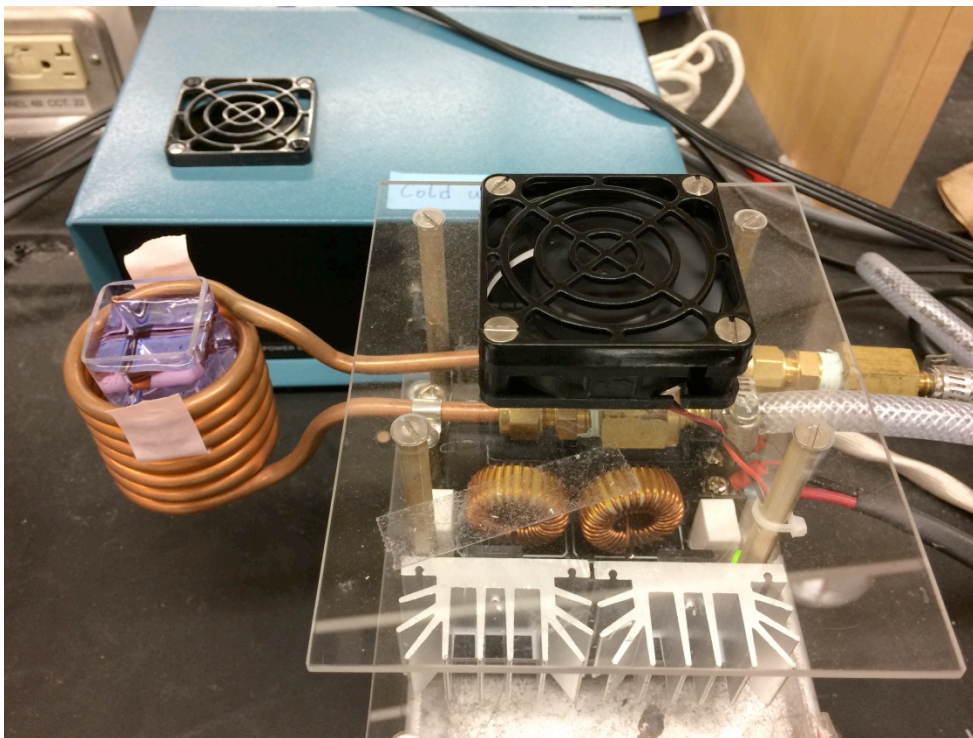
Figure B.1 Setup of high frequency magnetic field generator and reaction reservoir.

B.1.7 Enhanced Drug Release

A 5 mL aliquot of deionized water was added into the glass vial with an etalon loaded

with crystal violet, and cooling water was run before turning on the power. The

absorbance of the solution was determined with UV-Vis at different time periods.

B.2 Results and Discussion

B.2.1 Synthesis and Characterization

Chapter 3 fully characterized the microgels we synthesized and will not be repeated in

this appendix.

B.2.2 High Frequency Magnetic Field Response

It is known that ferromagnetic materials generate heat when exposed to a high frequency magnetic field. There are many commercial products available in the market. This property can be used in our etalons for sensing and drug release. When etalons made with iron are exposed to an external high frequency magnetic field, they will generate heat. The heat generated will cause the microgels layer within the etalon to shrink. As the sizes of the microgels decrease, the color of the etalon will change; this can be captured with an optical probe. A typical reflectance spectrum of the reflectance peak of the etalon (before and after application of external high frequency field) is shown in Figure B.2.
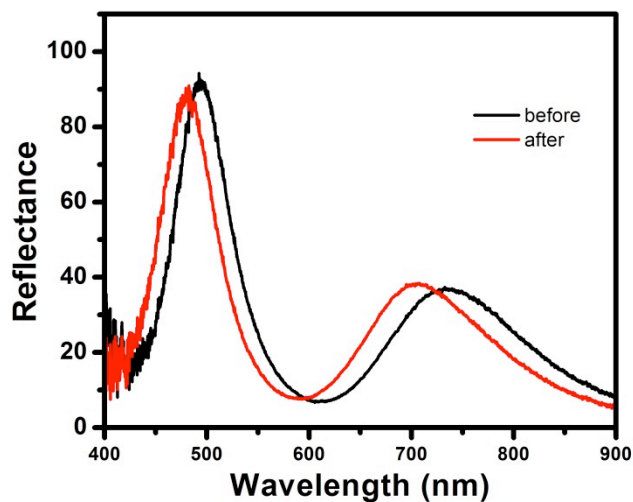
Figure B.2 Typical reflectance spectra of the reflectance peak of the etalon (before and after application of an external high frequency field).

We synthesized etalons with different compositions: iron as bottom layer/iron as top layer, iron as bottom layer/gold as top layer, gold as bottom layer/iron as top layer, and gold as bottom layer/gold as top layer. As can be seen in Figure B.3, in all cases, as the

exposure time of the etalon in the magnetic field is prolonged, the total peak shift of the reflectance spectra of the etalon increases accordinately. The etalons composed of pure gold have slight response to the magnetic field. However, when iron is used to replace gold on either layer to fabricate the etalon, the response to magnetic field increases dramatically in a similar way. The most significant response was observed when iron is used to make the etalon in both bottom and top layers.
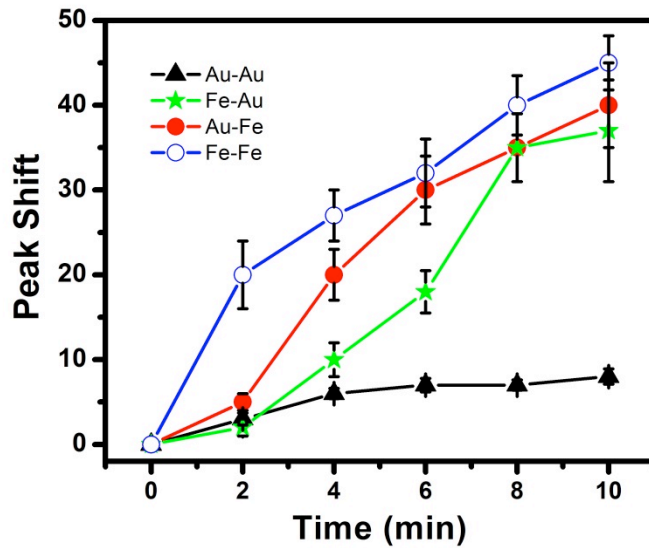
Figure B.3 Total peak shifts (in nm) of etalons made with different compositions when exposed to a high frequency magnetic field, as a function of exposure time.

B.2.3 Drug Delivery

From the research experience in Chapter 4, I concluded that heat will enhance the drug release from etalons. Therefore, we loaded crystal violet into the etalon made of iron in both bottom and top layers. A UV-Vis absorbance spectrometer was used to detect the release of crystal violet. The absorbance intensity at 500 nm was recorded; as can be seen

in Figure B.4, when an external magnetic field is applied, the rele   ase is enhanced. This

may be of interest in the area of biomedical research.
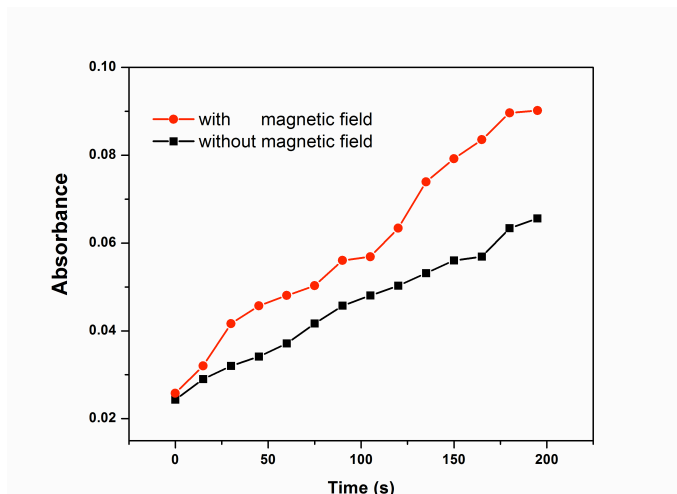
Figure B.4 Absorbance change of released crystal violet in solution with/without the external high

frequency magnetic field on for different time periods.

B.3 Conclusions

So far we have confirmed that we are able to use iron to replace gold to fabricate etalons

in order to enhance the high frequency-magnetic field response. This property could be

used in enhanced drug delivery.

Appendix C: Preliminary Results of Urease-Based Strategy for E. Coli Detection

C.1 Experimental Section

C.1.1 Materials and Instruments

N-isopropylacrylamide (NIPAm) was purchased from TCI (Portland,Oregon) and purified by recrystallization from hexanes (ACS reagentgrade, EMD, Gibbstown, NJ) prior to use. N, N- methylenebisacrylamide (BIS) (99%), acrylic acid (AAc) (99%), and ammonium persufate (APS) (98+%) were obtained from Aldrich (St. Louis, MO) and used as received. Sodium chloride was obtained from EMD (Millipore, Billerica, MA). Deionized (DI) water with a resistivity of 18.2 MΩ·cm was used. Cr (99.999%) was obtained from ESPI as flakes (Ashland, OR), while Au (99.99%) was obtained from MRCS Canada (Edmonton, AB). Urease powder from Canavalia ensiformis (Jack bean), maleimidobenzoic acid N-hydroxy-succinimide ester (MBS) was obtained from Sigma-Aldrich. DNA oligonucleotides with sequence 5'-TTTTT TTTTT TTTTT TGACA CAGCG TTCAA-3' were ordered from IDT. The 5' end of the DNA chain was modified with NH_2. Fisher's finest glass coverslips were 25 × 25 mm and obtained from Fisher Scientific (Ottawa, Ontario).

Annealing of Cr/Au was done in a Thermolyne muffle furnace from ThermoFisher Scientific (Ottawa, Ontario). A JUV electronbeam evaporator was used to deposit iron. Reflectance spectra were collected using a USB2000+ spectrophotometer, a HL-2000-FHSA tungsten light source, and a R400-7-VIS-NIR optical fiber reflectance probe, all from Ocean Optics (Dunedin, FL). The spectra were recorded using Ocean Optics Spectra Suite Spectroscopy Software over a wavelength range of 350−1025 nm.

C.1.2 Modification of Urease with DNA Aptamer

A solution of MBS (6.4 mM) was made by dissolving 2 mg MBS (6.4 μmol) in 1 mL of dimethyl sulphoxide (DMSO). Similarly, a urease solution was produced by dissolving 1.5 mg urease (3.3 nmol) powder in 1 mL of 1× PBS buffer (pH 7.2). A mixture of 1 nmol DNA oligonucleotides and 3.2 μL of the MBS solution (20 nmol) was prepared and adjusted to a final reaction volume of 100 μL with 1× PBS buffer and allowed to react at room temperature. After 1 h, the mixture was passed through a membrane based molecular sizing centrifugal column with a molecular weight cut-off of 3,000 Daltons (NANOSEP OMEGA, Pall Incorporation) in order to remove excess MBS. The column was washed with 50 μL of 1× PBS buffer three times, and the DNA was resuspended in 100 μL of 1× PBS buffer. Then, urease solution (1 mL, 3.3 nmol) was added to the MBS activated DNA, and the conjugation reaction was allowed to proceed at room temperature for 1 h. The mixture was filtered through a 300,000-Dalton cut-off centrifugal column. The DNA-urease conjugate (UrDNA) was washed with 50 μL of 1× PBS buffer three

times and resuspended in 100 µL of 1× PBS buffer. The concentration of the DNA-urease conjugate was estimated to be 10 µM.

C.1.3 DNA Aptamer Modified Urease for E.coli Detection

Different concentrations of E. coli solutions were prepared from a stock solution. Then, 0.5 mL of each E. coli solution was mixed with 10 pmol DNA-urease, and the suspension was incubated at room temperature for 1 h. After reaction, 75 µL of the resulting suspension was added on top of an etalon, which is stabilized with a urea solution of 50 mM, and allowed to react for 30 min.

C.2 Results and Discussion

As calculated, single strand DNA (in excess) was used to modify urease. We separated the excess DNA by centrifuging the solution with a filter. As shown in Figure C.1, the DNA oligonucleotides we used have an absorbance peak at 260 nm. DNA-modified urease has two absorbance peaks at around 260 nm and 290 nm. The 260 nm peak is attributed to the DNA backbone and the 290 nm peak to the urease protein.
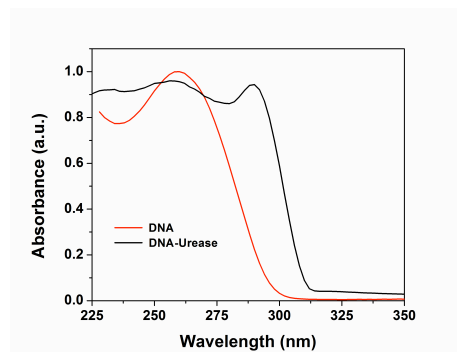
Figure C.1 Absorbance spectra of DNA and DNA-urease solution.

Mixtures containing 0.5 mL of E.coli solution of different concentrations and 10 pmol of the DNA-urease solution, with DNA-urease in excess, were prepared. On completion of the reaction, E.coli bacteria that are bound with DNA-urease were separated from the solution by centrifugation. The supernatant was collected and used for the following reaction: 75 μL of the supernatant was mixed with an etalon that is saturated with a 50 mM urea solution. The reflectance spectrum was recorded after 15 min. The total peak shift as a function of E.coli concentrations is shown in Figure C.2. As the concentration of E.coli increases, less DNA-urease is left in the solution. As a result, less ammonia is generated when reacting with urea, causing less swelling of the microgel layer. Therefore, we observe smaller peak shift in the reflectance spectrum.
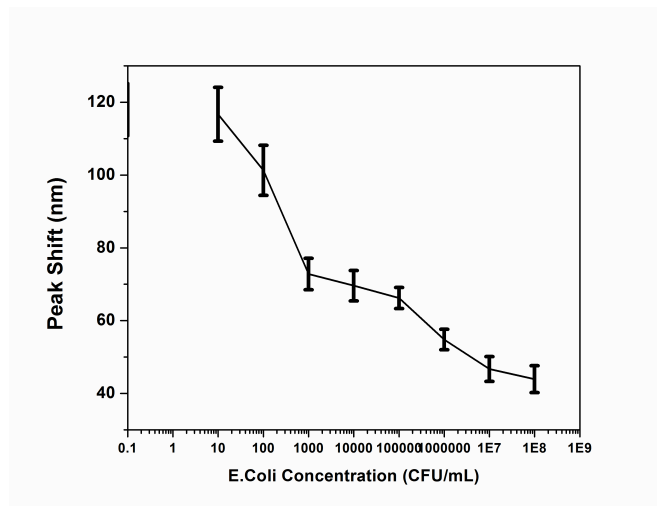
Figure C.2 The total reflectance peak shift from etalons that reacted with the resulting solution from different concentrations of E.Coli and DNA-urease.

To confirm the mechanism behind the response, we separated the supernatant obtained from the reaction of E.coli (10^3 CFU/mL) with DNA-urease. Then, we added the

supernatant to a urea solution in PBS buffer and measured the conductivity of the

solution after 30 min and 60 min. The original conductivity of the solution was 1427, it

increased to 1912 after 30 min and to 2298 after 60 min, as shown in Figure C.3. As

ammonia is generated in the solution, it will dissolve in water and increase the

conductivity.
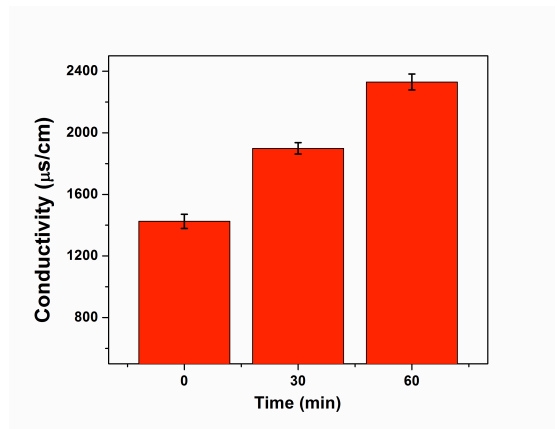
Figure C.3 Conductivity of a urea solution after addition of the supernatant obtained from reacting E.coli (10^3 CFU/mL) with DNA-urease for different time periods.

We used DLS to characterize directly the size change of the microgels with the

existence of DNA-urease. The size of a microgel solution was detected before and after

addition of DNA-urease and urea solution. As seen in Figure C.4, the size increased from

735 nm to 791 nm after 30 min and to 862 nm and 60 min. The size of microgels

increases due to the repelling accumulating positive charges generated by dissolved and

partially disassociated ammonia.
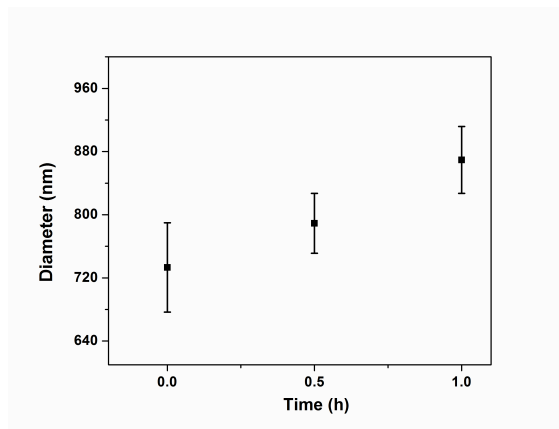
Figure C.4 Diameters of microgels after addition of the supernatant obtained from reacting E.coli (10^3 CFU/mL) with DNA-urease for different time periods.

C.3 Conclusions

Preliminary results show that DNA modified urease is able to react with E.coli. After separation, the excess DNA-urease will be left in the solution, which can degrade urea into ammonia that will interact with the microgels in the etalon, causing the size change of these microgels. The size change of the microgels can be tracked and recorded with an optical probe by collecting the reflectance spectrum. As the concentration of E.coli changes, the total reflectance peak shift changes accordingly. This might be deployed as a cheap and hand held E.coli sensor.